Modeling and Design of a Three-dimensional Inductor with Magnetic Core

Kanchana Surendra

Thesis submitted to the faculty of the Virginia Polytechnic Institute and State University in partial fulfillment of the requirements for the degree of

Master of Science
In
Electrical Engineering

Kathleen Meehan
William Davis
Cameron Patterson

August 10, 2011
Blacksburg, VA

Keywords: inductance, quality factor, parasitics

Modeling and Design of a Three-dimensional Inductor with Magnetic Core

Kanchana Surendra

Abstract

As the demand for portable electronic devices increase, the need to replace off-chip discrete devices with on-chip devices is imperative. Inductors are one such passive device that is widely used in low noise amplifiers, oscillators, etc. Current on-chip spiral inductors suffer from large parasitics and area for a meager value of inductance and quality factor. The need to overcome these issues has led to the development inductors with new geometries housing magnetic cores that show an enhanced inductance compared to the air core coil.

In this thesis, we discuss the design of a three-dimensional spiral inductor with a Co-Fe nanoparticle core that will be fabricated as per the process rules set by VT MT SPL. The changes in the value of the inductance, resistance, quality factor and parasitics are studied for varying number of turns of the coil, thickness of the coil, spacing between turns and different materials used as the coil. An optimum design incorporating the least parasitics and reasonable inductance is proposed.

Acknowledgements

I would like to thank my advisor Dr. Kathleen Meehan who has been very kind and extremely helpful in guiding me through my thesis. She has been really patient and supportive during my difficult times and has always encouraged me to look on the bright side of things. I am sincerely grateful to her for her guidance and thank her for her continued faith in me.

I would also like to extend my gratitude to the members on my committee Dr. William Davis and Dr. Cameron Patterson for their guidance and support.

I am forever grateful to my amazing family who has been very supportive and encouraging of my studies and graduate education. I could not have completed this work without the blessings of Dr. M. N. Surendra, my father, Mrs. Gowri Surendra, my mother and Mr. Madhav Surendra, my brother. Their love and support has helped me come a long way. I love you guys!

I would also like to thank my best friends Amit Rudra, Karl Periera, Santhoshkumar Sambamoorthy, Tania Mutmaina, Nikhil Gupta, Jatin Thakkar, Manasa Valipa, Navaneeta Dorbala, Jai Shanghavi, Gaurav Dongaonkar, Kevin Jones, Francisco, Nader Shehata, Mohini Verma and Sumitra Nair for their tremendous love, support and encouragement. My stay at Virginia Tech will always be memorable because of them. I am blessed to have friends like the Sparkling 12, Vinod Rai, Ritushree, Reena Frank, Vishwas Gowda, Mohan Talikoti, Santhosh Astagimath, Kuldeep Modi, Murali Krishna, Arun Balachandran, and Seema Kulkarni with whom I have shared the most wonderful and amazing times. I cannot imagine my life without you guys and I want you to know that I will always love and treasure each and every one of my friends.

Table of Contents

List of Figures

List of Tables

Chapter 1: Introduction

1.1 Motivation

Integrated RF circuits, including low noise amplifiers, mixers, switches and voltage controlled oscillators, have begun to replace discrete and hybrid components in wireless portable communication applications. Inductors play an important role in RFICs, motivating extensive work on the development of structures to achieve optimized performance. On-chip inductors are critical for enabling integrated wireless communication systems since the use of discrete components introduces parasitics, making the system integration and miniaturization difficult. Vertical, two-dimensional (2-D) and three-dimensional (3-D) structures have been proposed previously [3]-[8], with results showing improved inductance and quality factor as compared to planar structures. In recent times, integrated inductors manufactured using magnetic cores [9] and thin films [10], [11], have demonstrated a performance improvement of 30 times more than that of an air core inductor of an identical geometry.

Researchers using the Micron Technology Semiconductor Processing Laboratory (VT MT SPL) at Virginia Tech, have developed a new type of magnetic nanoscale material composed of Co-Fe, which shows a promising permeability of 120. Our aim is to design and simulate a three-dimensional inductor that can utilize the Co-Fe nanoparticles in its core in an electromagnetic simulation environment such as the Momentum, ADS as per the design rules designated for the students in ECE 4244/5244G, the processing laboratory course that uses the equipment located in the Virginia Tech Semiconductor Processing Laboratory. We hope to fabricate the inductor eventually based on the results of this thesis. An analysis of the sensitivity of the inductance with respect to observed run-to-run process variability will be performed to determine the expected component tolerance of the fabricated inductor.

1.2 Literature Review

The fundamental monolithic inductor is usually implemented as a spiral trace deposited on the passivation layer over a silicon substrate [4], as shown in Figure 1.2-1. The connection from the innermost turn can be taken out as a lead by an underpass or an air bridge. The design parameters are number of turns (n), metal width (w), metal spacing (s), diameter of outermost turn (d_o), diameter of innermost turn (d_i) and arithmetic mean

of inner and outer diameter (d_{avg}). The inductance [1] of the square planar coil is given by the equation

$$L = \frac{9.375\mu_0 n^2 d_{avg}^2}{(11d_0 - 7d_{avg})} \quad (1.1)$$

where μ_0 is the permeability of free space with a value of $4\pi*10^{-7}$ H/m.

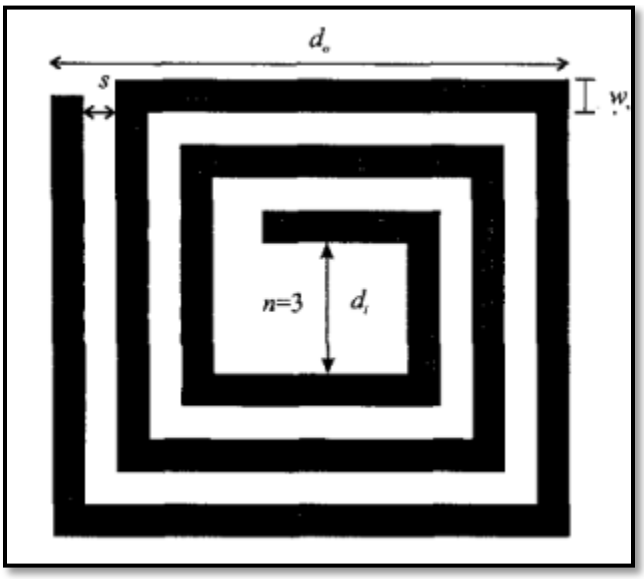

Figure 1.2-1: Planar Square Spiral Inductor [6] (©[2004] IEEE)

The spacing between metal segments in the spiral can be minimized to achieve the maximum inductance per unit area. There are several drawbacks to this design. First, there is considerable parasitic capacitance between the metal runs in the spiral as well as between the metal spiral and the underlying substrate. It is difficult to introduce a magnetic core into the design. It is observed that the conventional planar spiral inductors suffer from large size (~100 times larger than the transistors even for an inductance of L ~ a few nH) and low quality factors (Q < 10 in CMOS) due to various energy loss defects and are not suitable to real world radio frequency (RF) system-on-a-chip (SoC) applications [13].

An increased Q and self-resonance frequency, without process modifications, can be obtained by differentially driven inductors that have the potential to exhibit (ideally) double the Q and increased self-resonance frequency, with respect to single-ended spiral inductors, due to the reduced effect of the substrate shunt parasitic in the differential case [14]. As shown in Figure 1.2-2, when the voltages and currents at Ports 1 and 2 are excited 180° out of phase, the trace currents flow in the same direction, thus increasing the inductance per unit area. While the resulting device has improved performance, the size of the inductor has not decreased from that of the single input spiral inductor design.

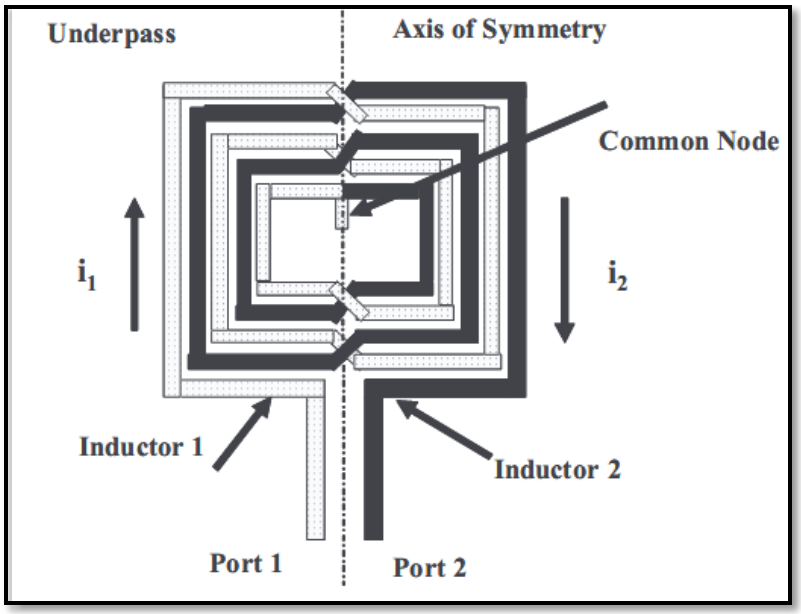

Figure 1.2-2: Symmetrical Differentially driven microstrip inductor [14] (©[2002] IEEE)

An optimal inductor solution would need to provide not only good performance, but also compatibility with the industrial-standard foundry processes [7]. Bulk etching and the use of thick sacrificial layers are not only expensive but also introduce issues of compatibility with existing foundry processes. A new three-dimensional (3-D) microstructure assembly process called PDMA, plastic deformation magnetic assembly [6], [7] was developed and is shown in Figure 1.2-3. Using the PDMA process, surface micromachined structures can be bent out of the substrate plane permanently and can maintain their profile without any external force. As the vertical spiral inductors are raised away from the substrate, the substrate loss, parasitic capacitances, and also the footprints of the inductors are reduced. The coupling between these vertical inductors and the substrate is comparatively lower than that of the in-plane ones. The ability to pull the inductor away from the substrate must be carefully integrated into the process flow. Due to their structure, handling and packaging of the circuit with a PDMA inductor must be cautiously performed to prevent damage to the inductor. Since the PDMA inductor stands vertical, its mass must be minimized to avoid the mechanical failures from flexing of the device structure.

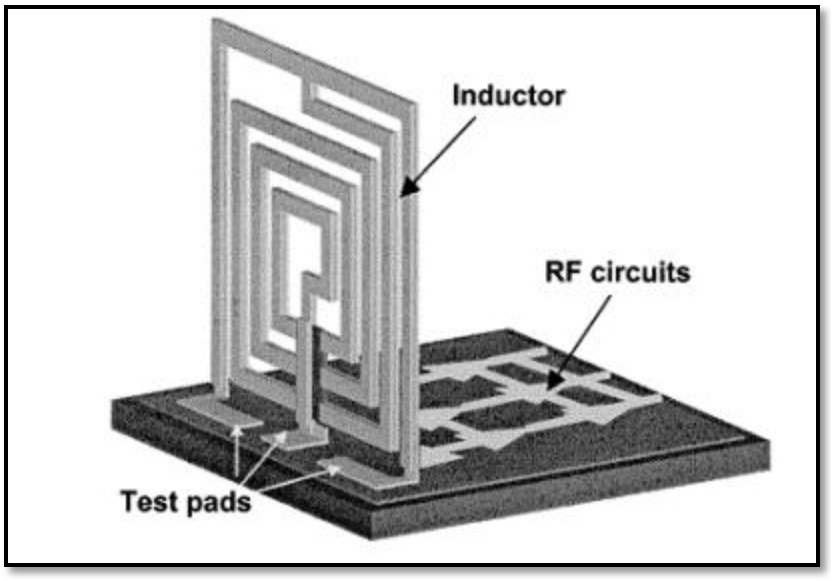

Figure 1.2-3: Vertical Spiral Inductor [7] (©[2003] IEEE)

Solenoid inductors are realized by the assembly of two-dimensional (2-D) multilayer structures [7]. A metal layer (metal-1) is first deposited onto the substrate and patterned as shown in Figure 1.2-4 (a). A number of such parallel metal traces are created forming the lower windings. Then, a second metal layer (metal-2) is deposited and patterned to form semi-circular wire leads as shown in Figure 1.2-4 (b). The two metal layers are separated by a sacrificial layer located between the two metallization and are connected only at via-holes, which are located at the ends of the parallel lines in metal-1 [7]. A magnetic material is then electroplated over the metal-2 patterns and the sacrificial layer is removed. The PDMA process [7] is then used to assemble the top-level winding structures (metal-2) into vertical position to form a three-dimensional solenoid inductor as shown in Figure 1.2-4 (c). Given the structure of PDMA, it is difficult to introduce a magnetic core and is currently not integrated with PDMA inductors. Fragility of the structure is again a drawback, though not as severe as the previous inductor structure.

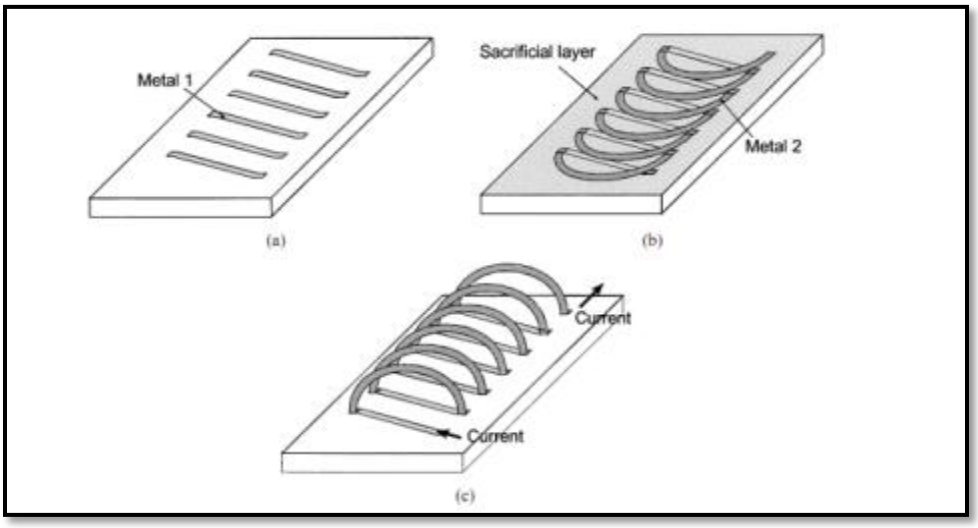

Figure 1.2-4: On chip Solenoid Inductor using PDMA process [7] (©[2003] IEEE)

1.2.1 Fabrication of magnetic cores

A high quality factor can be obtained by the use of a magnetic core with a small iron loss at high frequencies. Thin film microinductors [10] were prepared using multilayered CoNbZr/AIN film. The optimum conditions for a high Q were explored by varying the size of the magnetic core and the structure of the multilayer film and exciting coil. The quality factor (Q) and inductance (L) were observed to have higher values with decreasing thickness of individual magnetic layers and with increasing thickness of intermediate layers [10]. The multilayer thin film magnetic core as shown in Figure 1.2-5 helps reduce the demagnetizing field of the core, thereby increasing inductance. A drawback observed here is that the use of the multilayer thin film cores increases parasitic capacitances between the core and the coil, and this affects the resonant frequency of the device.

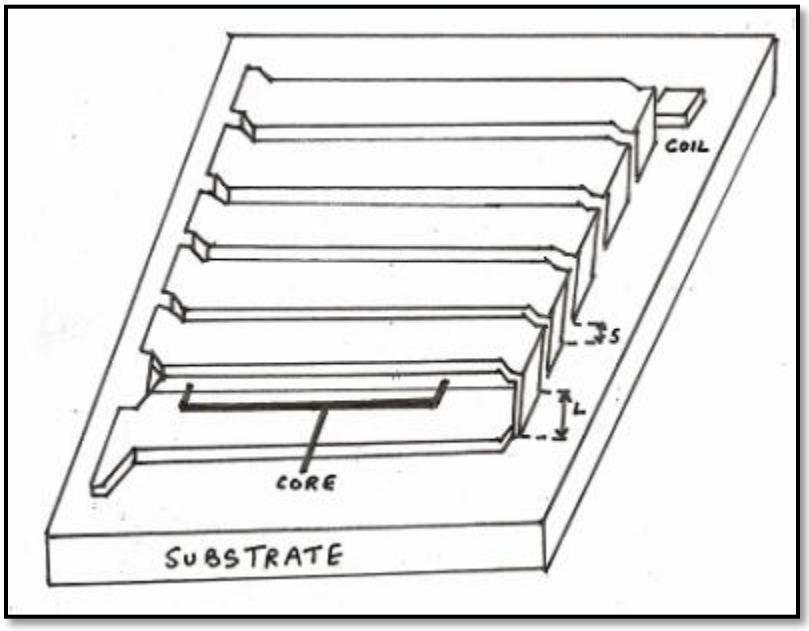

Figure 1.2-5: Inductor with magnetic core [10] (©[1993] IEEE)

Further advances show a toroidal inductor design [11], [15] in thin-film technology aiming at small-signal applications. In a whole new approach, a canted anisotropy is realized by sputtering the first magnetic layer on silicon and glass substrates, removing the samples from the vacuum chamber, and rotating them by 90^0. The insulating SiO_2 and a second magnetic layer are then sputtered with the tilted angle. A sketch of a double layer structure is given in Figure 1.2-6. The crossed anisotropy microinductors display a high inductance, quality factor and permeability. The inductance is sensitive to the angle of core rotation and can alter the resonant frequency.

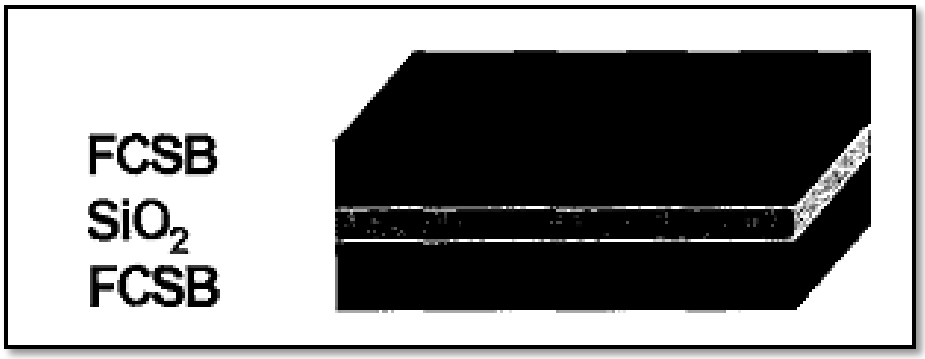

Figure 1.2-6: Sketch of a FeCoBSi double layer with crossed anisotropy [15] (©[2004] IEEE)

Magnetic nanocomposites [12] of high permeability can be used as cores in the inductor design. These composites consist of magnetic nanoparticles inside an insulating dielectric matrix or of a multilayer system of ferromagnetic thin films alternating with insulating layer [12] as described previously. Application of magnetic cores helps miniaturize the geometry and better confines the stray fields compared to air-core coil inductors. Figure 1.2-7 shows an example of a geometric model of a toroid with FeNiCo core used in HFSS. FeNiCo [12] shows promising material properties such as a hard axis permeability of 100 to achieve a ferromagnetic resonance frequency of 4.7 GHz.

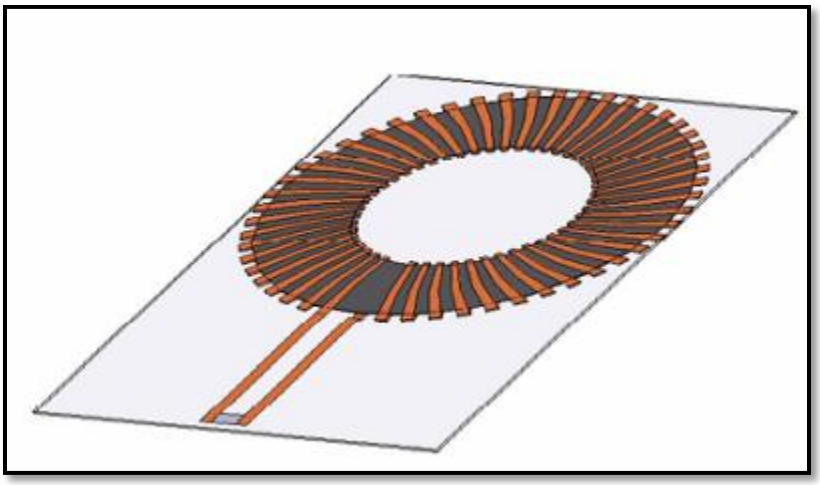

Figure 1.2-7: HFSS model of the toroid inductor with FeNiCo core [12] (©[2007] IEEE)

Incremental progress has been made using stacked structures for small size, special substrates for low losses, and three-dimensional structures for less parasitic effects. However, it is desirable for a full CMOS-compatible structure and integration technique [13] that can make super compact, transistor-size high-Q IC inductors. Ferrite films formed by conventional deposition techniques, such as the sol-gel method, sputtering, and pulsed laser deposition (PLD), are too thin (~1um) for magnetic coupling and require high temperature (>600°C) treatments for necessary crystallization and magnetic activation [13]. These procedures are also harmful to the Al or Cu metal interconnection in CMOS technologies. A fully CMOS compatible on-chip RF inductor with Ni-Zn-Cu and Co_2Z-type ferrite-partially-filled structure was fabricated using a

novel low-temperature nano-powder-mixed-photoresist filling technique [13]. Measured improvements up to +35% in L and +250% in Q as compared to an air core coil (few nH and Q<10) across a frequency range of 0.1-3.5 GHz are observed. The inductor structure is shown below in Figure 1.2-8. The Ground Signal Ground (GSG) test pads are used for S-parameter measurements.

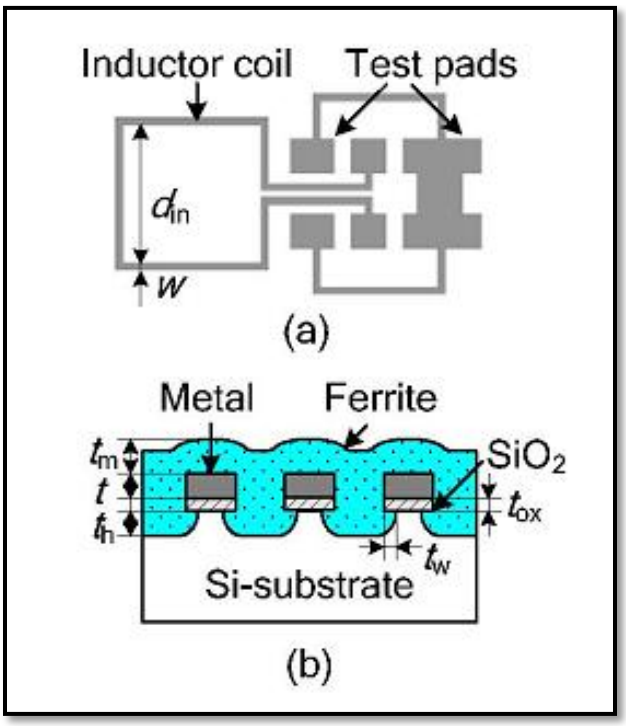

Figure 1.2-8: New ferrite-partially-filled inductor structure [13] (©[2007] IEEE)
(a) Coil with GSG pads. d_{in}: inner diameter, w: line width. (b) cross section of the inductor coil. t: metal thickness, t_{ox}: $Si0_2$ thickness, t_m: ferrite over metal thickness, t_h: thickness of ferrite filling below SiO_2 layer, t_w: lateral etching into bulk Si

1.3 Brief Description of the Project

A three-dimensional structure of a 100 nH inductor is designed in Agilent's Advanced Design System simulation software. The inductor is placed on a base of silicon substrate. The two levels of metal and vias are used to form a spiral structure as shown below in Figure 1.3-1. The core is comprised of the Co-Fe nanoscale material. The inductor is designed as per the current design rules being used in the semiconductor fabrication laboratory at Virginia Tech. The aim of the project is to simulate this particular three-dimensional structure and then to find the inductance value and its behavior upon variations in metal thickness and spacing, structure and frequency; the results of which will be used in the fabrication of the spiral inductor as future work.

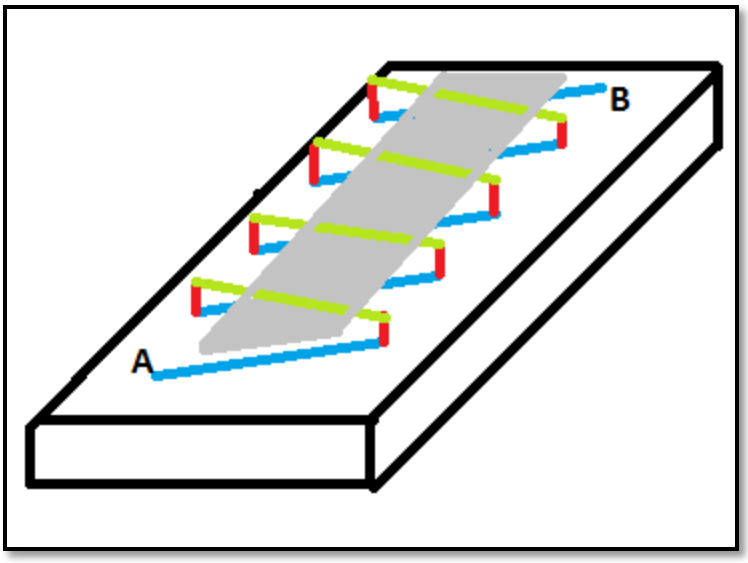

Figure 1.3-1: Proposed inductor

Figure 1.3-1 shows the proposed inductor structure where A and B are the two leads of the inductor. The lines in blue and green indicate the two levels of metal used and the metallization in vias are represented in red. The portion in gray is the Co-Fe magnetic core. The inductor is placed on the silicon substrate.

1.4 Thesis Organization

Chapter 2 provides a brief description of the process being used to simulate the inductor. It provides a brief introduction to S-parameters and describes the current design rules employed in the semiconductor fabrication laboratory at Virginia Tech. It also describes the materials used and their properties.

Chapter 3 provides a brief description of the parasitics and the state of the art software packages used in this project.

Chapter 4 reveals the mask set designed and describes the results of the simulations of the lumped model. It also provides the details of the sensitivity of the inductor with variations in process, materials used and the design structure.

Chapter 5 concludes the research work and provides suggestions for future work in designing and fabricating high performance inductors.

Chapter 2: Process Constraints and Scattering Parameters

2.1 Process Constraints

Post simulation, the inductor will be fabricated on silicon. The process is required to comply by the standard rules of fabrication observed in the Micron Technology Semiconductor Processing Laboratory (VT MT SPL). The simulations on the inductor have been performed keeping in mind the dimensions and process constraints used in the laboratory. The purpose is to build a three-dimensional inductor replicating a solenoid structure at its best. It was limited to an area of 1 mm^2 to 1.5 mm^2 as most on chip inductors do not exceed this size. The dimensions of the inductor were chosen based on a reference model as mentioned in [9]. The general structure to be constructed is briefly discussed here.

Horizontal strips of metal-1 in red are first laid out as shown in Figure 2.1-1. The vias or contacts are the rectangular structures in blue placed at every edge of the metal-1 strip. Following this the diagonal strips of metal-2 in yellow are placed connecting the vias and forming a three-dimensional structure, as shown in Figure 2.1-2. The metals and vias used are comprised of aluminum, which is the standard metal used in the VT MT SPL. The conductivity of aluminum used is $3.7x10^7$ Siemens/meter (S/m). The minimum thickness of the metal layers is 1 µm and the minimum spacing between the two metal strips is also 1 µm thick. The vias are required to be a minimum of 1 µm x 1 µm x 1 µm in dimension.

After the metal layers have been placed, the characteristics of the substrates are edited next. Silicon is the most widely used substrate in the semiconductor industry. It can be made to behave as a conductor in a controlled manner depending on the quantity and quality of dopants introduced while remaining stable under adverse conditions. Hence the substrate used in this project is silicon with a permittivity of 11.9, a conductivity of 0.00156 S/m and a thickness of 400 µm. The insulator is made of silicon dioxide (SiO_2) which extends above the silicon substrate and covers the entire structure of the inductor, as shown in Figure 2.1-3. The magnetic core used comprised of CoFe nanoparticles with a permeability of 120 with a minimum thickness of 1 µm. Simulation results for varying thickness of the core and other parameters are provided in Chapter 3.

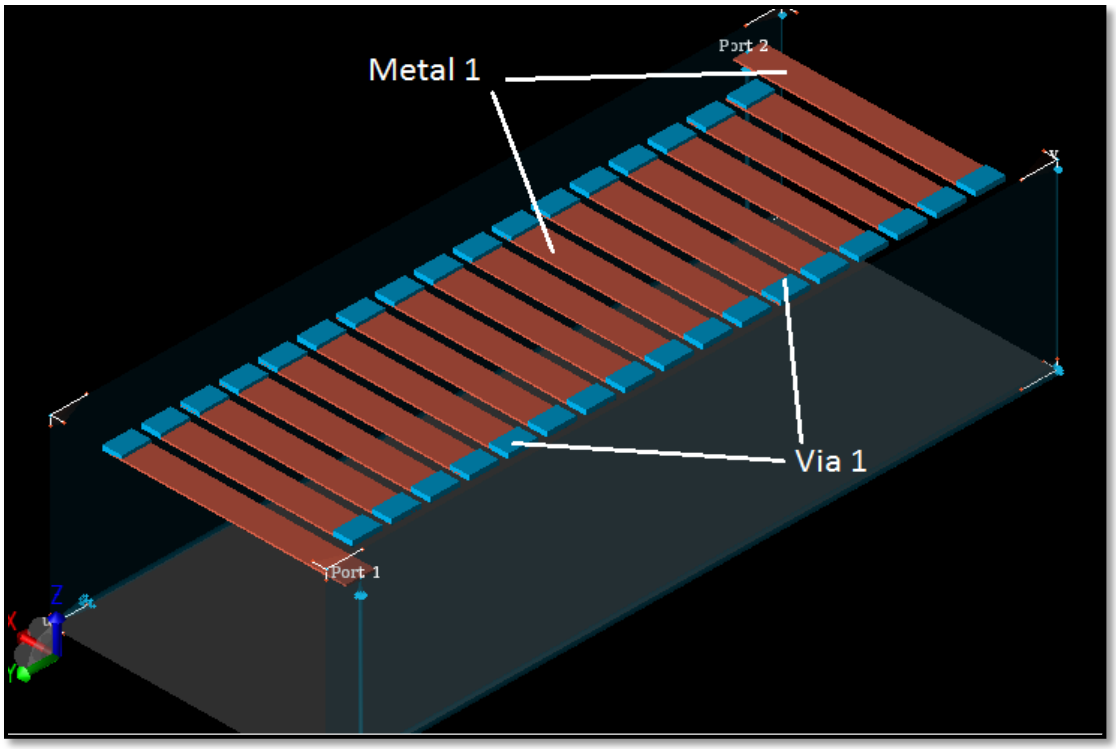

Figure 2.1-1: Horizontal strips of metal-1 and via-1

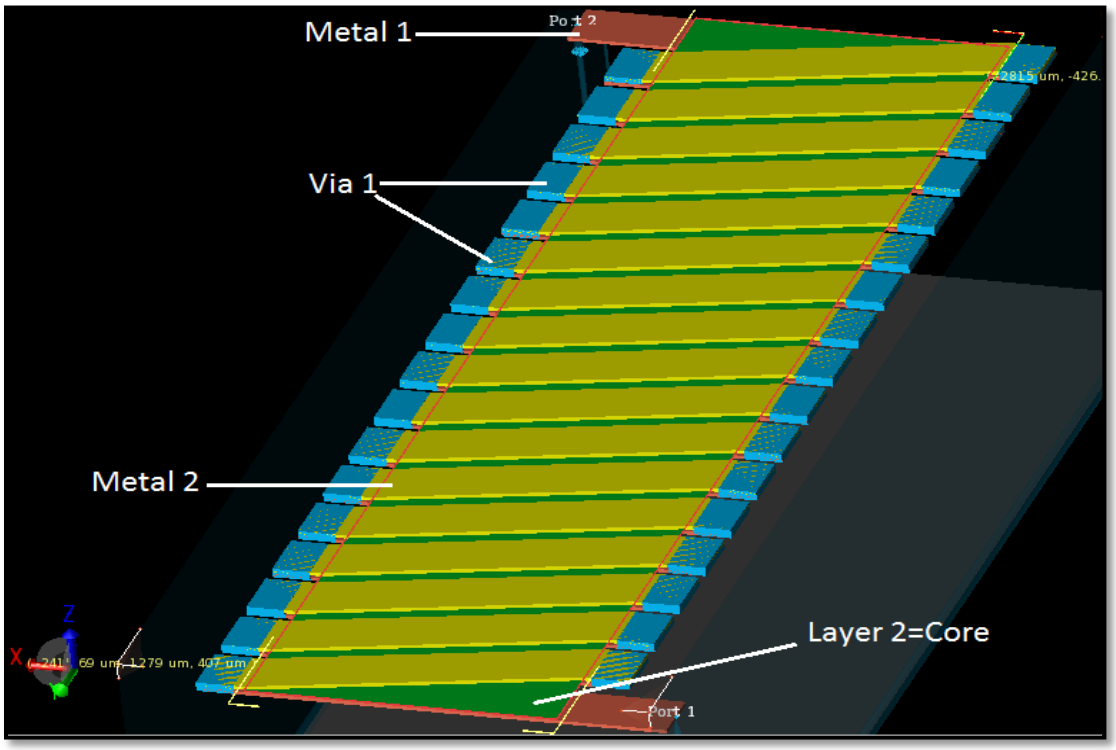

Figure 2.1-2: Three-dimensional inductor shown with core

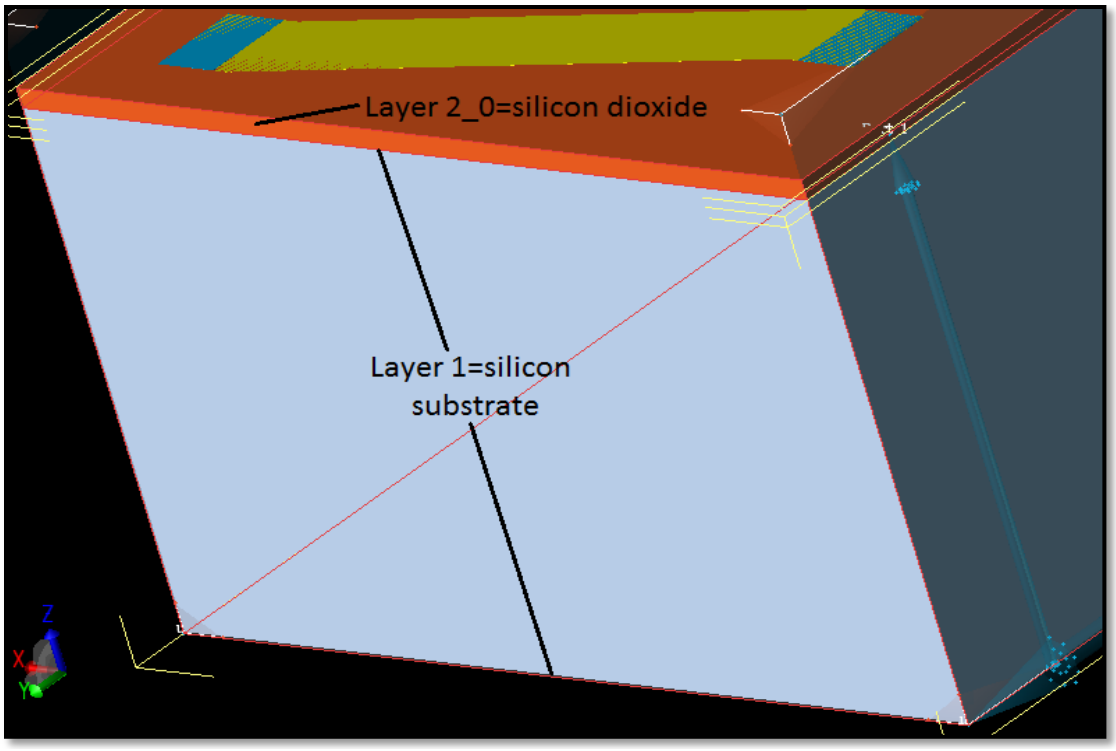

Figure 2.1-3: Substrate structure

2.2 Scattering Parameters

2.2.1 Introduction

Linear networks and nonlinear networks operating with signals sufficiently small to cause the networks to respond in a linear manner can be completely characterized by parameters measured at the network terminals (ports) without regard to the contents of the networks [18]. Knowing the parameters of a network, its behavior in any external environment can be predicted, without regard to the contents of the network. This can easily be achieved by the use of scattering parameters that represent these networks as a black box and predict the external behavior of the components inside the black box. Scattering parameters or S-parameters are important in microwave and RF design because they are easier to measure and work with at high frequencies as compared to other kinds of parameters such as the impedance (Z), admittance (Y) or hybrid (H) parameters. Scattering parameters are conceptually simple, analytically convenient, and capable of providing a great insight into a measurement or design problem [18].

Measuring most other parameters calls for the input and output of the device to be successively opened and short circuited [17]. This can be particularly difficult at RF frequencies where lead inductance and capacitance can make short and open circuits

difficult to obtain. A few disadvantages are that tuning stubs are required at each measurement frequency to reflect short or open circuit conditions to the device terminals, and a tuning stub shunting the input or output may cause a transistor to oscillate, making the measurement invalid. S-parameters provide a comparatively simpler choice as they can be used to express many electrical properties such as gain, return loss, voltage standing wave ratio (VSWR), etc of inductors, capacitors, resistors, integrated circuits, etc. without a tuning stub.

2.2.2 Using S-parameters

The ease with which scattering parameters can be measured makes them especially well suited for describing transistors and other active devices. Let us consider a 2-port scattering matrix for a black box with an input port (Port 1) and output port (Port 2) as shown in the Figure 2.2-1.

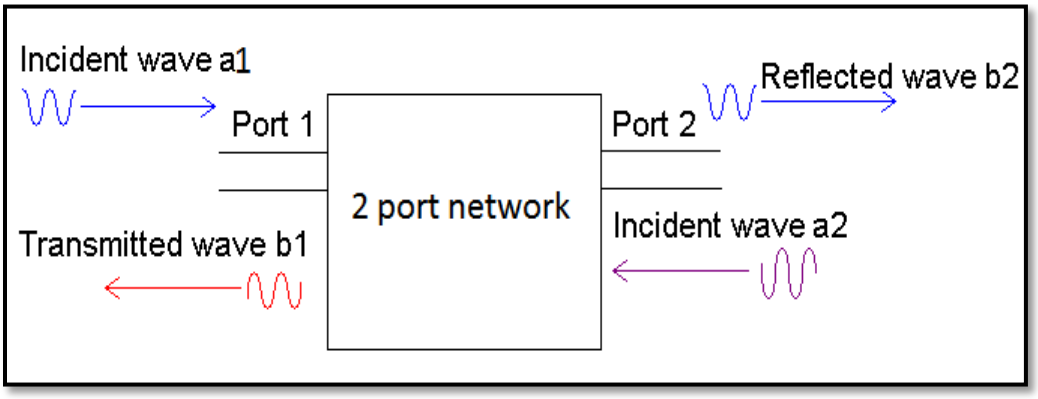

Figure 2.2-1: Two – port network

Scattering parameters can be used to provide a complete description of the network as seen from its ports [19]. They are measured by sending a signal into the network or black box and detecting the reflected or transmitted waves that exit from each port. Power, voltage and current can be considered to be in the form of waves traveling in both directions.

Let us consider an input wave (a_1) incident at Port 1. If the output Port 2 is terminated by connecting it to matched load impedance then there are no reflected waves at Port 2. Hence there is no input wave (a_2) on Port 2. If the input wave on Port 1 (a_1) is not terminated by a matched load impedance at the input, then this gives rise to a reflected wave at Port 1 ($s_{11}a_1$) and a transmitted wave at Port 2, which is absorbed in the termination on port 2.

a_1 is the incident wave at Port 1 and the transmitted wave available at Port 2 is b_2.
a_2 is the incident wave at Port 2 and the transmitted wave available at Port 1 is b_1.

The linear equations describing the 2-port network are:

$$b_1 = s_{11}a_1 + s_{12}a_2 \quad (2.1)$$

$$b_2 = s_{21}a_1 + s_{22}a_2 \quad (2.2)$$

The S-parameters [18] can now be defined as follows:

$s_{11} = \left.\frac{b_1}{a_1}\right|_{a_2=0}$ = Input reflection coefficient with the output port terminated by a matched load

$s_{22} = \left.\frac{b_2}{a_2}\right|_{a_1=0}$ = Output reflection coefficient with the input port terminated by a matched load

$s_{21} = \left.\frac{b_2}{a_1}\right|_{a_2=0}$ = Forward transmission gain with the output port terminated by a matched load

$s_{12} = \left.\frac{b_1}{a_2}\right|_{a_1=0}$ = Reverse transmission gain with the input port terminated by a matched load

We now apply the knowledge of S-parameters to determine the electrical characteristics of the inductor. The layout of the inductor has been created in a tool called Electro Magnetic Professional (EMPro), an EM simulation software design platform used to analyze the three-dimensional electromagnetic effects of components such as high-speed and RF IC packages, bond-wires, antennas, on-chip and off-chip embedded passives and PCB interconnects [20].

The inductor behaves as a two port network shown in the Figure 2.2-2 below. The open ends of the inductor are terminated by ports with a 50 ohm voltage source and are alternately excited by the tool to get the different S-parameters. As S-parameters are frequency dependent, a finite element method (FEM) simulation is run incorporating an adaptive frequency sweep to capture the S-parameter values for this structure over a range of frequencies.

Once the S-parameters for the desired frequency range are obtained, the values are imported in another tool called Advanced Design System (ADS) by Agilent to calculate the impedance parameters and the value of the inductance. The series resistance and quality factor are derived from these values.

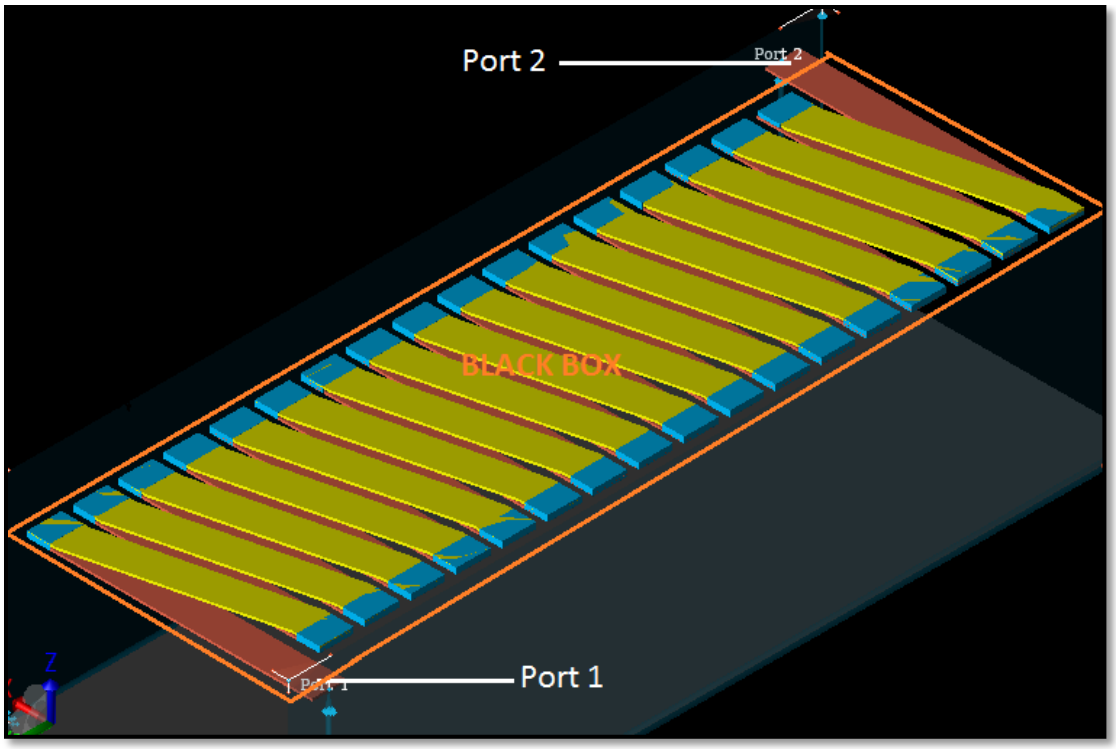

Figure 2.2-2: Inductor as a two - port network

Chapter 3: Tools

3.1 Introduction

There are a number of sophisticated electromagnetic simulation tools available in the market. Each one incorporating as many features possible to more accurately model and calculate the field solution for various applications. A few of the popular simulation software used in the industry are:

- HFSS™ (High Frequency Simulation Software), a simulation tool by ANSYS for 3D full-wave electromagnetic field simulation used in the design of high-frequency and high-speed component design [21].

- IE3D™ SSD, from Mentor Graphics, incorporates the industry's only Full-Wave three-dimensional Method-of-Moments (MoM) EM simulation implementation. The MoM provides full three-dimensional capability in the frequency domain, treating both planar and three-dimensional high frequency structures in a multilayer environment [22].

- Agilent's Momentum is a three-dimensional planar electromagnetic (EM) simulator used for passive circuit modeling and analysis. It accepts arbitrary design geometries (including multi-layer structures) and uses frequency-domain Method of Moments (MoM) technology to accurately simulate complex EM effects including coupling and parasitics [23].

- Electromagnetic Professional (EMPro) is Agilent EEsof EDA's EM simulation software design platform for analyzing the three-dimensional electromagnetic (EM) effects of components such as high-speed and RF IC packages, bondwires, antennas, on-chip and off-chip embedded passives and PCB interconnect [20].

- CST MICROWAVE STUDIO® (CST MWS) is a specialist tool for the three-dimensional EM simulation of high frequency components, which are used is applications such as mobile communication, wireless design, signal integrity, and electromagnetic compatibility/interference [24].

A majority of the tools are state of the art software packages and are not freeware. The trial versions for most of the tools are unavailable and, thus, our options to experiment with different tools were limited. As Virginia Tech had a license for Agilent EEsof's ADS tool package, Momentum was initially chosen as the EM simulator for this project. Although it proved to be a very valuable tool, Momentum had a few

shortcomings. As a result, EMPro, a simulation tool that is also from Agilent, was used in conjunction with Momentum for more accurate representation and evaluation of the inductor structure.

3.1.1 Momentum

Momentum [23] is a three-dimensional planar electromagnetic (EM) simulator that enables RF and microwave designers to significantly expand the range and accuracy of the passive circuits and circuit models. It can analyze random shapes on multiple substrate and metal layers. It is a powerful simulation tool that takes into account coupling and parasitic effects as well, making it a ideal tool for customized passive circuit design-as is our case of the three-dimensional inductor.

A few of the key features of Momentum is that it can easily compute S, Y, Z parameters for a given planar structure. Vias that connect one layer to another can also be simulated; enabling designers to more fully and accurately simulate multilayer RF/MMIC's, printed circuit boards, hybrids, and Multi-Chip Modules (MCMs) [23]. The simulator is based on the Method of Moments (MoM) technology that is particularly efficient for analyzing planar conductor and resistor geometries and generates EM accurate models [23].

Momentum EM simulator has a fast computational time due to its efficient meshing mechanism, adaptive frequency sampling and threaded NlogN solver. It can simulate the skin effect, substrate effect, thick metals, multiple dielectrics/substrates, parasitic coupling and even radiation.

As a result of its above capabilities, Momentum EM proved to be the most appropriate tool at hand to use in this project. Momentum EM is an add-on feature to Agilent EEsof's ADS. The ADS environment is easy to use and a number of online help materials is available on how to do circuit/layout simulations. As the proposed inductor structure is three-dimensional and the circuit component of such a structure is not readily available in the ADS library, the inductor had to be manually laid out in ADS. The procedure observed in Momentum, ADS is described below:

1. The ADS package being used is a 2009 version Update 1. The ADS tool is invoked and a new project is started with the standard length being micron.

2. A "New Layout" window is selected under "Window" in the ADS toolbar. This opens up an empty layout editor window in which the drawings can be made as shown in Figure 3.1-1

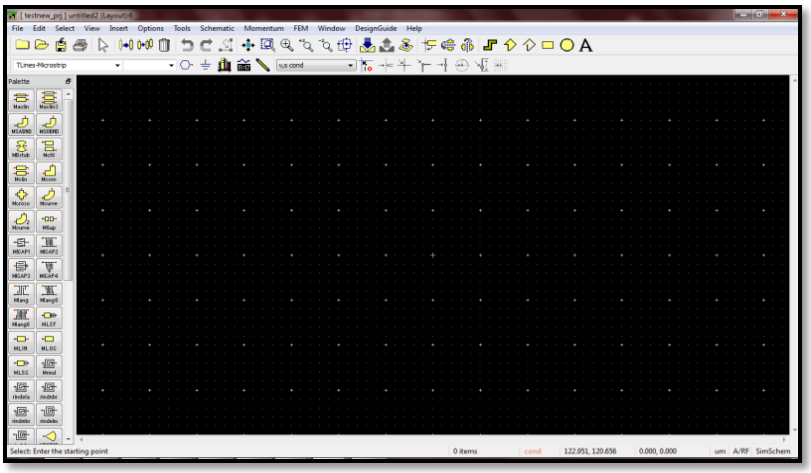

Figure 3.1-1: New Layout Window

3. The name of the current layer selected is displayed in the toolbar. The metals and vias to be used are first selected from the layer editor window by setting the appropriate layer name and binding type. Using more descriptive names can help identify the layer that each part of the circuit is drawn on.

    - To do this, select the "Layers" under "Options" tab in the tool bar. A layout editor window as shown in Figure 3.1-2 opens up and in the "Advanced" tab the following changes are made. "Cond" and "Cond-2" layers are renamed as metal-1 and metal-2 respectively in the "Name" and "Binding List field" sections.

    - The "hole" is renamed as via-1 in the "Name" field and under "Binding list" via-1, metal-1 and metal-2 are written. Via-1 provides a connection from metal-1 to metal-2. In this proposed inductor the metals and via made of aluminum, copper, gold, and silver are simulated.

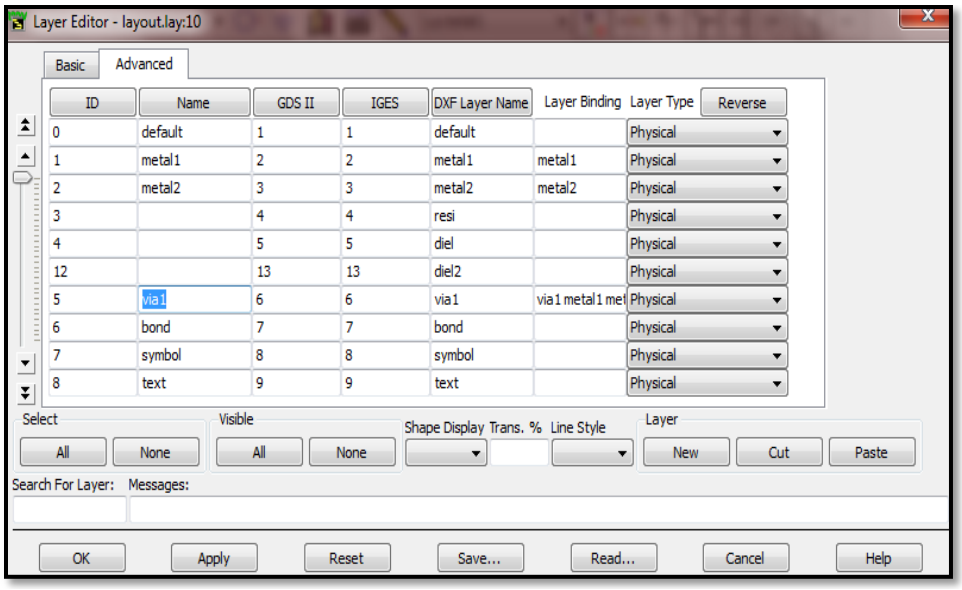

Figure 3.1-2: Layer Editor Window

4. Using either "Insert" commands or toolbar icons, different shapes can be placed in the layout.

    - Metal-1 (red) first selected from the toolbar and either a "path" or "create polygon" is selected to draw horizontal strips of metal 1 depending on the number of turns. The first and last strips are extended in opposite directions so as to include the ports and allow for a proper boundary to be created for simulations.

    - Via-1 (blue) is next selected from the tool bar and "rectangular" vias are then laid out at the edges of each strip of metal-1.

    - Metal-2 (yellow) is next selected and "create polygon" is chosen to draw the diagonal strips of metal-2 connecting vias and metal-1 as shown in Figure 3.1-3. The entire structure is laid out keeping in mind the design rules being followed in VT MT SPL.

    - Two 50 ohm single mode ports of metal-1 are then placed at the two ends of the extended coil.

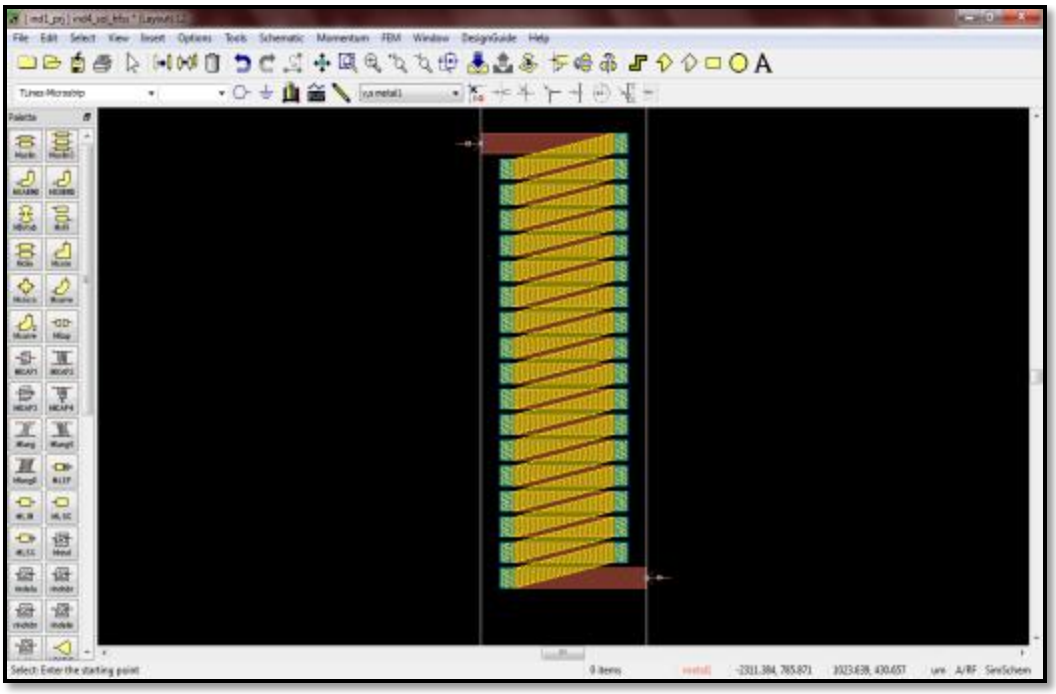

Figure 3.1-3: Inductor structure in ADS

Once this structure is complete, the substrate characteristics need to be set. Substrate layers define the dielectric media, ground planes, air or other layered material. By mapping layout layers to metallization layers, we can position the layout layers that the circuit is drawn on within the substrate.

- A predefined silicon substrate is selected from Momentum > Substrate > Open

- The substrate layers are edited next by clicking on Momentum > Substrate > Create/Modify. The silicon substrate of 400 µm with a permittivity of 11.9 and conductivity of 0.00156 S/m is selected as layer 1, which sits above a closed GND as shown in Figure 3.1-4.

- A new layer 2_0 is added and it is an insulator made up of SiO_2 with a permittivity of 3.9. Layer 3 is also another layer of the same insulator. The thickness of the insulator layer below the metal windings should be at least 1 µm and no more than 5 µm.

- Layer 2 is a magnetic core with a permeability of 120 that sits above layer 2_0. The core can extend up to 80 µm and is sandwiched between layer 2_0 and layer 3.

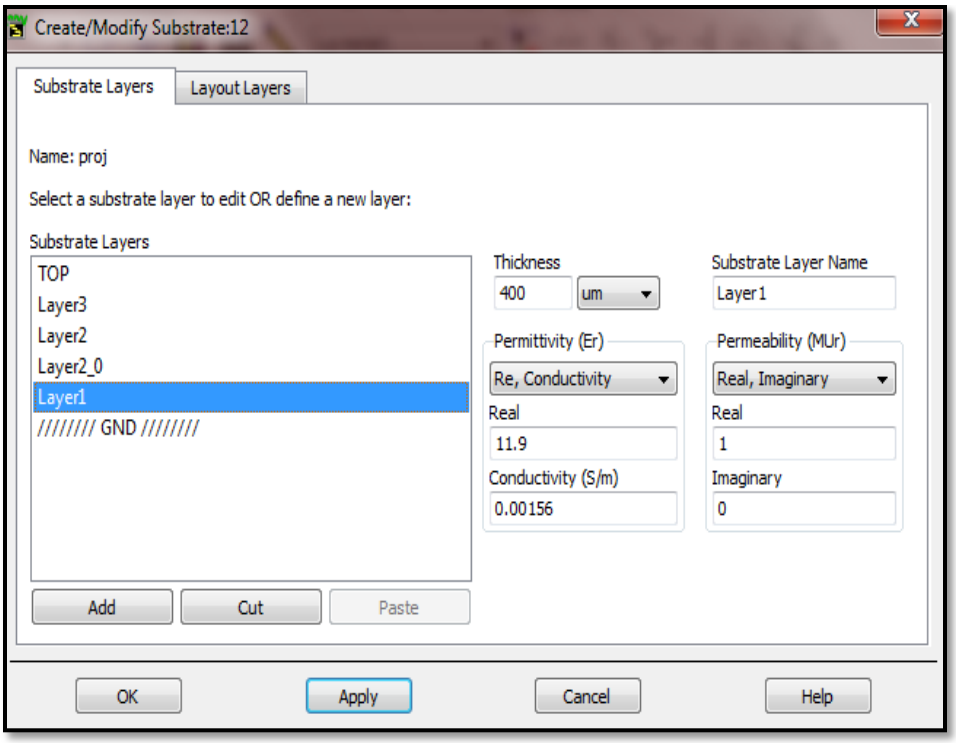

Figure 3.1-4: Create/Modify Substrate layers window

- In the "Layout layers" tab the layout mapping is done. A strip of metal-1 with a conductivity of 3.7×10^7 S/m is introduced above layer 1 with appropriate thickness. Another strip of metal-2 with the same conductivity above is introduced above layer 3. The metal strips must be at least 1 µm but no more than 10 µm thick.

- The connectivity from metal-1 to metal-2 is then provided by via-1 by connecting it through the layers 2_0, 2 and 3. The topmost layer after layer 3 is an open boundary of air as shown in Figure 3.1-5. The changes are saved and structure is then simulated under S-parameters.

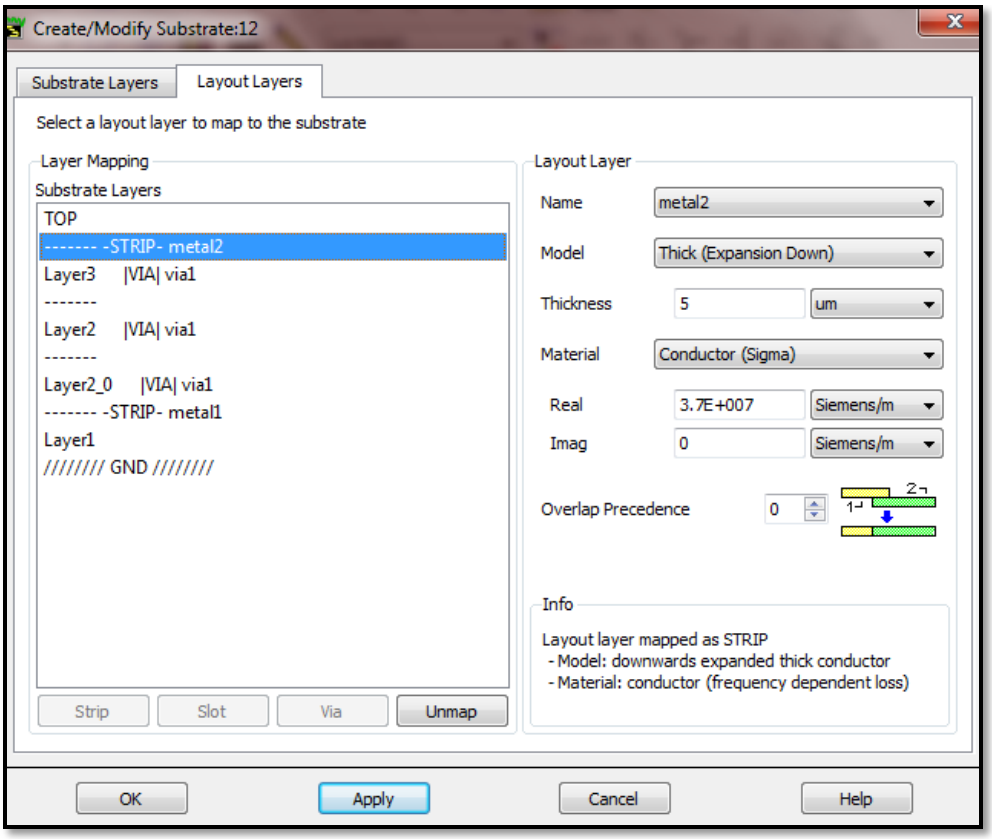

Figure 3.1-5: Create/Modify Layout layers window

5. The simulation profile is opened under Momentum > Simulation > S-parameter. A frequency sweep type of "Adaptive" is selected as it uses a fast, highly accurate method of comparing sampled S-parameter data points to a rational fitting model. The range of frequency chosen is 1 MHz to 20 GHz and the profile is "updated". The "template" specified is a 2 port spiral and a data set name is provided for the results to be displayed. The simulation begins when the "simulate" button is clicked as shown in Figure 3.1-6. After the simulation is completed, a data display window pops up containing graphs of the effective inductance, resistance and quality factor versus frequency as shown in Figure 3.1-7.

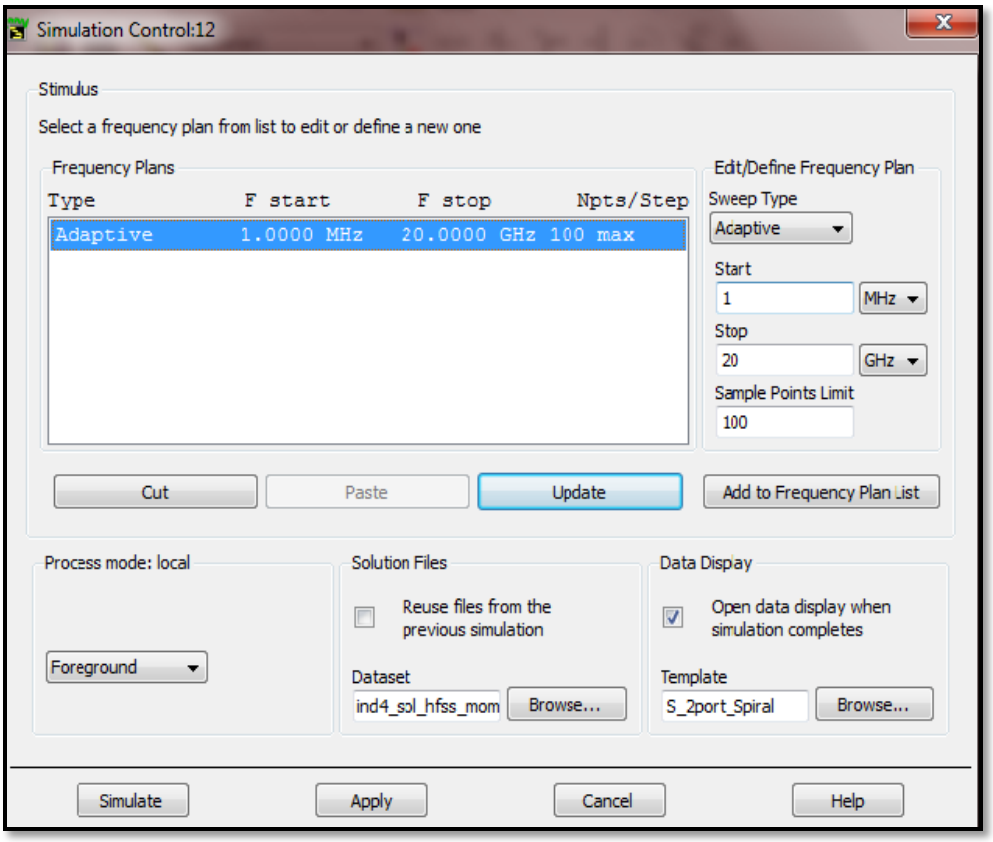

Figure 3.1-6: S-parameter simulation window

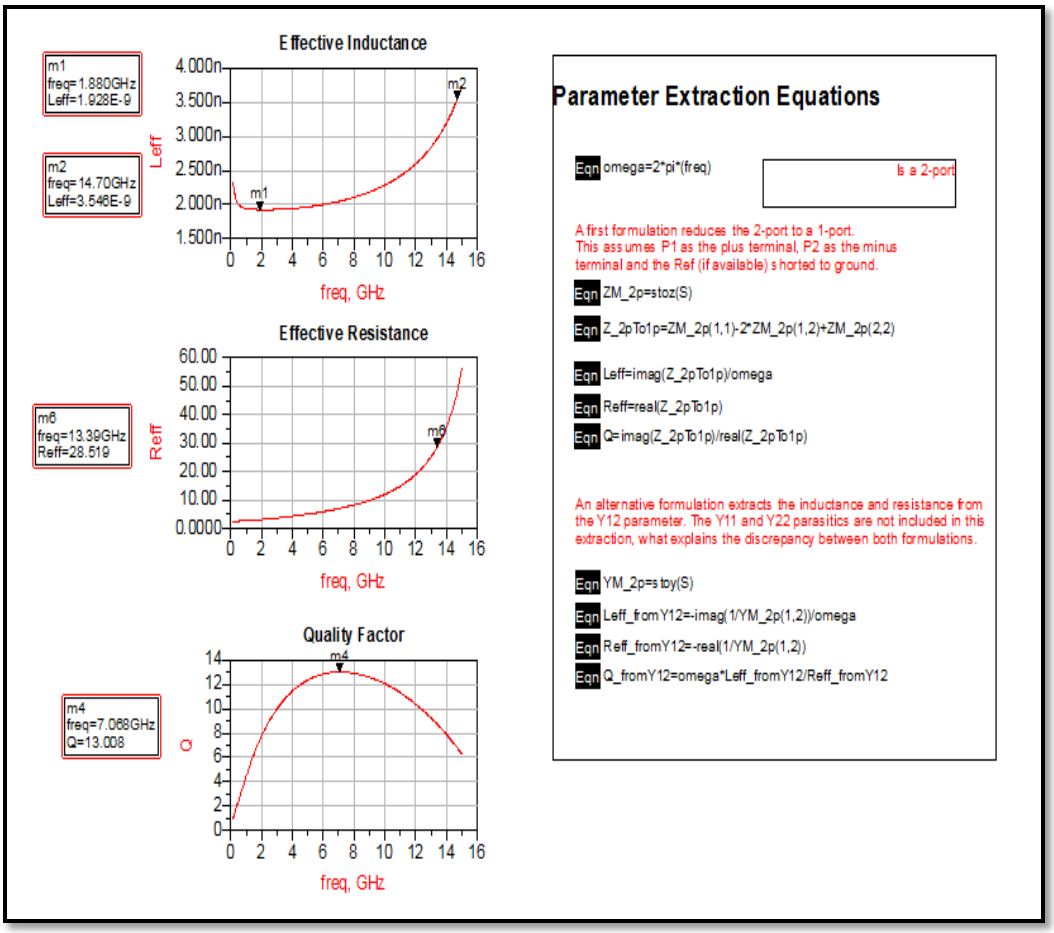

Figure 3.1-7: Simulations results showing Effective Inductance, Resistance and Quality Factor

Shortcomings:

1. Momentum can simulate planar conductor geometries, with planar substrates in a three-dimensional space [23]. The planar conductors have currents flowing only in the horizontal planes without a vertical component. Vias are conductors that act as a bridge to transfer currents from lower metal layers to higher metal layers along the vertical direction without a horizontal component. As a result of these limitations on current flow, Method of Moments is considered to be a 2.5D simulator.

2. Momentum does not allow editing substrate geometries in the horizontal plane. This becomes particularly difficult as we want to introduce a core that sits inside the coil structure, away from the boundaries.

As a result, Electro Magnetic Professional (EMPro), another three-dimensional EM simulation tool by Agilent, was explored to overcome the above problems.

3.1.2 Electromagnetic Professional (EMPro)

EMPro [20] EM simulation software features a modern design, simulation and analysis environment, high capacity simulation technologies and integration with the industry's leading RF and microwave circuit design environment, Advanced Design System (ADS) for fast and efficient RF and microwave circuit design. Unlike Momentum, three-dimensional structures can now be analyzed accurately in EMPro using the same FEM simulator available in ADS. Finite Element Method (FEM) is a fast numerical computational technique in the frequency domain, which proves particularly useful for RF/microwave applications. This technique can handle arbitrary shaped structures such as bondwires, conical shape vias and solder balls/bumps where z-dimensional changes appear in the structure [20].

The EMPro version currently available in Virginia Tech is 2010.07 and is compatible with ADS 2009 Update 1. The layout structure drawn in Momentum can easily be exported to EMPro and further editing can be made. The procedure followed in EMPro is listed below:

1. To export the existing layout from the ADS layout window to EMPro, we choose FEM > export to EMPro > Launch EMPro and import this design from the toolbar.

2. EMPro opens up and the design is imported exactly as it is in ADS. The material properties along with the geometries can be edited here. The magnetic core of layer 2 is edited using the geometry options to fit inside the coil structure as shown in Figure 2.1-2.

3. The design is saved and an FEM simulation for an adaptive frequency range of 1 MHz to 15 GHz is run as shown in Figure 3.1-8. The results are available in the "results" window.

4. As EMPro does not display the inductance directly, a work around was found for this. The S-parameters from EMPro are saved in a citi file format. In the ADS data display window, under Tools > Data file tool, the citi file is read and the inductance, resistance and quality factor of the new structure simulated in EMPro is displayed without any loss of data in the same way as in Figure 3.1-7.

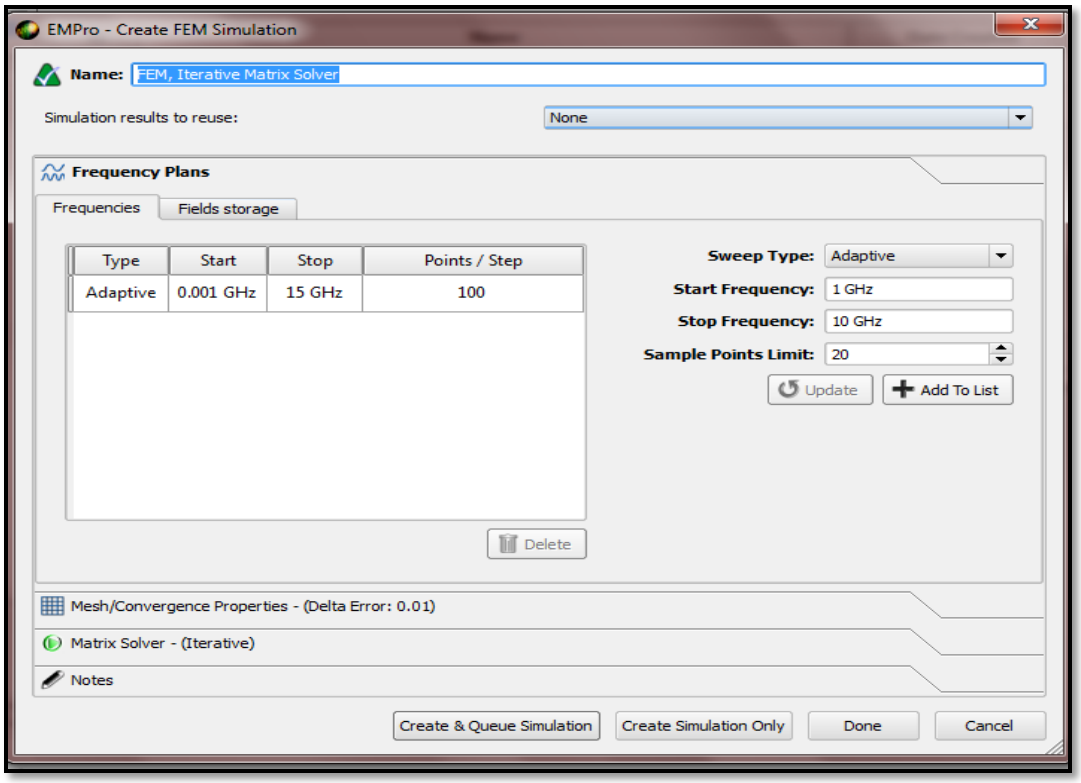

Figure 3.1-8: FEM simulation window in EMPro

3.2 Parasitics

An "ideal inductor" can be defined as one that has a pure inductance, with no resistance or capacitance terms. In simple terms an ideal inductor is one that does not dissipate or radiate energy. However, a real inductor's performance is determined by its layout design and its physical characteristics regarding the loss mechanisms like resistive losses of the metal windings and substrate losses [25]. Thus, the inductance value obtained from simulating the above structure in Figure 2.1-2 does not represent the absolute value of the inductance of the coil. The main hindrance is the presence of parasitics [1] comprising of stray capacitances and resistances like:

- Coupling capacitance between the turns of the coil in both metal-1 and metal-2
- Capacitance of the oxide (C_{ox})
- Capacitance of the silicon substrate (C_{sub})
- Eddy current effects due to the resistance of substrate (R_{sub})
- Resistances of the metal-1 and metal-2 and via-1 (R_s)

- Fringing capacitance of the coil (C_f)

At high frequencies, the stray capacitances begin to affect the inductor's behavior, and at a certain frequency, real inductors can behave as resonant circuits, becoming self-resonant. At frequencies above this, the capacitive reactance becomes the dominant part of the impedance and the inductor has no significance. At higher frequencies, resistance and resistive losses in inductors increase significantly due to skin effect in the inductor's winding wires. Core losses also contribute to inductor losses at higher frequencies. Given the three-dimensional structure of the inductor, there can be other unforeseen losses in the coil and substrate. Figure 3.2-1 represents the sub-circuit of a planar on chip spiral inductor [1], which can be used here to represent the common parasitics. L_s is the inductance of the coil.

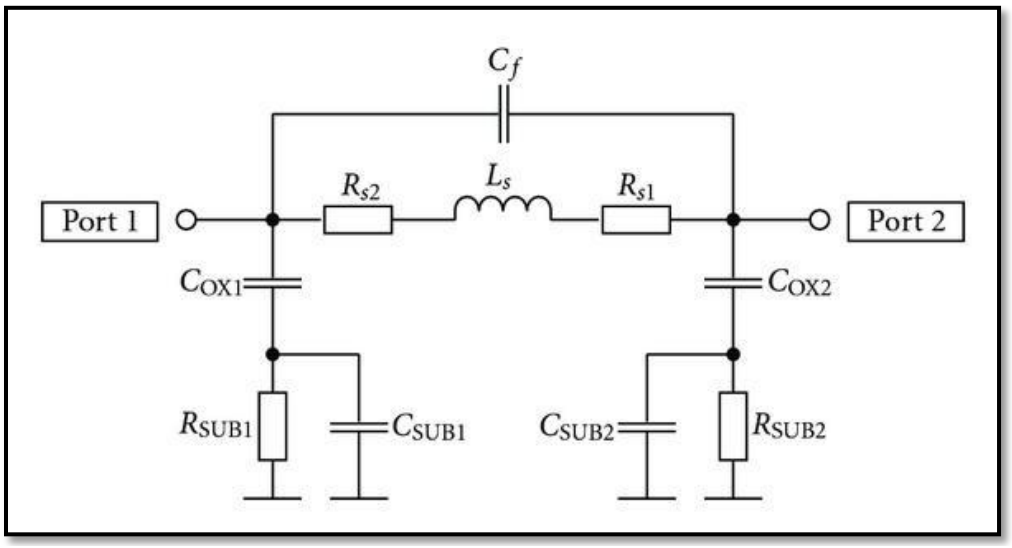

Figure 3.2-1: Sub-circuit of an on chip inductor [25]

The parasitic resistance can be reduced by the use of higher conductivity materials and increasing the thickness of the windings. The coupling capacitance between the windings is in series and, hence, their effective capacitance is lower compared to planar spiral inductors. The substrate coupling and effects can be overcome by new fabrication methods as mentioned in [25]. One outcome of the simulations run on the structure described in Figure 2.1-2 is the identification of a set of materials and the dimensions that minimize these parasitic, which will be described in Chapter 4.

Chapter 4: Results and Discussion

4.1 Inductor Design

The schematic of an inductor with magnetic core listing various parameters used in the representative model [9] model are shown in Figure 4.1-1. N is the number of turns of the coil, Lc is the length of the coil, La (Lm) is the length of the air core (magnetic core), Wm is the width of the magnetic core, Wv is the width of the via, Gv is the via overhang, Sv is the via size, Sp is the spacing between turns, Wa is the width of the air core, Tc is the thickness of the coil, Tm is the thickness of the magnetic core, Ta is the thickness of the air core and H is the height of the structure.

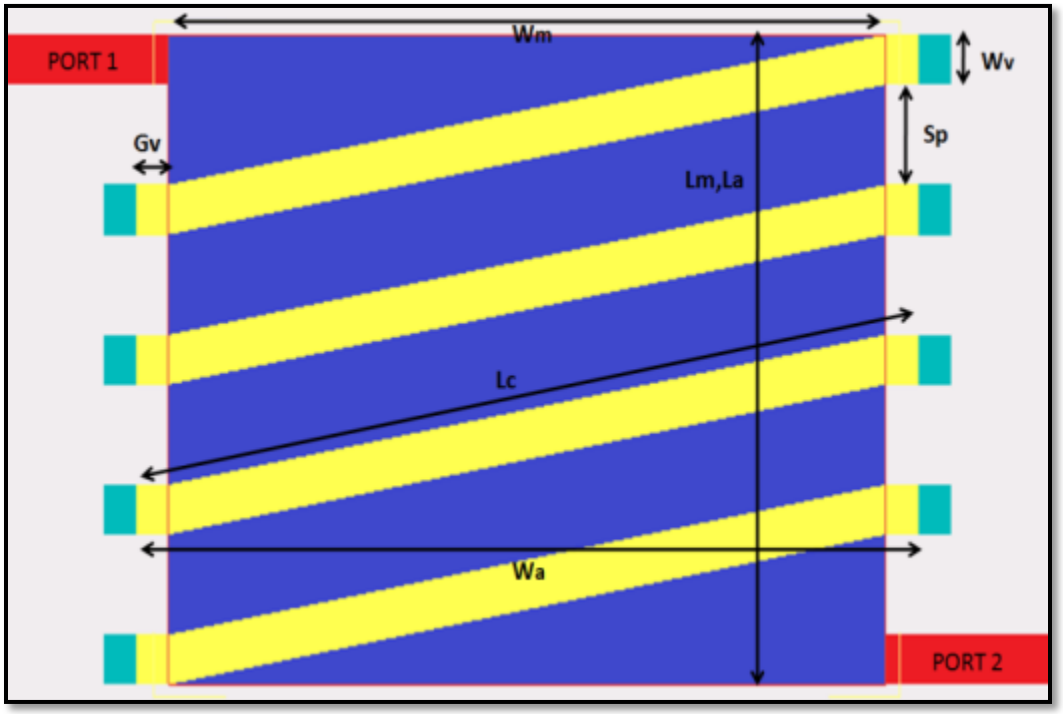

(a)

(b)

Figure 4.1-1: Integrated solenoid inductor with magnetic core: (a) top view and (b) cross-sectional view

The expression for the inductance of the integrated solenoid inductor with air core, L_{AC}, is modified from the Wheeler formula based on the comparison with the experimental and simulation results [9] and can be written as:

$$L_{AC} = L_{Winding} + L_{Parasitic} \tag{4.1}$$

$$\text{where } L_{Winding} = \frac{10\pi\mu_o a^2 N^2}{9a+10L_a}, \tag{4.2}$$

$$a = \sqrt{\frac{(W_a + 2S_v)(T_a + 2T_c)}{\pi}} \tag{4.3}$$

The winding inductance $L_{Winding}$ depends on the cross section area of the core, which includes the vias and the coils surrounding the air core. The parasitic inductance $L_{Parasitic}$ represents effects due to parasitics at the ports. Upon the introduction of a magnetic core, the inductance should be enhanced by the relative permeability (μ_r) of the core [26].

$$L_{Solenoid} = \frac{\mu_o \mu_r N^2 W_m T_m}{L_m} \tag{4.4}$$

This equation proves to be an over estimate of the actual inductance achieved as it does not take into consideration the effect of the demagnetization field [9]. This reduces the relative permeability as a higher magnetizing field is required to overcome the demagnetizing field to obtain the same magnetization. Lee et al. [9] suggests an expression for the inductor with a magnetic core as

$$L_{MI} = L_{AC} + \Delta L \tag{4.5}$$

$$\text{where } \Delta L = \frac{\mu_o \mu_r N^2 W_m T_m}{L_m [1 + N_d (\mu_r - 1)]} \tag{4.6}$$

ΔL represents the increase in inductance due to the magnetic contribution and N_d is the demagnetizing factor.

At lower frequencies, the expression for series resistance [9] is expressed as a sum of the resistances of the coil over the air core, the connection to the via and the via itself.

$$R_{AC} = 2N\rho\left[\frac{T_c}{W_m T_c} + \frac{(S_v + 2G_v)}{W_v T_c} + \frac{T_c + T_a}{S_v{}^2}\right] \tag{4.7}$$

where ρ is the electrical resistivity of the coil material. At higher frequencies the current tends to flow on the surface of the conductor making the effective current carrying cross sectional area smaller than that at lower frequencies. This effect is the skin effect [1] and the depth at which the current flows is the skin depth. As a result of this effect we observe an increase in resistance and lower skin depth at higher frequencies. The skin effect is not prominent at lower frequencies but can increase the resistance to a large amount at higher frequencies. An estimate for the series resistance [1] incorporating the skin depth is shown below.

$$R = \frac{L}{w\sigma\delta\left(1 - e^{-\frac{t}{\delta}}\right)} \tag{4.8}$$

where L is the length, w is the width, t is thickness, σ is the conductivity and δ is the skin depth of the coil. The skin depth [1] is a function of the frequency and is written as

$$\delta = \sqrt{\frac{2}{\omega\sigma\mu_0}} \tag{4.9}$$

where ω is the angular frequency and μ_0 is the permeability of free space. Thus the equation (4.7) may be re-written as

$$R_{AC} = 2N\rho\left[\frac{\frac{T_c}{W_m T_c} + \frac{(S_v + 2G_v)}{W_v T_c} + \frac{T_c + T_a}{S_v{}^2}}{\delta\left(1 - e^{-\frac{T_c}{\delta}}\right)}\right] \tag{4.10}$$

Another important parameter that decides the usefulness of an inductor is the quality factor (Q). It is defined as the ratio of the energy stored to the energy dissipated in

the circuit. The energy is stored in the inductive and capacitive elements in terms of magnetic and electric field and the energy is dissipated by the resistances in the circuit in the form of heat. The quality factor [1] is frequency dependent and can be written as

$$Q = \frac{\omega * \text{Maximum energy stored}}{\text{Power Loss}}, \tag{4.11}$$

$$Q = \frac{\omega}{\Delta\omega} = \frac{f_r}{\Delta f} \tag{4.12}$$

where $\omega=2\pi f_r$ is the angular frequency and f_r is the resonant frequency and Δf is the bandwidth of the circuit. The equations (4.1) through (4.12) provide a rough estimate to the values of inductance, series resistance and quality factor. The practical values as we see in the simulation results ahead vary quite a bit from the theoretical values.

The finite element method (FEM) simulations for the proposed inductor structure have been carried out for various metallic windings made of aluminum, gold, copper, and silver. The structure has been simulated in the frequency range of 1 MHz to 15 GHz by varying the parameters such as the thickness of the metal windings, number of turns/spacing between turns and thickness of the core while maintaining a fixed area of the structure to 1-1.2 mm^2. The simulation results are displayed and discussed in the following sections.

4.2 Air core vs. Magnetic core

A solenoid with an air core (μ_r=1) of 80 µm thickness (T_a), 5 turns (N) each with 10 µm thickness (T_c) and 20 µm wide (W_v) separated by 40 µm spacing (S_p) was simulated and compared with an identical structure encasing a magnetic core of 70 µm thick (T_m). The relative permeabilities (μ_r) of the magnetic core used for the simulation are 120 and 1500. High permeability magnetic cores were chosen to observe the increase in the value of the inductance as predicted from equations (4.5) and (4.6). The simulations have been run for four metals aluminum, gold, copper and silver with the conductivities of each of these metals being $3.7x10^7$ S/m, $4.52x10^7$ S/m, $5.96x10^7$ S/m and $6.3x10^7$ S/m respectively. The most common metals used as metallization layers in industry today are aluminum and copper as they are easily available, cost effective and reliable. We observe in our simulations that silver and copper prove to be the top two metals that show promising results in the frequency range of 5 GHz to 15 GHz because of their higher conductivity.

4.2.1 Inductance

Figure 4.2-1 shows the inductance plotted over a range of frequencies for the various core permeabilities. The relative permeability of the magnetic core material used is 120 and 1500. Figure 4.2-1 (a) is the inductance plot of the air core over the frequency range 1 MHz - 5 GHz. This plot displays a lot of random incomprehensible data for all the metals. The inductance here seems to oscillate between being positive and negative for very short ranges of frequency. Also there seems to be a fall in the inductance value between the frequencies 4.7 GHz and 5.525 GHz that occurs in the graphs of all the three structures. We observe that this random variation disappears upon significantly increasing the number of turns of the coil as seen in Figure 4.2-1 (e), which represents a magnetic core coil with 10 turns and a permeability of 120. We observe that the random variations are now limited between 1 MHz to 2.5 GHz and continue to reduce with increasing number of turns as we see in the later sections. It is difficult to say exactly why there is so much noise at lower frequencies for fewer turns. One reason could be that the parasitics are more pronounced for a smaller structure at lower frequencies than at higher frequencies, causing this behavior. As this region does not provide any useful data, we plot the region where the inductance remains more or less positive with frequency for all the following graphs.

Figure 4.2-1 (b) displays the inductance of the air core between the frequency range of 5 to 15 GHz. The graph shows the behavior of the four metals aluminum (red), gold (blue), silver (green), and copper (pink). The curves for gold and aluminum are under the curve for silver and are not visible for the given axes limits. For the frequency range of 5-10 GHz, all the four metals display almost identical inductance values. The on-chip inductor model shown in Figure 3.2-1 indicates that the circuit exhibits a parallel self-resonance. Hence, the inductance increases before the resonance value and becomes capacitive (negative inductance) after the resonance value. The peak inductance for the air core coil in Figure 4.2-1 (b) for copper is shown to be 104 nH at 13.4 GHz clearly where as the other metals do not show a sharp peak. It shows that copper tends to have a higher inductance compared to the rest of the metals for the air core coil.

Figure 4.2-1 (c) and (d) are the inductance graphs for the solenoid with a magnetic core. All four metals here exhibit similar pattern and have their parallel self-resonance around 13.6 GHz. The inductance improvement observed with the introduction of a magnetic core is not very large compared to an air core as one would expect from the equations (4.5) and (4.6), but we notice a more stable set of inductance values before the 5.25 GHz. Also the peak of the value of inductance for all the four metals before resonance in Figure 4.2-1 (c) and (d) is 107 nH and 108.5 nH, which is a small increase (3-4 nH) from the air core coil. For frequencies higher than 5 GHz, silver shows the highest inductance amongst other metals.

According to the equations, the magnetic core inductor must have a much higher value of inductance compared to the air core inductor. Below is an estimate of the theoretical values calculated from equation (4.1) and (4.5):

$\mathbf{L_{AC}} = 5.011$ nH

$\mathbf{L_{winding(\,\mu r=120)}} = L_{AC} + \Delta L = 5.011x10^{-9} + 23.15x10^{-9} = 28.16$ nH

$\mathbf{L_{winding(\,\mu r=1500)}} = L_{AC} + \Delta L = 5.011x10^{-9} + 24.23x10^{-9} = 29.24$ nH

As we can see the theoretical values indicate a constant and higher value compared to what we see the graphs. It is difficult to say what parameters are acting against the coil to cause this degraded value and is still being thought upon. As numerous resources [9]-[15], [26] suggest that an increase in inductance is definitely observed for increase in permeability, we experiment with other probable parameter variations keeping μ_r=120 to see the effects on the inductance, resistance and quality factor in the following sections.

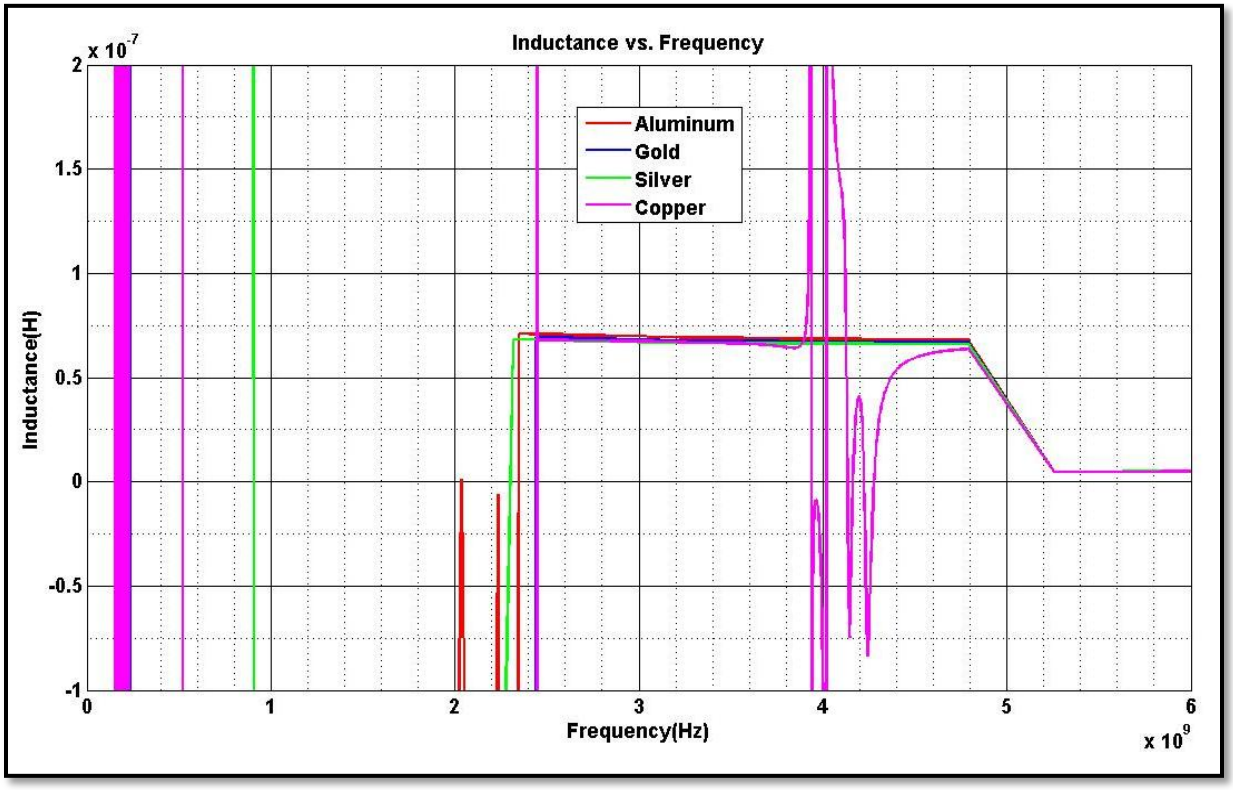

(a)

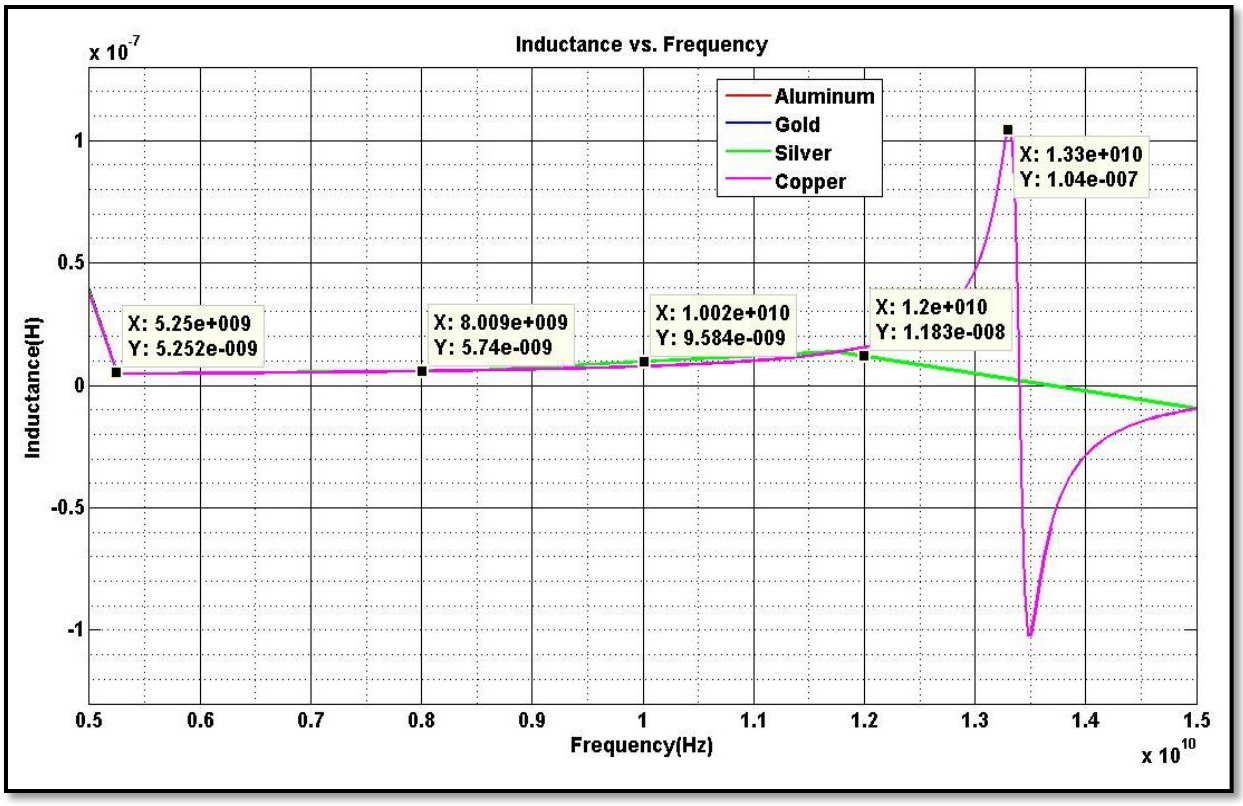
Inductance vs. Frequency
x 10^-7
Aluminum
Gold
Silver
Copper
X: 1.33e+010
Y: 1.04e-007
X: 5.25e+009
Y: 5.252e-009
X: 8.009e+009
Y: 5.74e-009
X: 1.002e+010
Y: 9.584e-009
X: 1.2e+010
Y: 1.183e-008
Inductance(H)
Frequency(Hz)
x 10^10

(b)

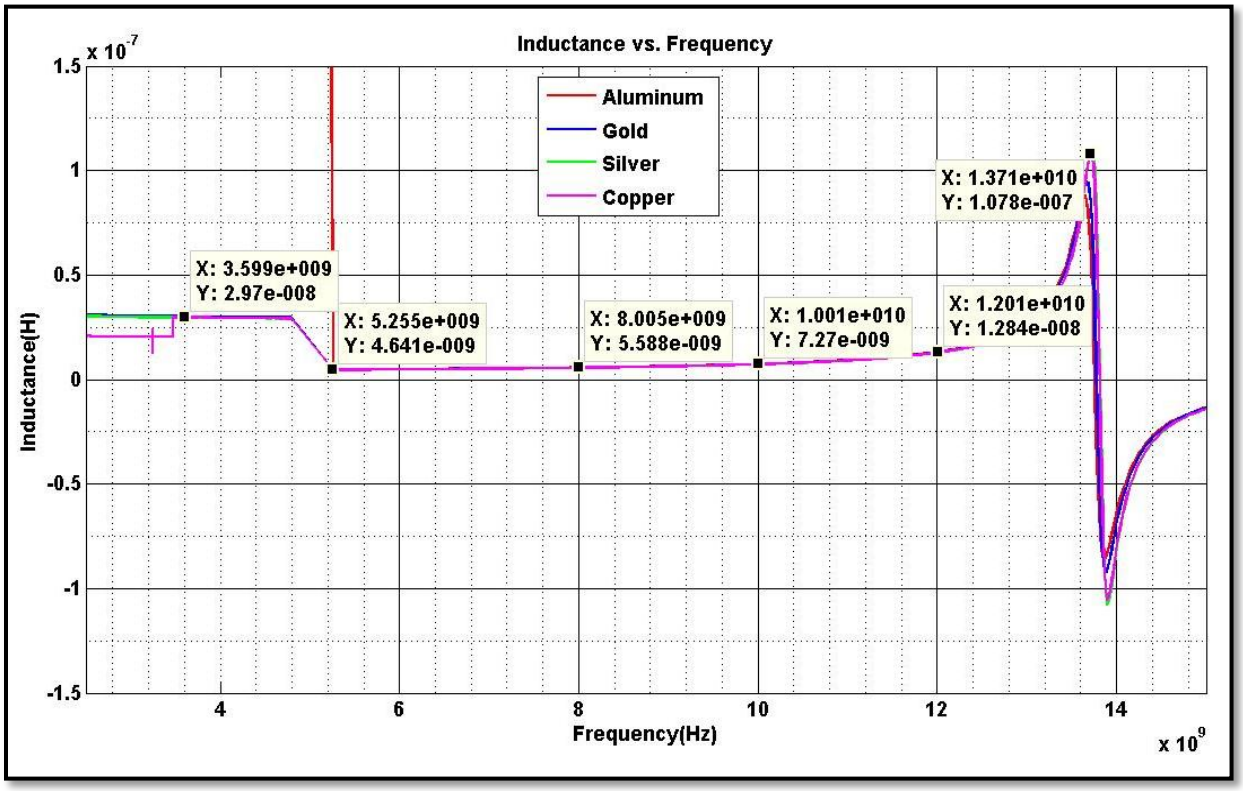
Inductance vs. Frequency
x 10^-7
Aluminum
Gold
Silver
Copper
X: 1.371e+010
Y: 1.078e-007
X: 3.599e+009
Y: 2.97e-008
X: 5.255e+009
Y: 4.641e-009
X: 8.005e+009
Y: 5.588e-009
X: 1.001e+010
Y: 7.27e-009
X: 1.201e+010
Y: 1.284e-008
Inductance(H)
Frequency(Hz)
x 10^9

(c)

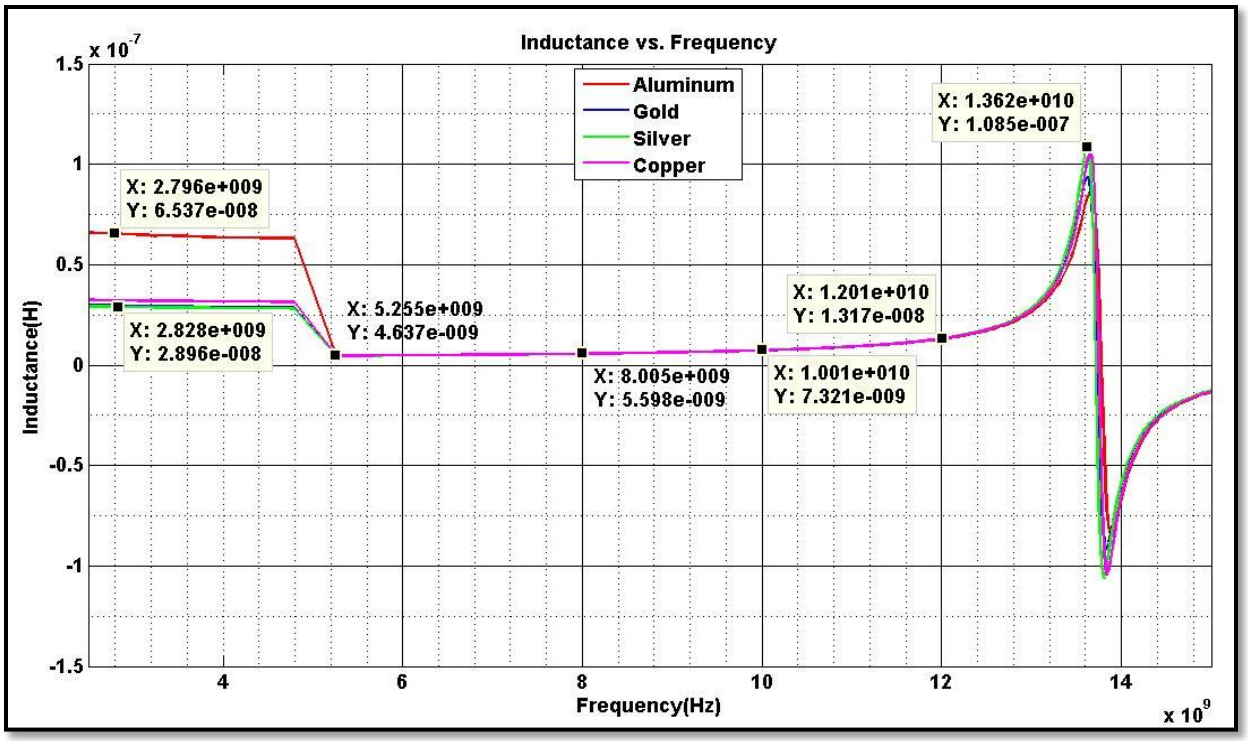

(d)

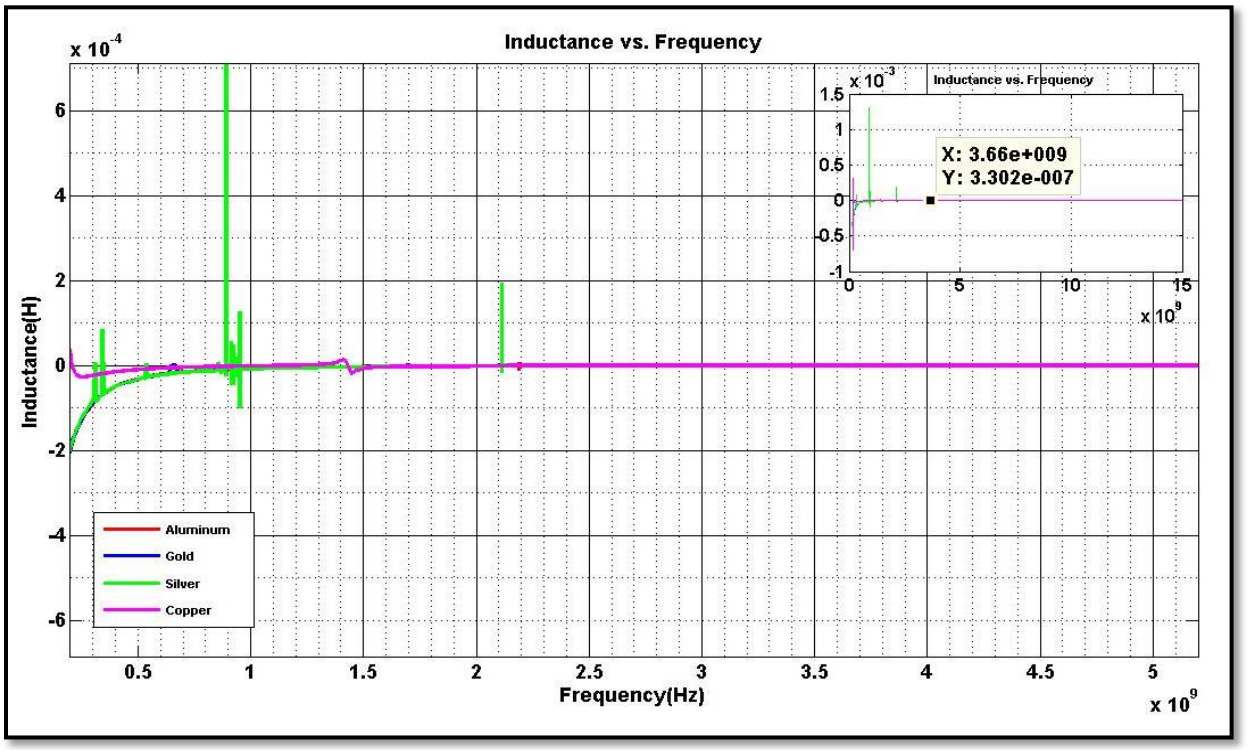

(e)

Figure 4.2-1: Inductance of (a) air core inductor with 5 turns in 0-5 GHz, (b) air core inductor with 5 turns in 5-15 GHz, (c) magnetic core inductor with 5 turns and μ_r=120, (d) magnetic core inductor with 5 turns and μ_r=1500, and (e) magnetic core inductor with 10 turns and μ_r=120 in 0-5 GHz

4.2.2 Resistance

Figure 4.2-2 shows the resistance graphs for the different structures. As observed earlier there are a lot of spikes and random variations below 5 GHz and hence the graph has been magnified for the range 5-15 GHz. An inset of the resistance versus frequency is provided for a view of the whole distribution. The y-axis on the inset is a logarithmic plot of the resistance. We observe that on the whole the resistance shows an increasing value from 1 MHz-15 GHz and this is due to the occurrence of skin effect. At parallel self-resonance, the reactances (X_L, X_C) cancel each other out and the circuit becomes purely resistive. For the air core, the maximum resistance at the resonant frequency of the circuit is as high as 17 kΩ for copper whereas the other three metals remain in the range of 3 Ω to 53 Ω for the frequency 5-15 GHz. The reason why only copper behaves in the manner it does is not known.

With the magnetic core, all four metals exhibit similar parallel resonance and resistance peaks as shown in Figure 4.2-2 (b) and (c). As relative permeability is a measure of how well a circuit can accommodate magnetic fields and provide least resistance, we can expect a drop in the resistances for increasing μ_r. The resistance for μ_r=120 has reduced by almost 3 Ω and 30 Ω at 10 GHz and 12 GHz but the peak resistance is almost 1 kΩ more than the air core. The peak for μ_r=1500 has reduced to almost 17.6 kΩ from 18.4 kΩ. It is observed that the resistances begin to get more stable at lower frequencies with increase in relative permeability. At increasing frequencies, the resistance for μ_r=1500 increases compared to μ_r=120 because the magnetic contribution to the resistance is more significant than the coil contribution [9].

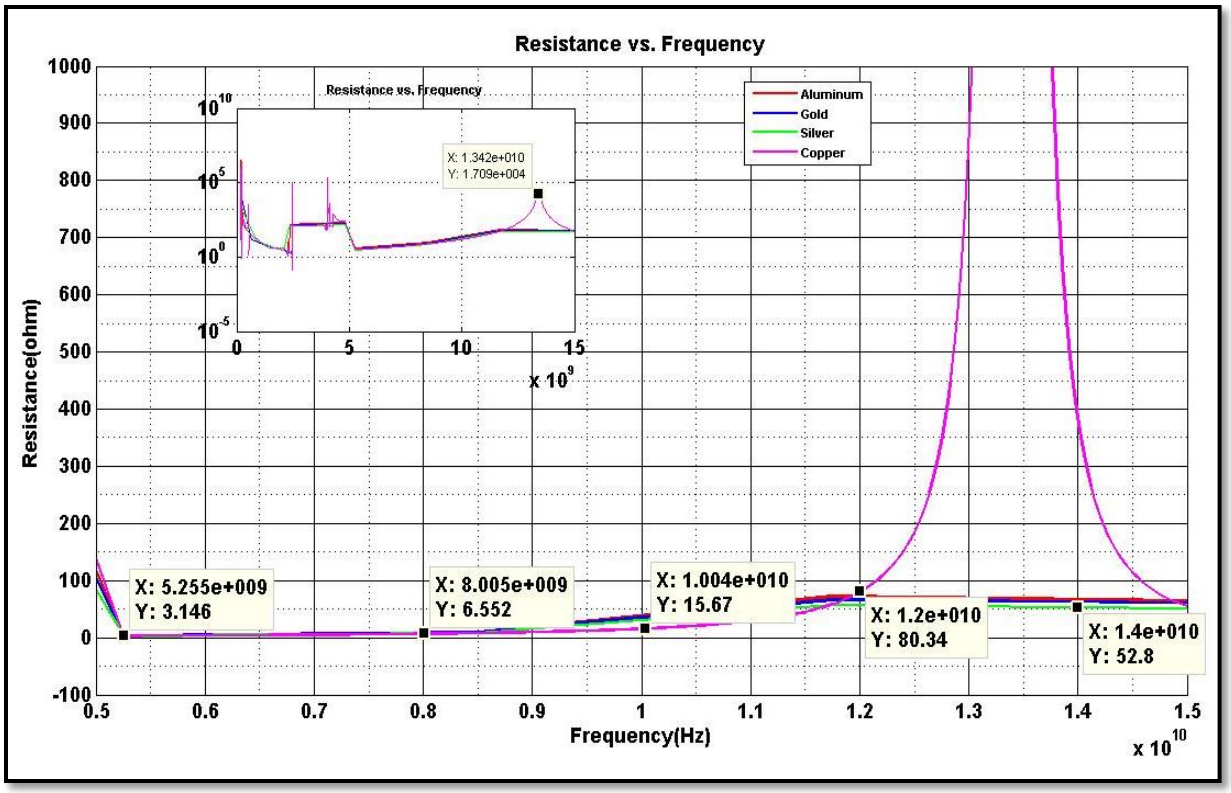
Resistance vs. Frequency
Resistance vs. Frequency
Aluminum
Gold
Silver
Copper
X: 1.342e+010
Y: 1.709e+004
x 10^9
Resistance(ohm)
Frequency(Hz)
x 10^10
X: 5.255e+009
Y: 3.146
X: 8.005e+009
Y: 6.552
X: 1.004e+010
Y: 15.67
X: 1.2e+010
Y: 80.34
X: 1.4e+010
Y: 52.8

(a)

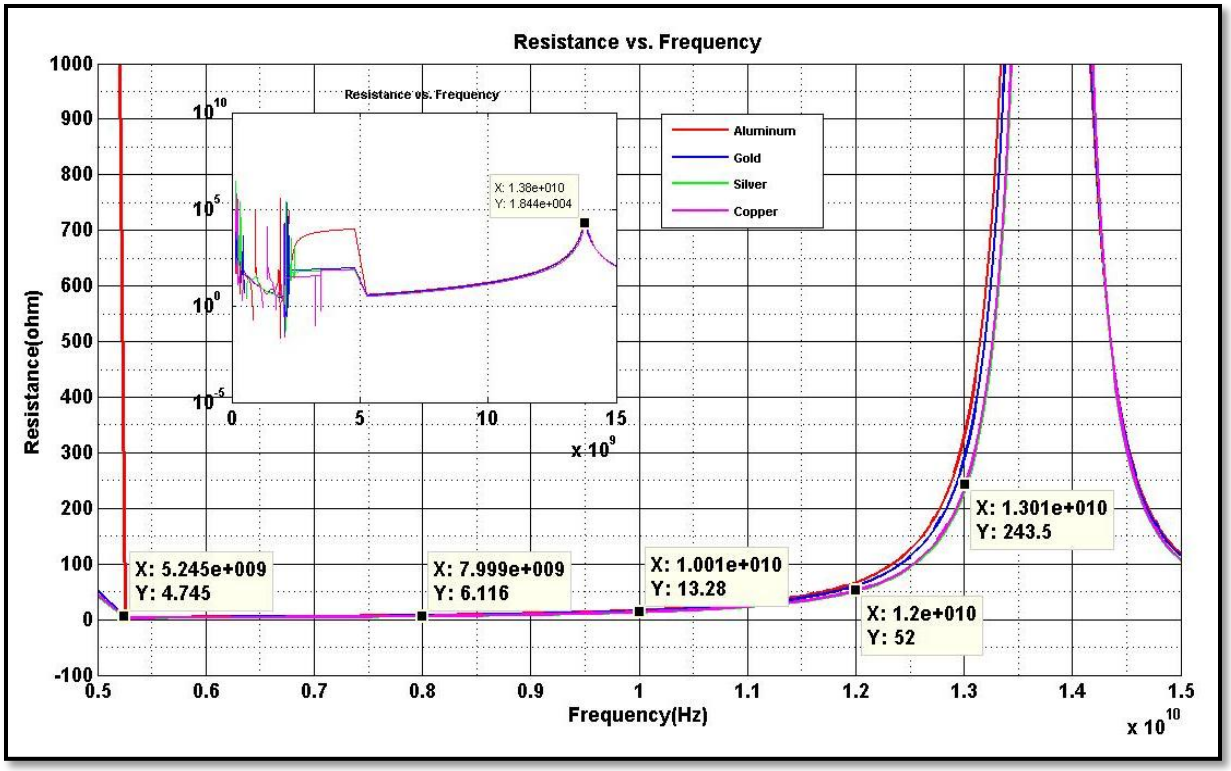
Resistance vs. Frequency
Resistance vs. Frequency
Aluminum
Gold
Silver
Copper
X: 1.38e+010
Y: 1.844e+004
x 10^9
Resistance(ohm)
Frequency(Hz)
x 10^10
X: 5.245e+009
Y: 4.745
X: 7.999e+009
Y: 6.116
X: 1.001e+010
Y: 13.28
X: 1.2e+010
Y: 52
X: 1.301e+010
Y: 243.5

(b)

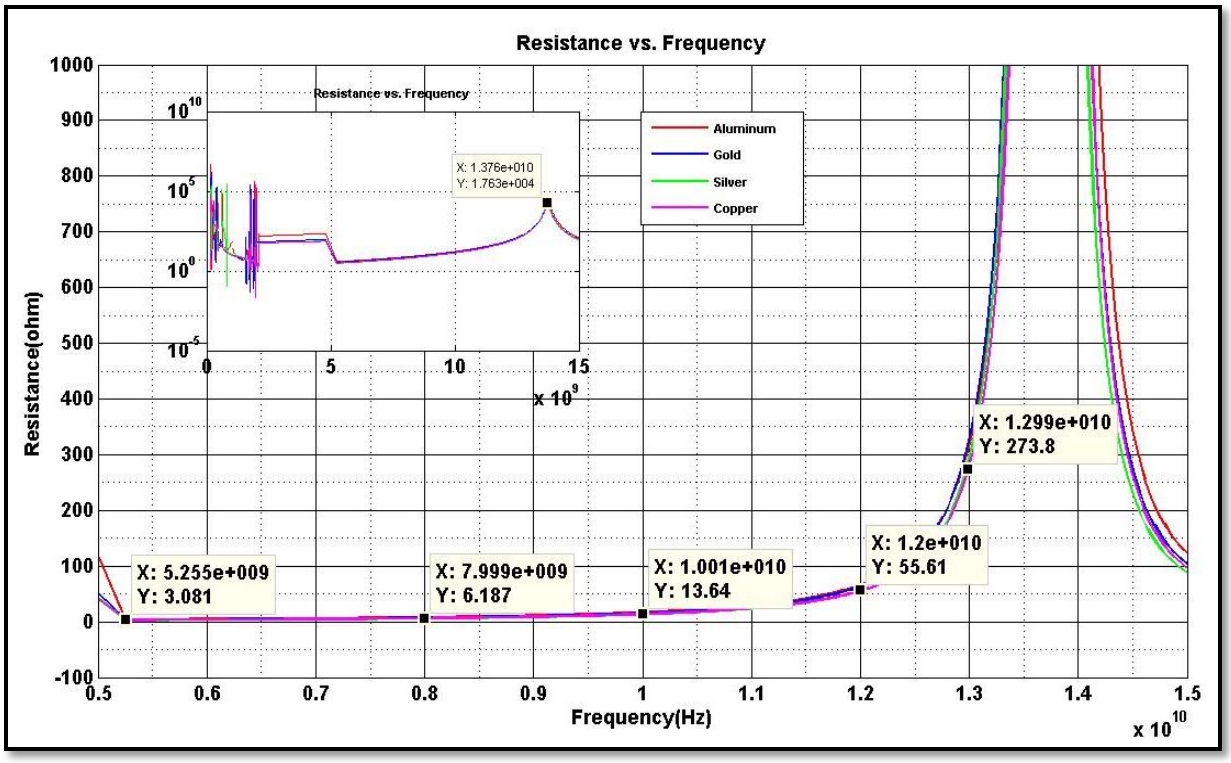

(c)

Figure 4.2-2: Resistance of (a) air core inductor (b) magnetic core inductor with μ_r=120, and (c) magnetic core inductor with μ_r=1500

4.2.3 Quality Factor

Figure 4.2-3 shows the quality factor for the three structures. As seen in the inset of Figure 4.2-3 (a), a logarithmic graph displays the quality factor versus frequency. There is a gap in the inset graph between the frequencies of 1-4 GHz due to negative values of the quality factor. Also seen are the spikes and random data prior to 5 GHz. Hence a magnified section between 5-15 GHz has been provided for better clarity.

The peak value of Q occurs for silver for all the three graphs at approximately 5.26 GHz and begins to lower with increasing frequency. All the metals are seen to exhibit the same kind of behavior with different peaks. The quality factor for the magnetic core in Figure 4.2-3 (b) and (c) have a smaller slope compared to the air core and reduce more slowly in value. The addition of the magnetic core showed an increase in inductance values and hence a better quality factor can be observed. Also with the increase in relative permeability, the quality factor below 5 GHz shows more stable values. The gradual drop in quality factor for higher frequencies is due to the increase in power dissipation. The quality factor has a value zero at the parallel resonant frequency.

The increase in power dissipation and hence the deterioration of the quality factor can be attributed to the various losses in the inductor and the substrate:

- The Ohmic losses due to the resistance of the coils and vias.
- Losses due to the skin effect that increases the resistance at higher frequencies.
- Proximity effect: This is another form of increase in resistance at higher frequencies due to the proximity of windings carrying magnetic fields. This induces eddy currents in the coils, which again run on the surface of the coils at high frequency due to skin effect.
- The losses in the core due to eddy currents induced by the magnetic field. This loss increases with size of the core.
- The losses in the substrate due its resistance and eddy currents.

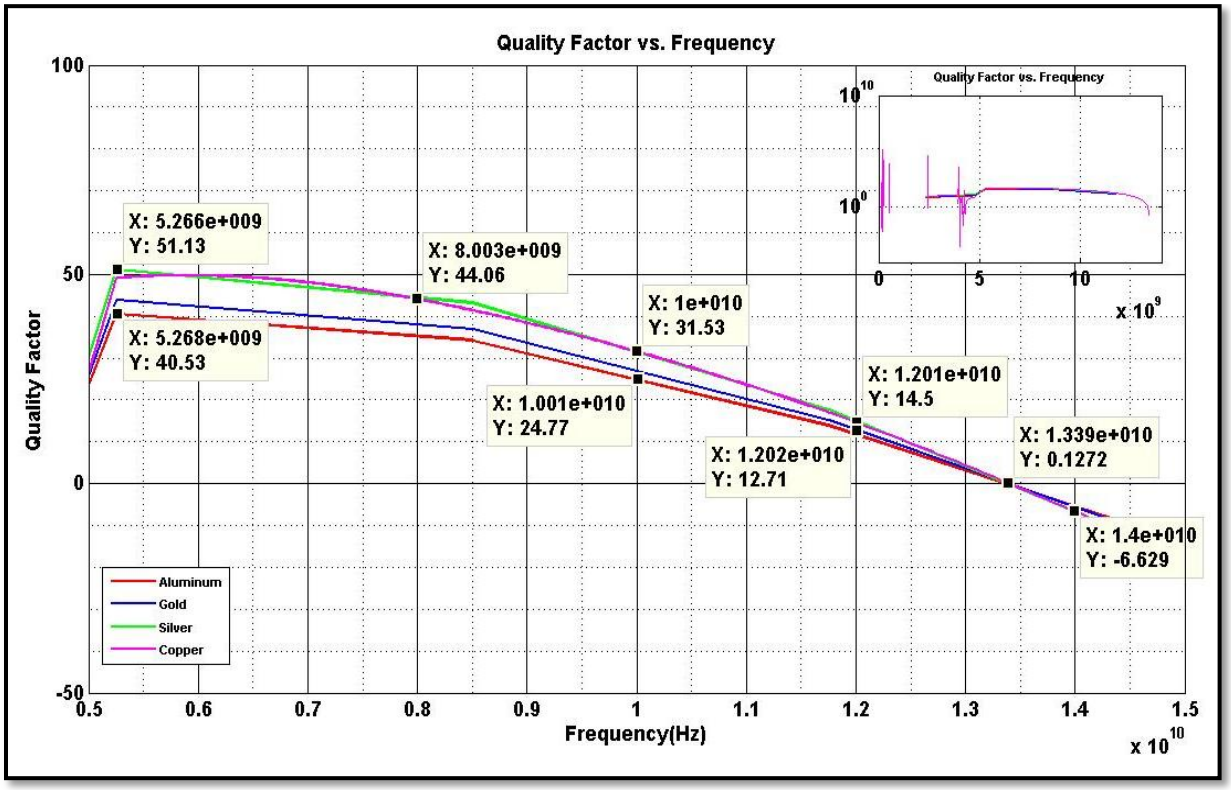

(a)

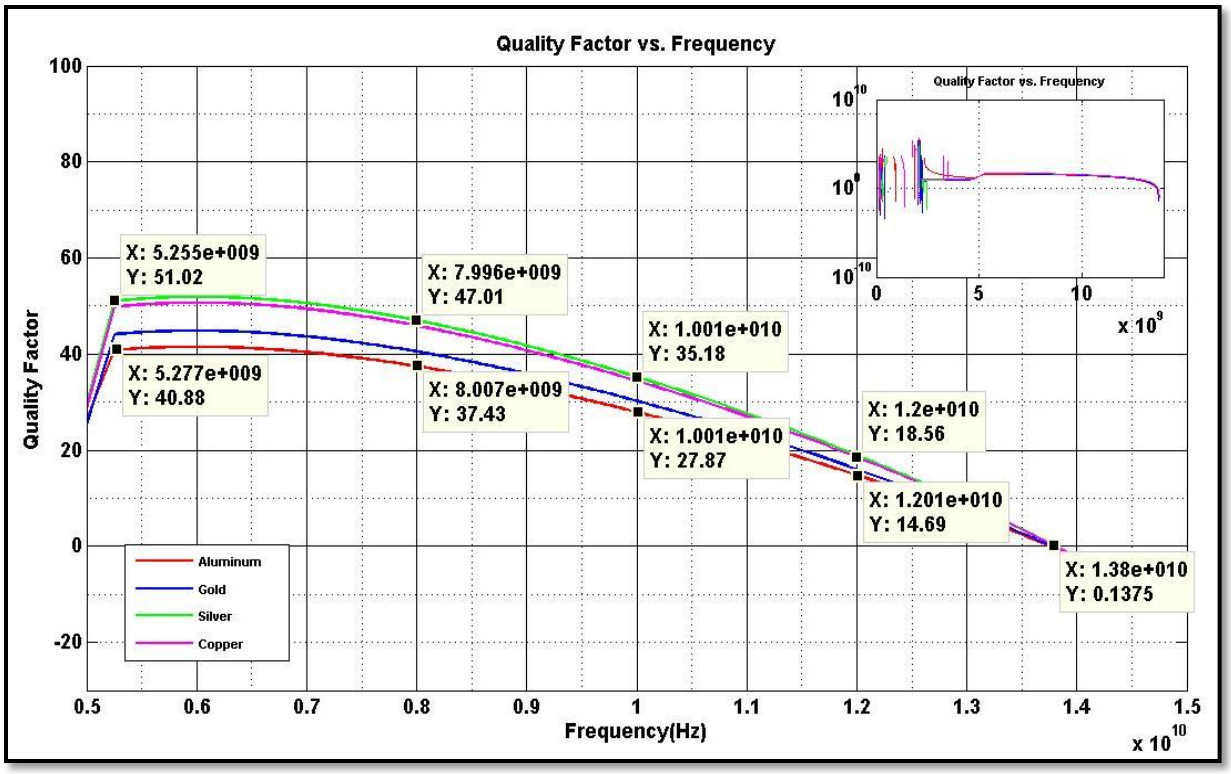

(b)

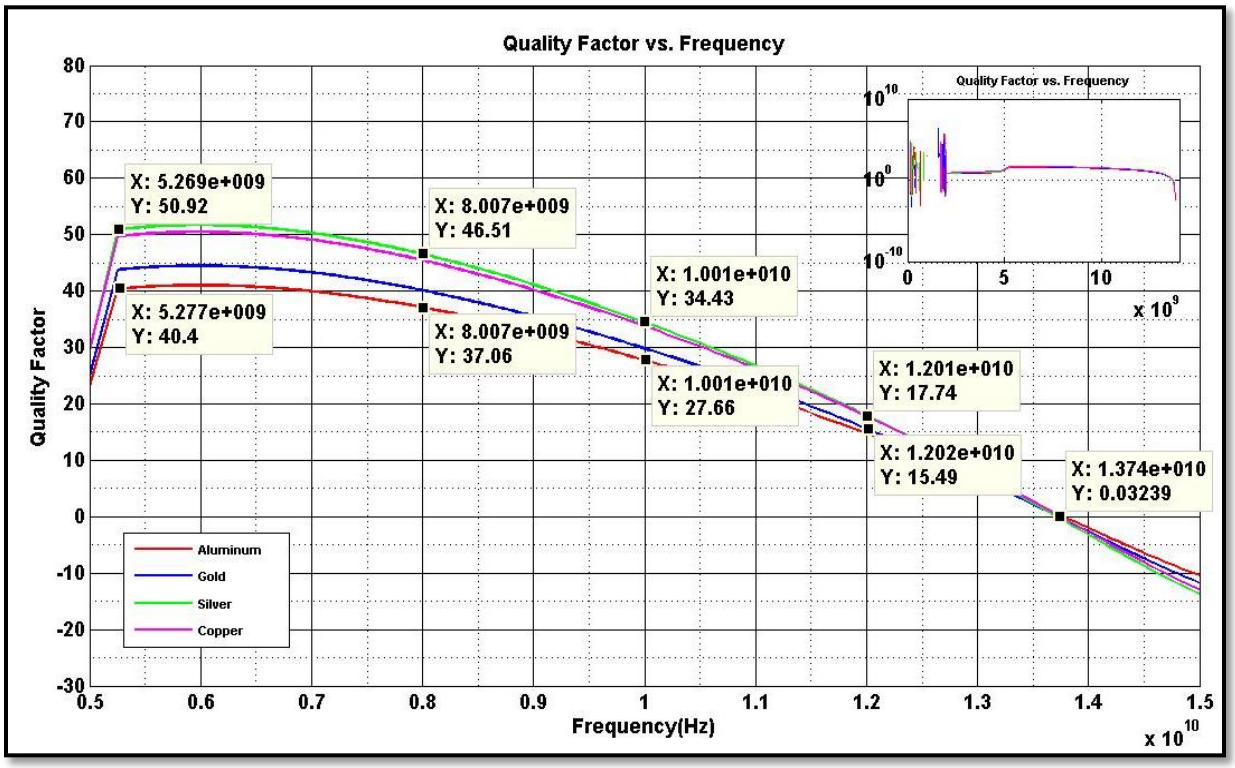

(c)

Figure 4.2-3: Quality Factor of (a) air core inductor (b) magnetic core inductor with μ_r=120, and (c) magnetic core inductor with μ_r=1500

4.3 Increase in insulator thickness

The substrate is one of the major reasons for power loss. The conductive nature of the silicon substrate aids the development of eddy currents from magnetic fields and causes power loss. To lower the losses and improve the quality factor, we can introduce an insulating layer of silicon dioxide between the lower metal and the substrate. The silicon dioxide insulates the metal from the substrate and hence reduces the formation of eddy currents in the substrate. The thicker the insulation layer, the lower are the substrate losses. However we are limited to use a maximum of 5 µm thickness as supported by VT MT SPL. Below are the simulation results of the structure with and without the increase in the thickness of the oxide layer. The structure under consideration is an 18 turn coil with 72 µm width and 5 µm thick encasing a magnetic core of 1 µm thick and μ_r=120.

4.3.1 Inductance

The inductance of the coils with and without the increase in oxide layer thickness below the metal-1 is shown in Figure 4.3-1 below. It is observed all the metals follow the same pattern of the curve. The inductance for aluminum is seen to be the highest while silver displays the least inductance for both structures. The curve for silver in Figure 4.3-1 (b) is hidden below the curve for copper. The enhanced silicon dioxide structure displays an increase of nearly 0.2 nH compared to that of the non-enhanced layer of silicon dioxide. The inductance continues to increase and would reach its peak close to the resonance frequency, which is beyond the limit of the given graph. We also observe that the number of turns and hence the area used in this structure is greater than that of the structure used in Section 3.2, which eliminates any noise-like pattern below 5 GHz.

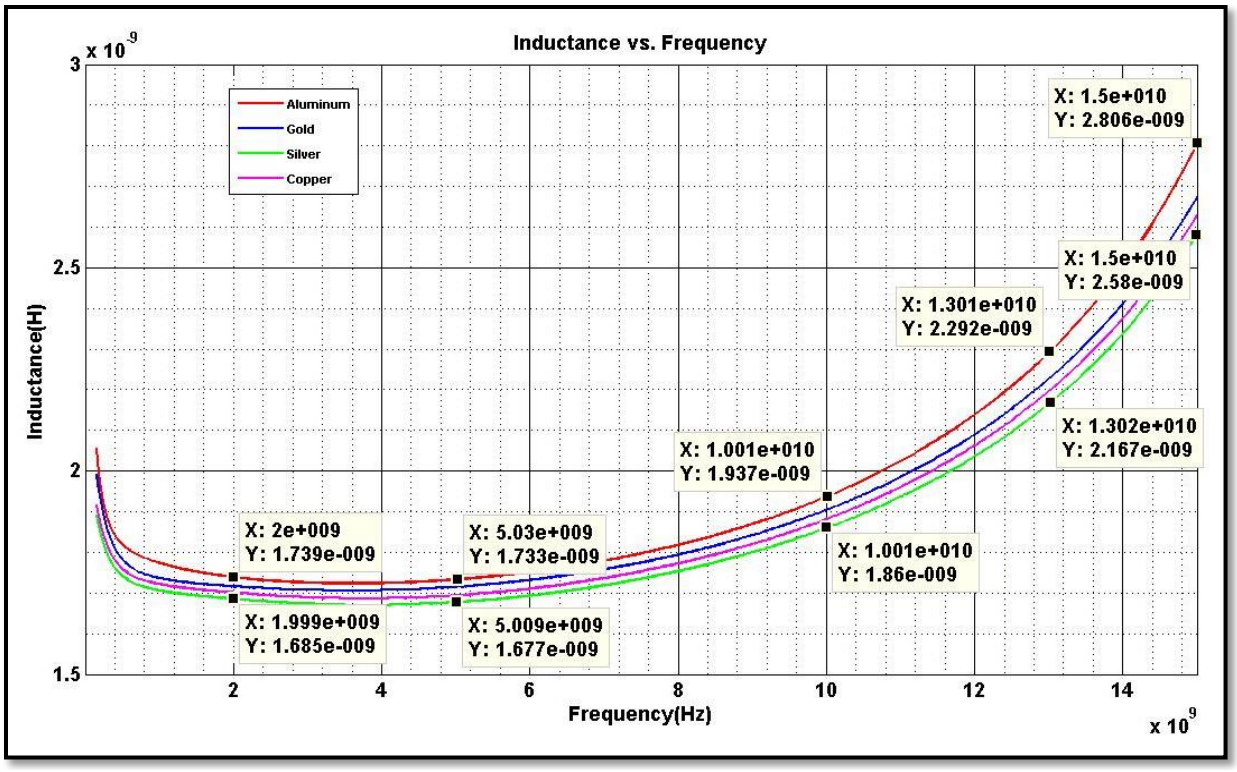

(a)

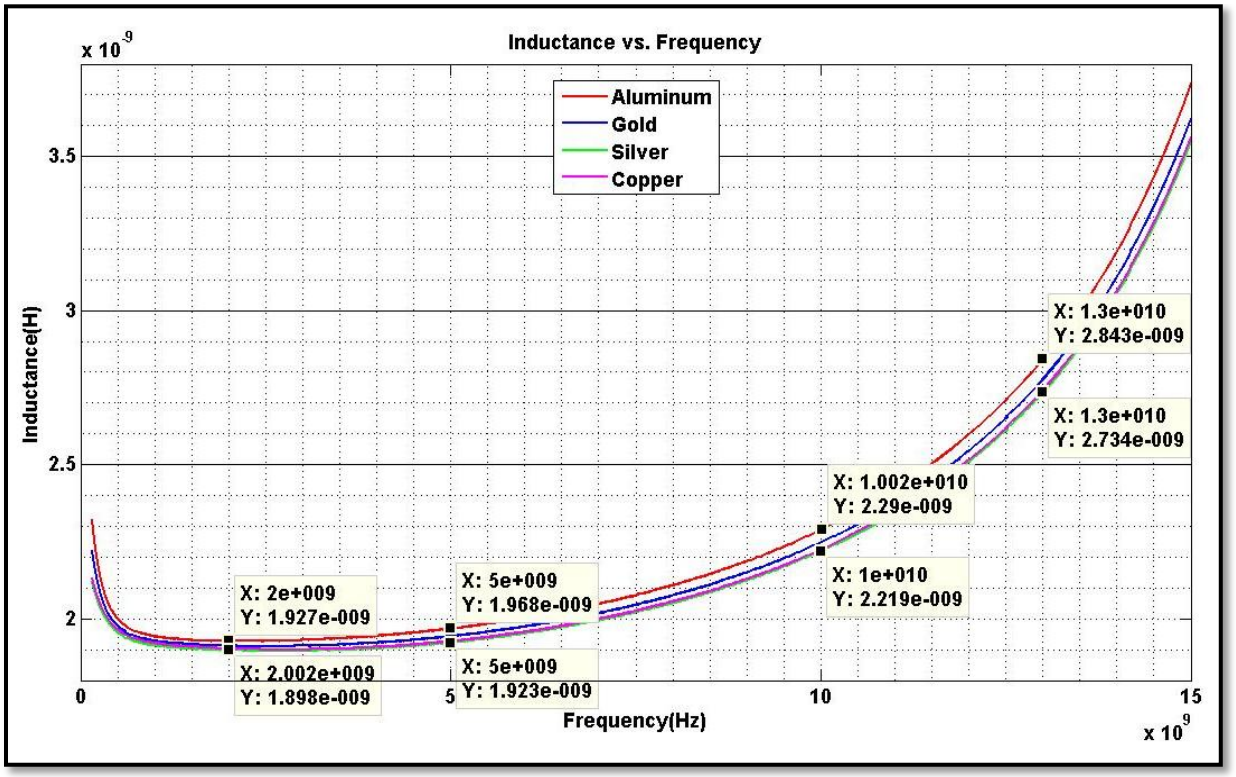

(b)

Figure 4.3-1: The inductance of (a) metal-1 touching substrate and (b) metal-1 separated by 5 μm thick SiO_2 from substrate

4.3.2 Resistance

Figure 4.3-2 (a) and (b) show the resistance of the inductor structure. All the four metals follow the same pattern of the curve but their slopes are different. The resistance of the four metals at lower frequencies is not very different from each other but show unique values at higher frequencies. Aluminum again takes the lead in both structures for higher resistance curve and silver for the least, which is justified by the fact that aluminum has the lowest conductivity among the four metals. The resistance is seen to be increasing for all metals except for aluminum and this increase can be attributed to the new resistance offered by the insulator. The resistance curve for the enhanced insulator thickness rises more slowly for aluminum, lowering the resistance at a few places.

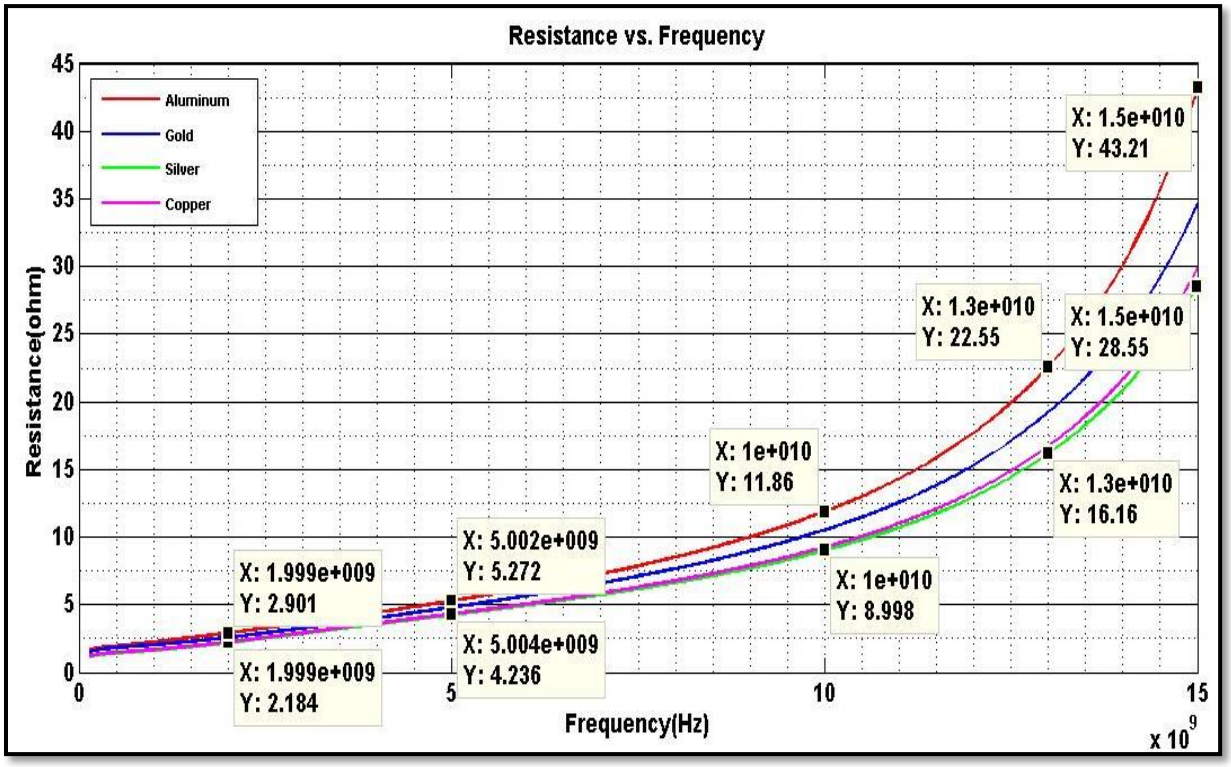

(a)

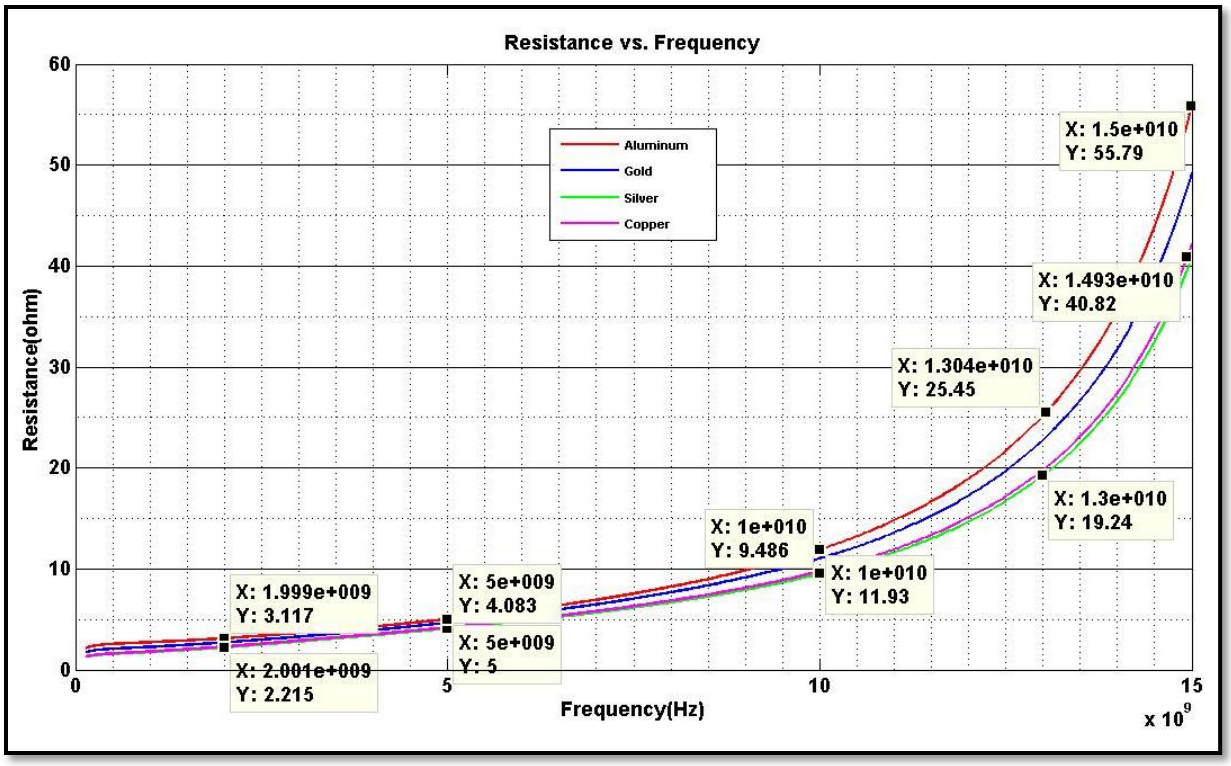

(b)

Figure 4.3-2: The resistance of (a) metal-1 touching substrate and (b) metal-1 separated by 5 µm thick SiO_2 from substrate

4.3.3 Quality Factor

Figure 4.3-3 (a) and (b) show the quality factor of the inductor structure. The peak quality factor is seen to be 13.3 for silver at 8 GHz while aluminum displays a peak of 10 at 7.1 GHz. We expect to see an increase in the quality factor with the enhanced structure containing silicon dioxide layer due to the reduction in losses. The quality factor observed in Figure 4.3-3 (b) shows a good improvement with the increase in the insulation oxide thickness. Silver again dominates with a peak quality factor of 15.5 at 7.3 GHz while aluminum has a peak of 13 at 7.1 GHz. The curves for the enhanced structure with silicon dioxide layers have higher peaks and are narrower. This can be seen from equation (4.12) that a higher quality factor implies a lower bandwidth. The parasitic capacitance C_{ox} also reduces with the increase in the silicon dioxide thickness between the metal layer and the substrate. The resistive losses are more contained to the substrate and do not affect the main inductor structure as much.

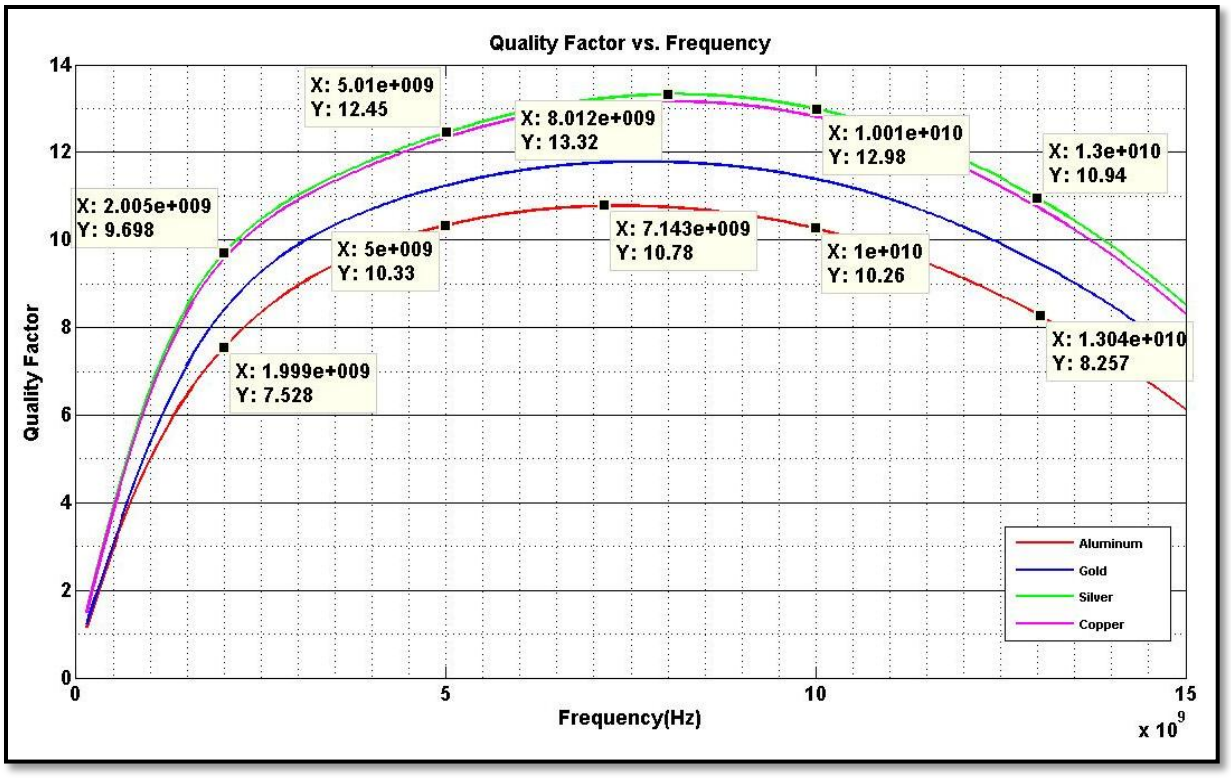

(a)

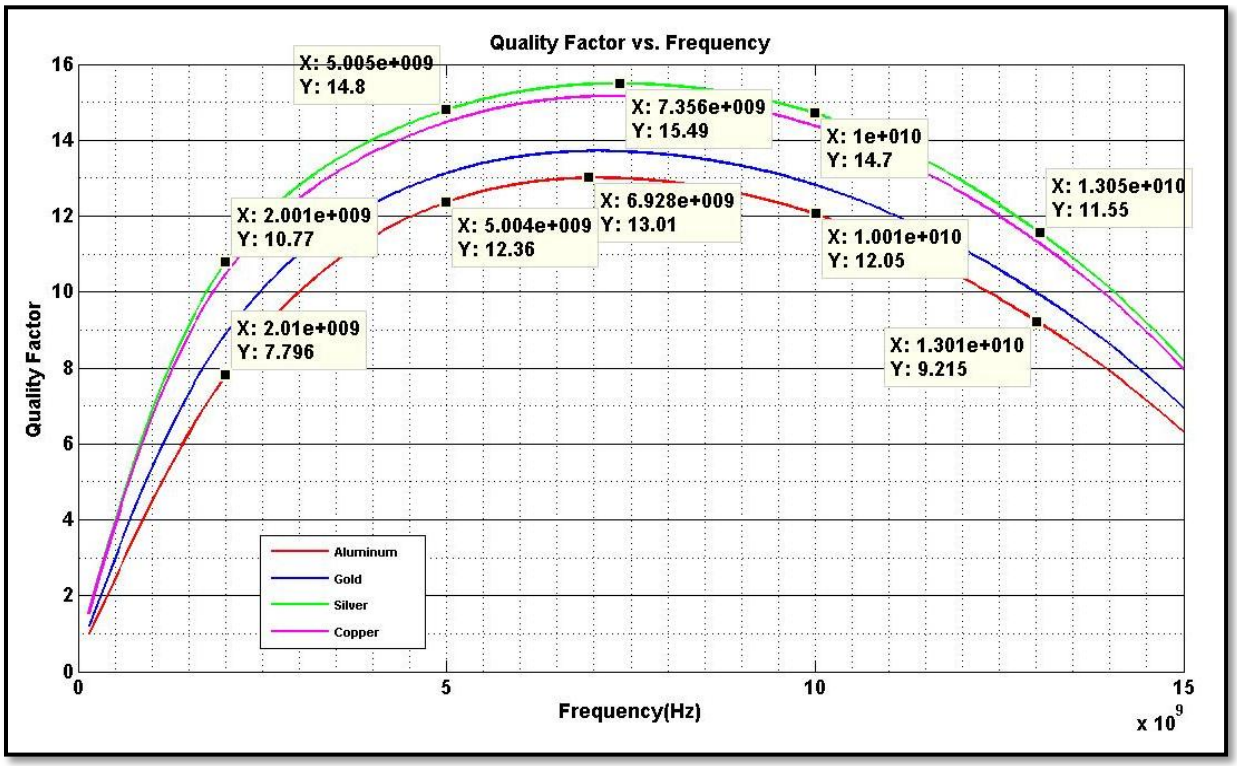

(b)

Figure 4.3-3: The quality factor of (a) metal-1 touching substrate and (b) metal-1 separated by 5 µm thick SiO_2 from substrate

4.4 Effect of variable spacing between turns

For a fixed area, if the number of turns of the coil are increased then according to equation (4.6) we can expect an increase in the value of the inductance but this also increases the parasitic capacitances due to smaller spacing between turns. Thus to observe the effects of variable spacing, an inductor with a metallic winding of 5 µm thick and 20 µm wide with a magnetic core of 70 µm thick and μ_r=120 was simulated and the results are shown below. All other parameters apart from the spacing and number of turns are kept constant.

4.4.1 Inductance

Figure 4.4-1 shows the inductance of the coil with increase in spacing. All four metals follow the same behavior for a given structure but have different peak inductance values. Of the four metals, silver again stands out with the highest inductance values. Figure 4.4-1 (a) displays the inductance for 35 turns with a spacing of 30 µm. An inset shows the plot of the entire range of the inductance versus frequency. The maximum inductance is 725 nH at 3.2 GHz. The parasitic capacitances such as the oxide capacitance, coupling capacitance between turns and turn to core, and the fringing capacitance all resonate with the series inductance forming a parallel resonant circuit. The effect of capacitance between the turns, and from turns to core is maximized with increasing number of turns for a given area.

It is observed that for the given configuration, the inductance tends to reduce with increase in spacing. This can be attributed to the following reasons:

- Lower number of turns from equation (4.6) implies a lower inductance value,
- The magnetic coupling between turns reduces with increase in spacing and hence the inductance reduces.

Therefore we observe a drop in the inductance values for 40 µm and 60 µm spacing. As a consequence of increased spacing, the inductance drops, the parasitic coupling capacitance reduces and the self resonant frequency increases. The self resonant frequency defines the frequency beyond which the inductor circuit behaves like a capacitor. Therefore with the drop in parasitic capacitance, the number of zero crossings (resonant frequency) of the inductance also reduces.

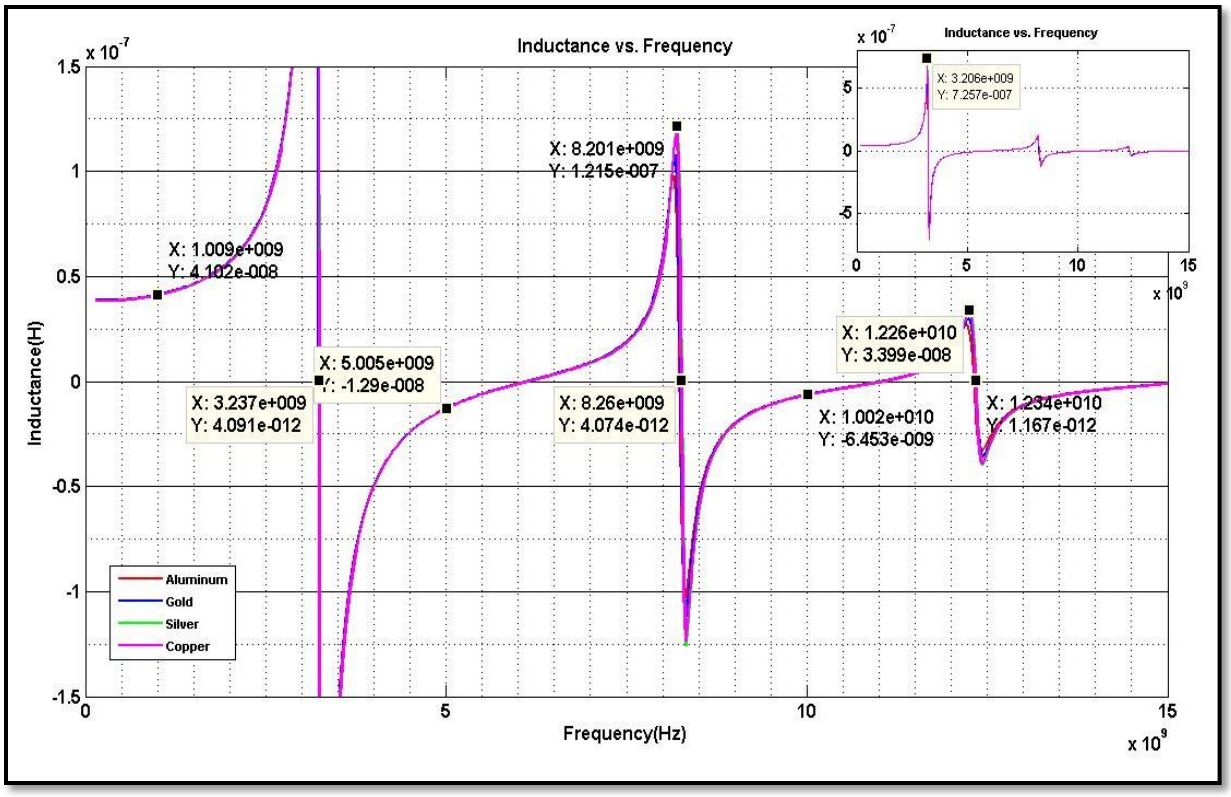
Inductance vs. Frequency
x 10^-7
Inductance(H)
Frequency(Hz)
x 10^9
X: 1.009e+009
Y: 4.102e-008
X: 3.237e+009
Y: 4.091e-012
X: 5.005e+009
Y: -1.29e-008
X: 8.201e+009
Y: 1.215e-007
X: 8.26e+009
Y: 4.074e-012
X: 1.002e+010
Y: -6.453e-009
X: 1.226e+010
Y: 3.399e-008
X: 1.234e+010
Y: 1.167e-012
Aluminum
Gold
Silver
Copper
Inductance vs. Frequency
X: 3.206e+009
Y: 7.257e-007

(a)

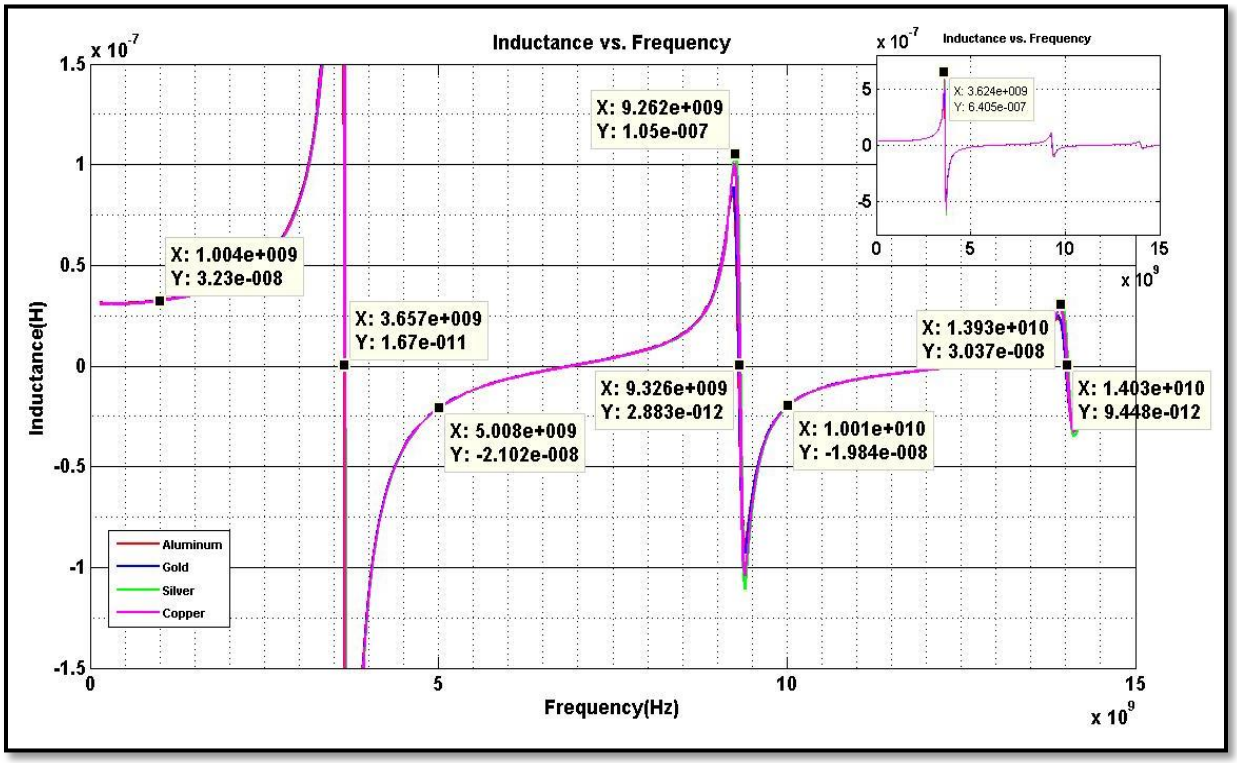
Inductance vs. Frequency
x 10^-7
Inductance(H)
Frequency(Hz)
x 10^9
X: 1.004e+009
Y: 3.23e-008
X: 3.657e+009
Y: 1.67e-011
X: 5.008e+009
Y: -2.102e-008
X: 9.262e+009
Y: 1.05e-007
X: 9.326e+009
Y: 2.883e-012
X: 1.001e+010
Y: -1.984e-008
X: 1.393e+010
Y: 3.037e-008
X: 1.403e+010
Y: 9.448e-012
Aluminum
Gold
Silver
Copper
Inductance vs. Frequency
X: 3.624e+009
Y: 6.405e-007

(b)

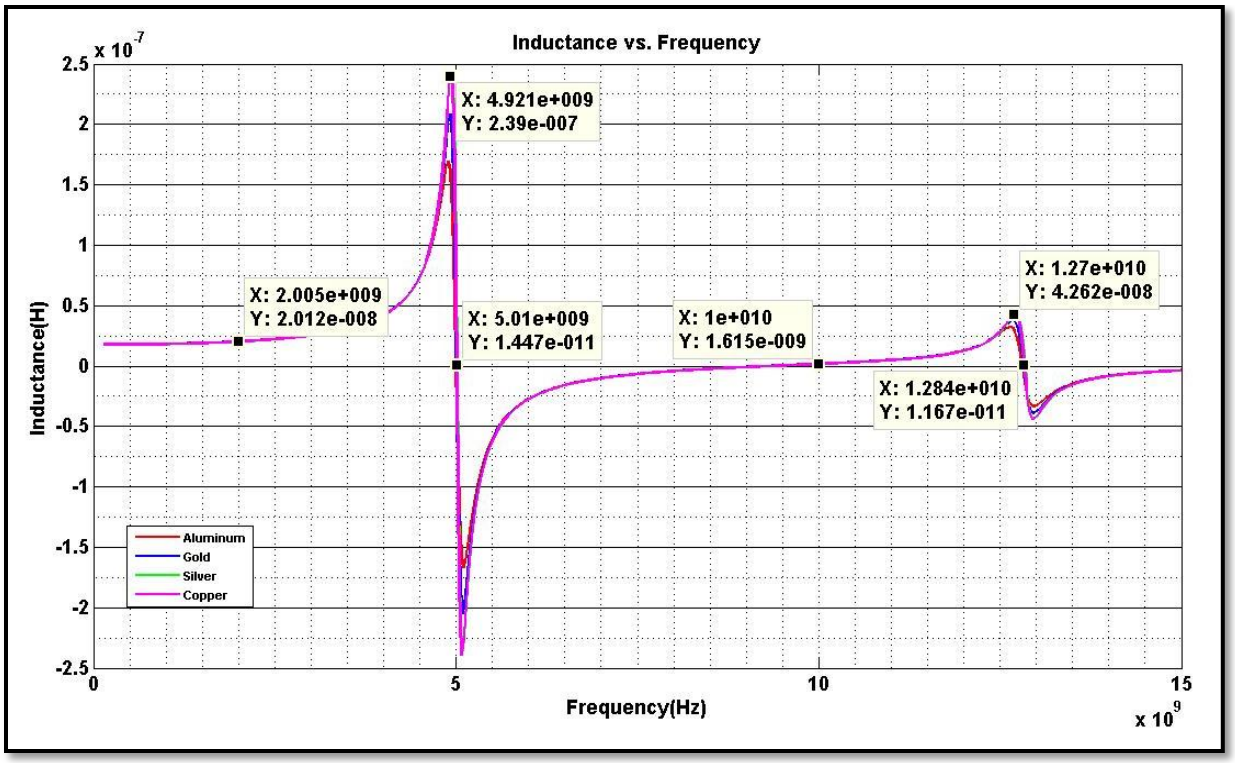

(c)

Figure 4.4-1: The inductance for a spacing of (a) 35 turns and 30 μm, (b) 29 turns and 40 μm, and (c) 22 turns and 60 μm

4.4.2 Resistance

Figure 4.4-2 shows the resistance of the coil for increase in spacing. The observed resistances are extremely high at self resonant frequencies and hence a logarithmic graph of the resistance versus frequency is provided in the inset. All four metals display similar behavior and peaks for a given structure with silver showing the least resistance. The peaks in the resistance graph occur due the presence of a parallel self-resonant circuit formed by the parasitic and the inductor coil. At resonance, the circuit impedances cancel each other out and the circuit becomes purely resistive displaying a high resistance.

Figure 4.4-2 (a), (b) and (c) show a peak of 29 kΩ at 3.2 GHz, 27 kΩ at 3.6 GHz and 13 kΩ at 5 GHz. The drop in resistance for 60 μm spacing is the maximum compared to 30 μm spacing of turns. The structure used for Figure 4.4-2 (a) has the highest number of turns compared to the rest and hence a large coil length. This increases the resistance of the coil as well as the parasitics. With the increase in spacing and reduced number of turns, the resistance can be decreased by a large amount.

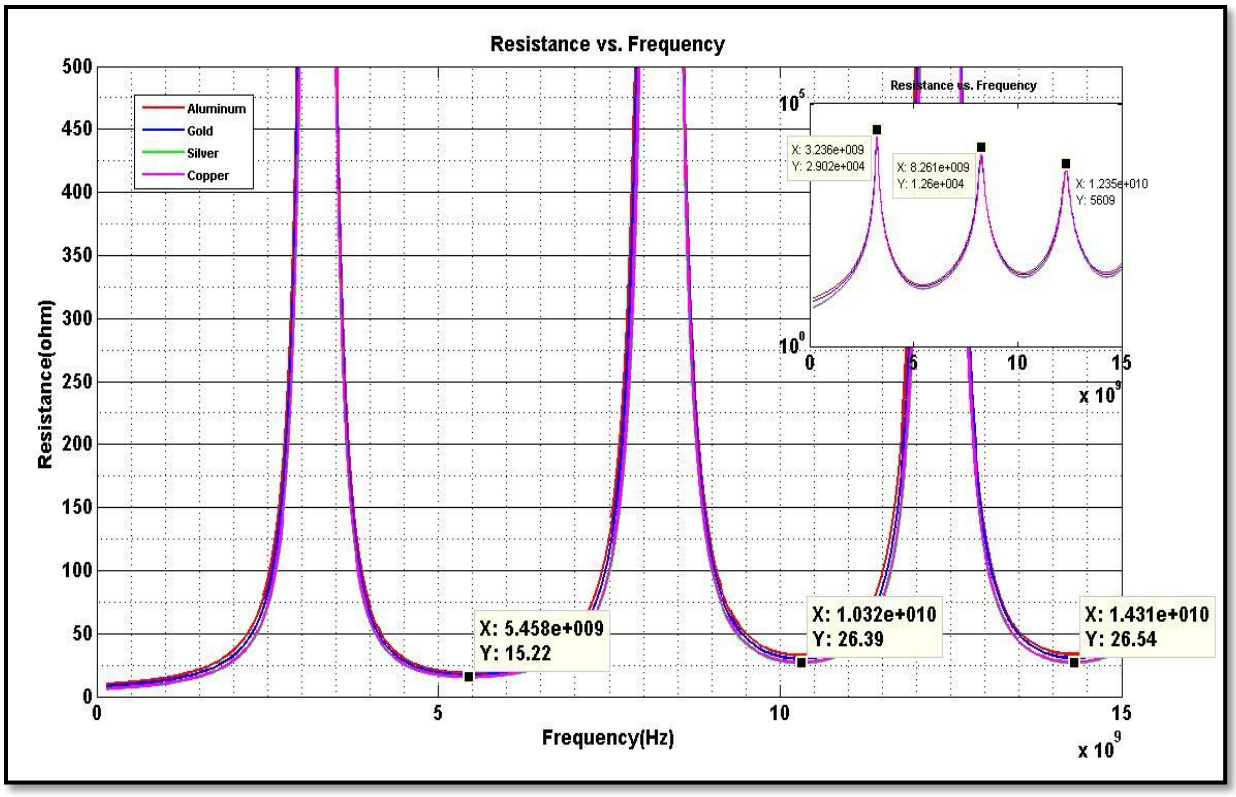
Resistance vs. Frequency
Aluminum
Gold
Silver
Copper
Resistance(ohm)
Frequency(Hz)
x 10^9
X: 5.458e+009
Y: 15.22
X: 1.032e+010
Y: 26.39
X: 1.431e+010
Y: 26.54
Resistance vs. Frequency
X: 3.236e+009
Y: 2.902e+004
X: 8.261e+009
Y: 1.26e+004
X: 1.235e+010
Y: 5609

(a)

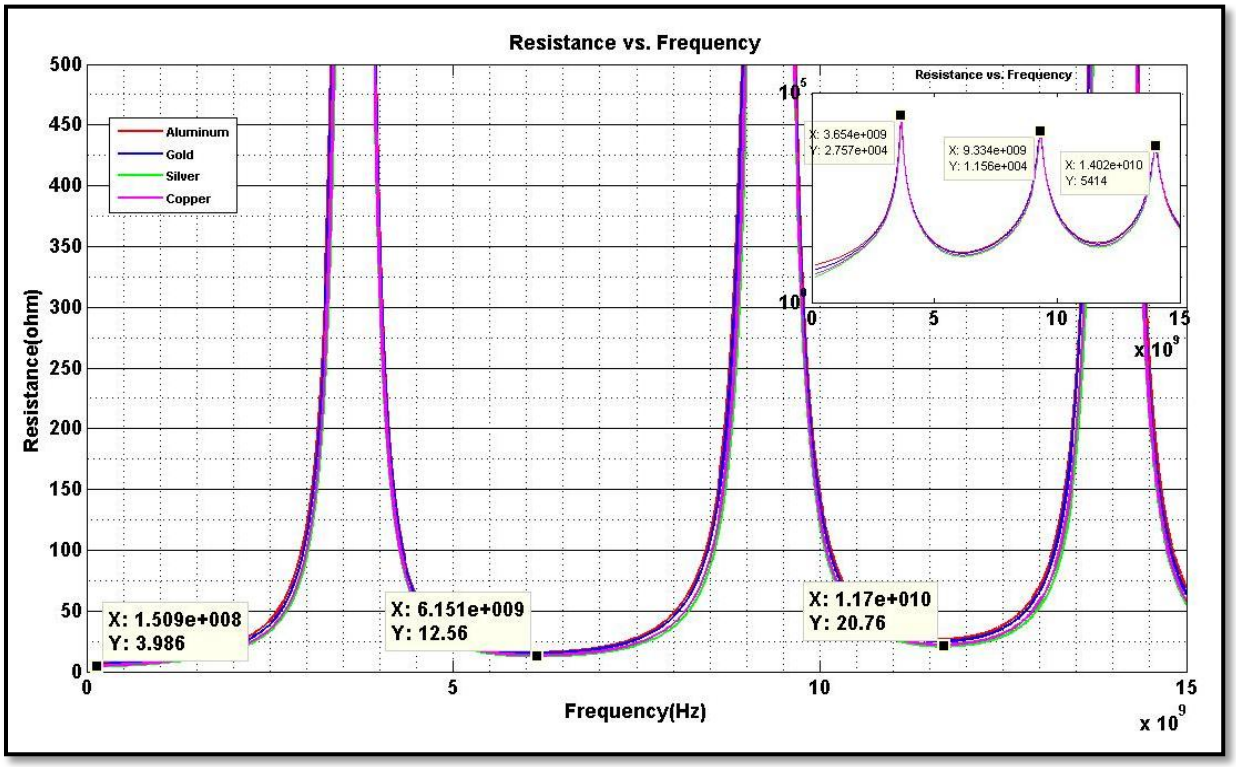
Resistance vs. Frequency
Aluminum
Gold
Silver
Copper
Resistance(ohm)
Frequency(Hz)
x 10^9
X: 1.509e+008
Y: 3.986
X: 6.151e+009
Y: 12.56
X: 1.17e+010
Y: 20.76
Resistance vs. Frequency
X: 3.654e+009
Y: 2.757e+004
X: 9.334e+009
Y: 1.156e+004
X: 1.402e+010
Y: 5414

(b)

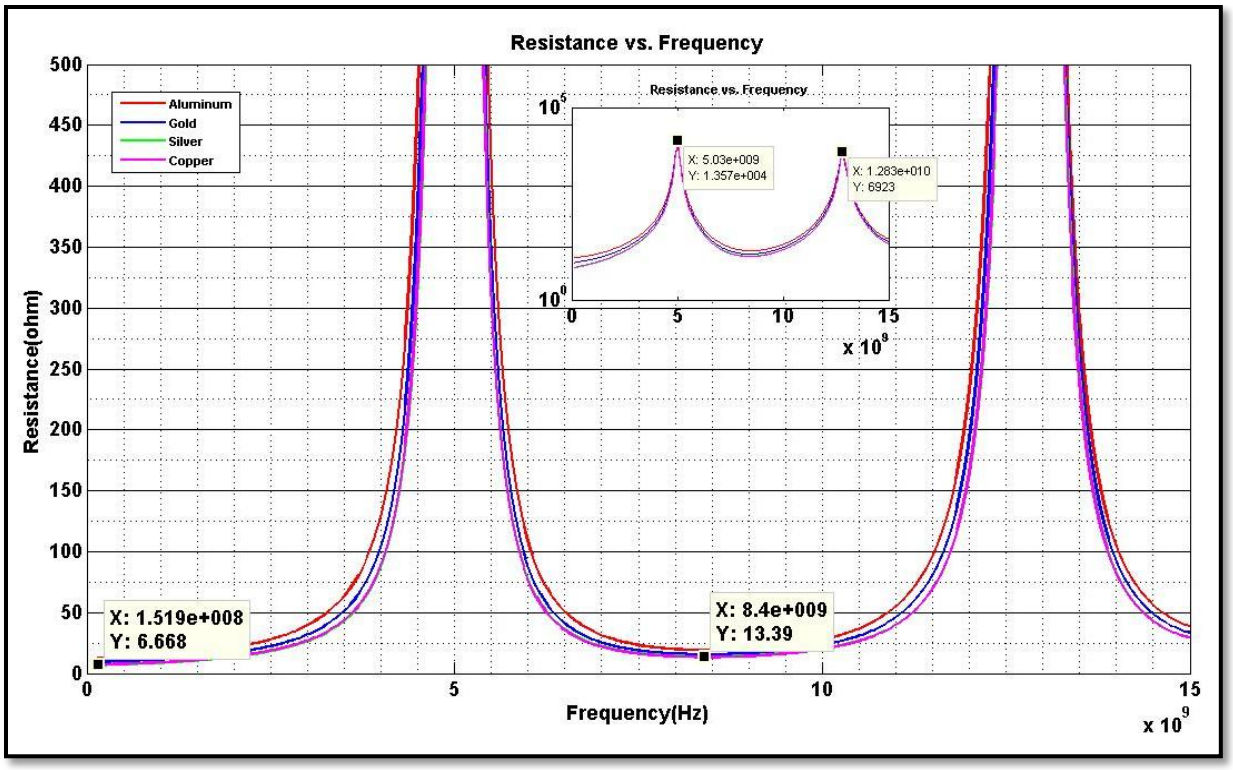

(c)

Figure 4.4-2: The resistance for a spacing of (a) 35 turns and 30 μm, (b) 29 turns and 40 μm, and (c) 22 turns and 60 μm

4.4.3 Quality Factor

Figure 4.4-3 shows the quality factor of the inductor. At lower frequencies, the quality factor for each of the metals in Figure 4.4-3 (a) and (b) display a unique peak but at higher frequencies, the positive peak of the quality factor of all metals seems to merge at the same peak making Q almost independent of metal used as the coil at higher frequencies. At lower frequencies, it is observed that silver dominates and provides the highest quality factor and aluminum yields the lowest quality factor.

The quality factor becomes zero at the resonant frequency because the inductance/capacitance values are also zero at the same frequency, implying that there is no energy stored in the circuit. The quality factor for Figure 4.4-3 (b) is 31 at 1.5 GHz, which is higher than the peak of 28.2 at 1.47 GHz for Figure 4.4-3 (a). This increase in quality factor can be attributed to the lowering of resistance, and hence, a drop in the power consumed by a smaller coil length. Figure 4.4-3 (c) shows a lower peak compared to Figure 4.4-3 (b) and this may be due to the fact that the increased spacing now affects the inductance to a greater extent such that the drop in inductance value causes a drop in the quality factor. The damping nature of values with increasing frequency observed in all the graphs are due to the skin effect, parasitics and other core losses. Therefore a

tradeoff can be made between number of turns and spacing depending on the parameter of interest.

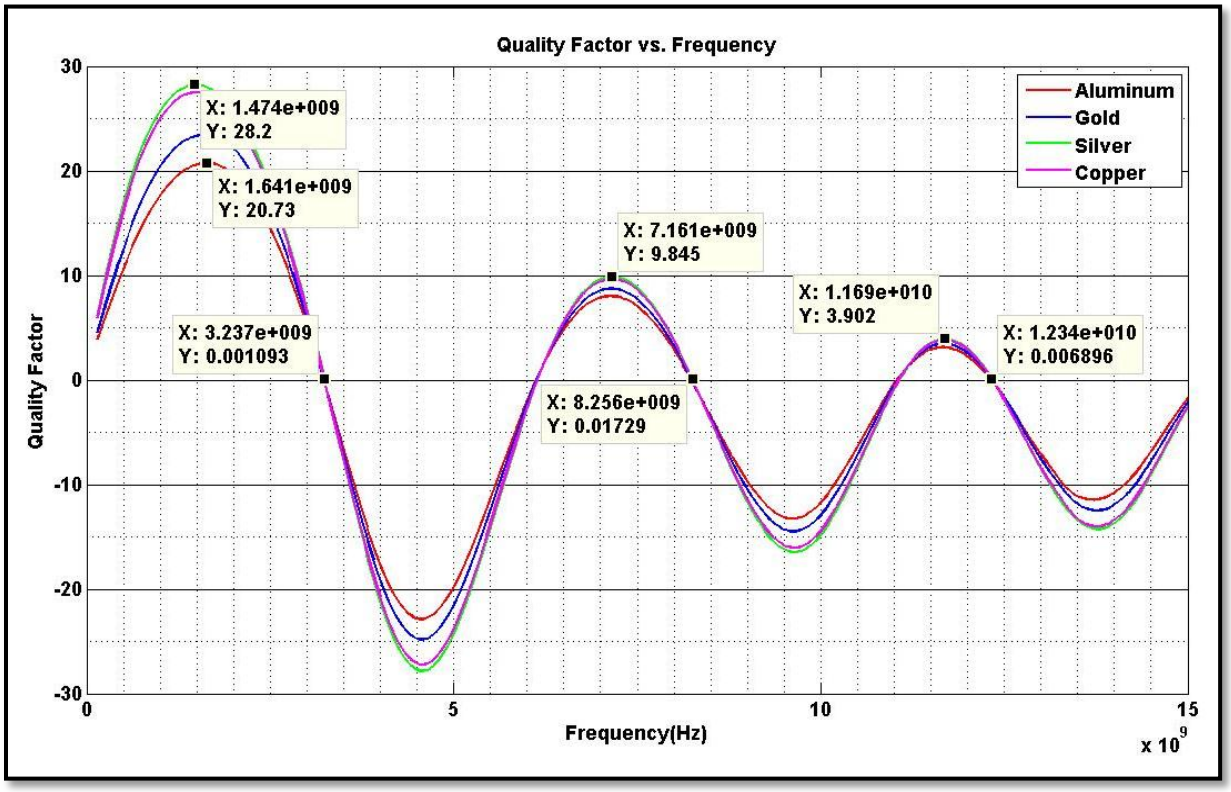

(a)

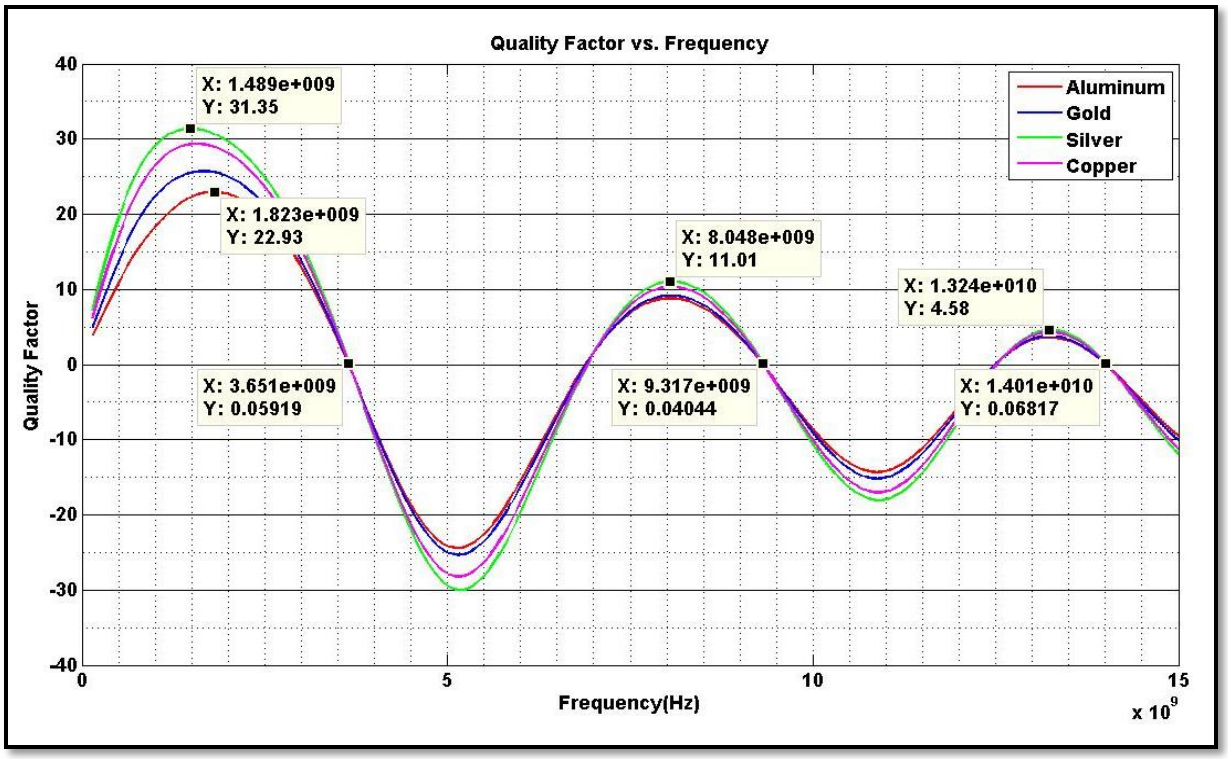

(b)

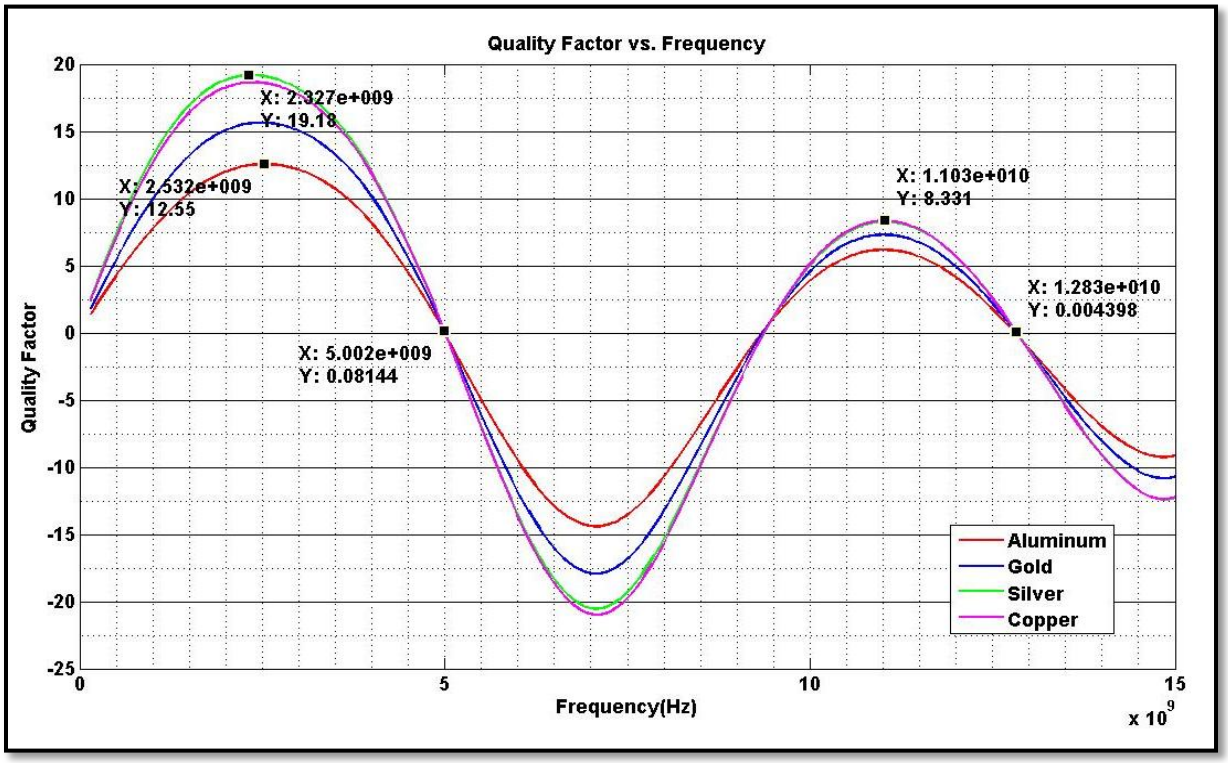

(c)

Figure 4.4-3: The quality factor for a spacing of (a) 35 turns and 30 μm, (b) 29 turns and 40 μm, and (c) 22 turns and 60 μm

4.5 Effect of variable thickness of the core for 5 μm thick metal

For a given inductor structure, if the thickness of the magnetic core were increased then from equation (4.6) we should expect an increase in the inductance values. To observe the effect of varying core thickness we simulate an inductor with 29 turns, each turn being 5 μm thick and 20 μm in width separated by 40 μm spacing while maintaining other parameters constant. The magnetic core material used is constant and has a relative permeability of 120. Below are the results.

4.5.1 Inductance

Figure 4.5-1 shows the inductance of the structure for increasing core thickness. The inset provides a complete plot of inductance vs. frequency distribution. The graph in Figure 4.5-1 (a) shows the inductance for the least core thickness (5 μm). The graph displays an inductance curve similar to the ones discussed in Section 3.4.1. All four metals display similar curve characteristics but with different peak values. It is observed that silver provides the highest inductance of 587 nH at 3.6 GHz and the inductances are found to be the maximum just before the self resonant frequency occurs. Increasing the core thickness to 20 μm does not increase the inductance by any visible amount as seen in Figure 4.5-1 (b). Increasing the core thickness further to 40 μm shows a visible increase in the inductance peak to 619 nH as seen in Figure 4.5-1 (c). Further increase in the core to 60 μm reduces the value of the first peak of the inductance to 609 nH but the second peak rises to 103 nH as seen in Figure 4.5-1 (d). A final increase in the core thickness to 80 μm increases the first peak to 640 nH and the second peak to 105 nH. Thus, we observe that the increasing core thickness does confirm with the equation in (4.6) in increasing the inductance. The self resonant frequency (inductance = 0) is seen to be increasing with core thickness as well.

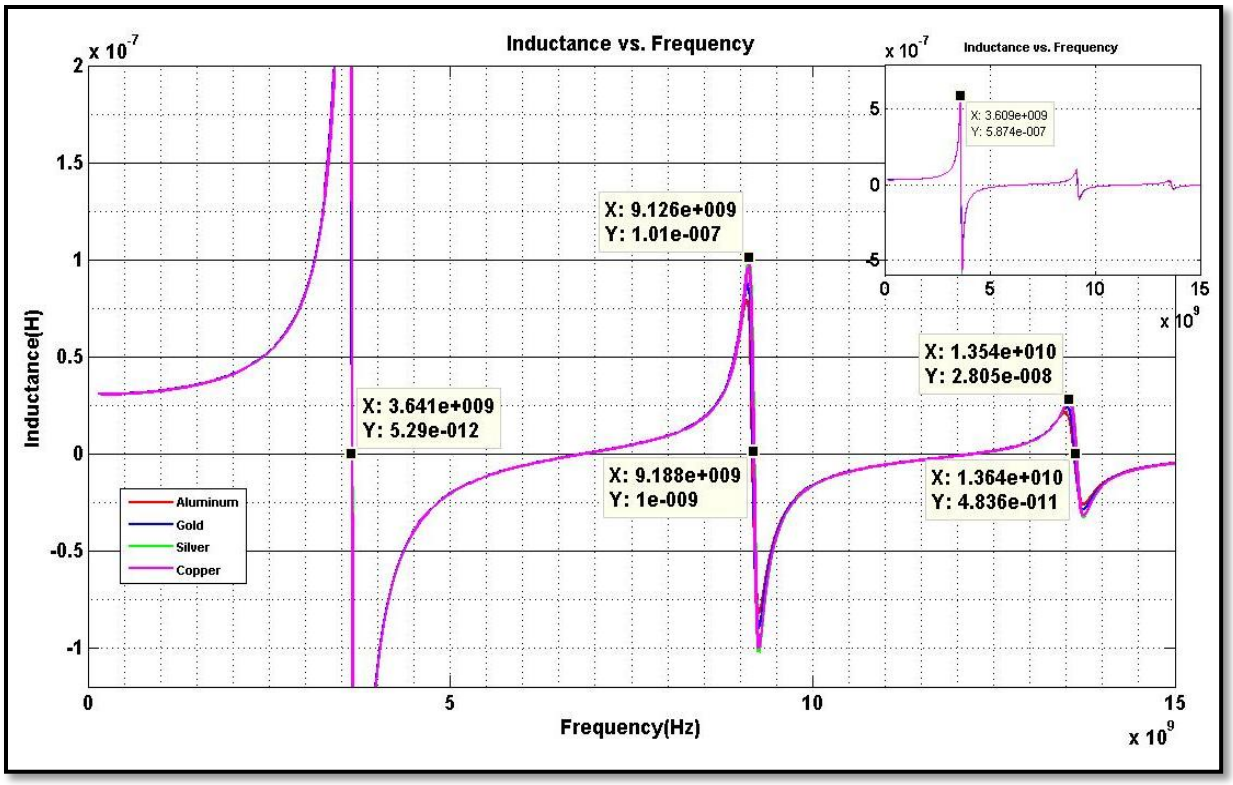
Inductance vs. Frequency
x 10^-7
Inductance(H)
Frequency(Hz)
x 10^9
X: 9.126e+009
Y: 1.01e-007
X: 3.641e+009
Y: 5.29e-012
X: 9.188e+009
Y: 1e-009
X: 1.354e+010
Y: 2.805e-008
X: 1.364e+010
Y: 4.836e-011
Aluminum
Gold
Silver
Copper
Inductance vs. Frequency
x 10^-7
X: 3.609e+009
Y: 5.874e-007

(a)

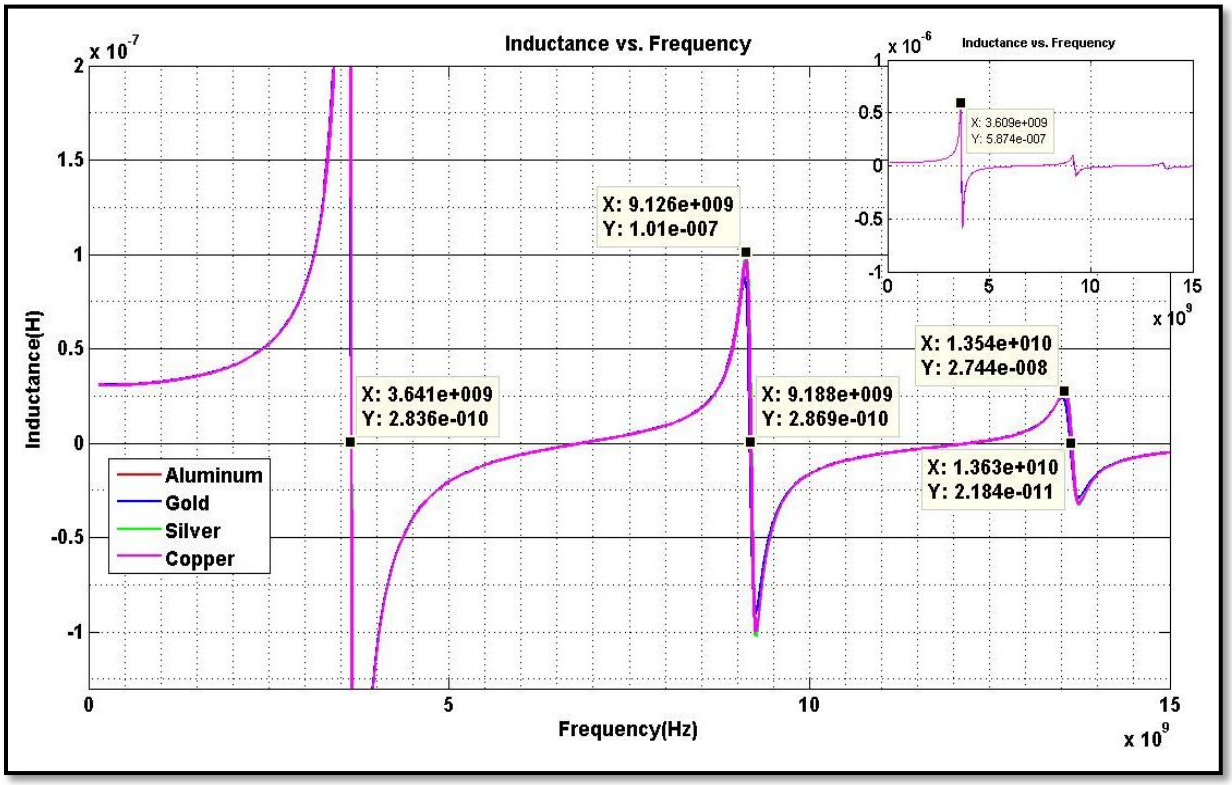
Inductance vs. Frequency
x 10^-7
Inductance(H)
Frequency(Hz)
x 10^9
X: 9.126e+009
Y: 1.01e-007
X: 3.641e+009
Y: 2.836e-010
X: 9.188e+009
Y: 2.869e-010
X: 1.354e+010
Y: 2.744e-008
X: 1.363e+010
Y: 2.184e-011
Aluminum
Gold
Silver
Copper
Inductance vs. Frequency
x 10^-6
X: 3.609e+009
Y: 5.874e-007

(b)

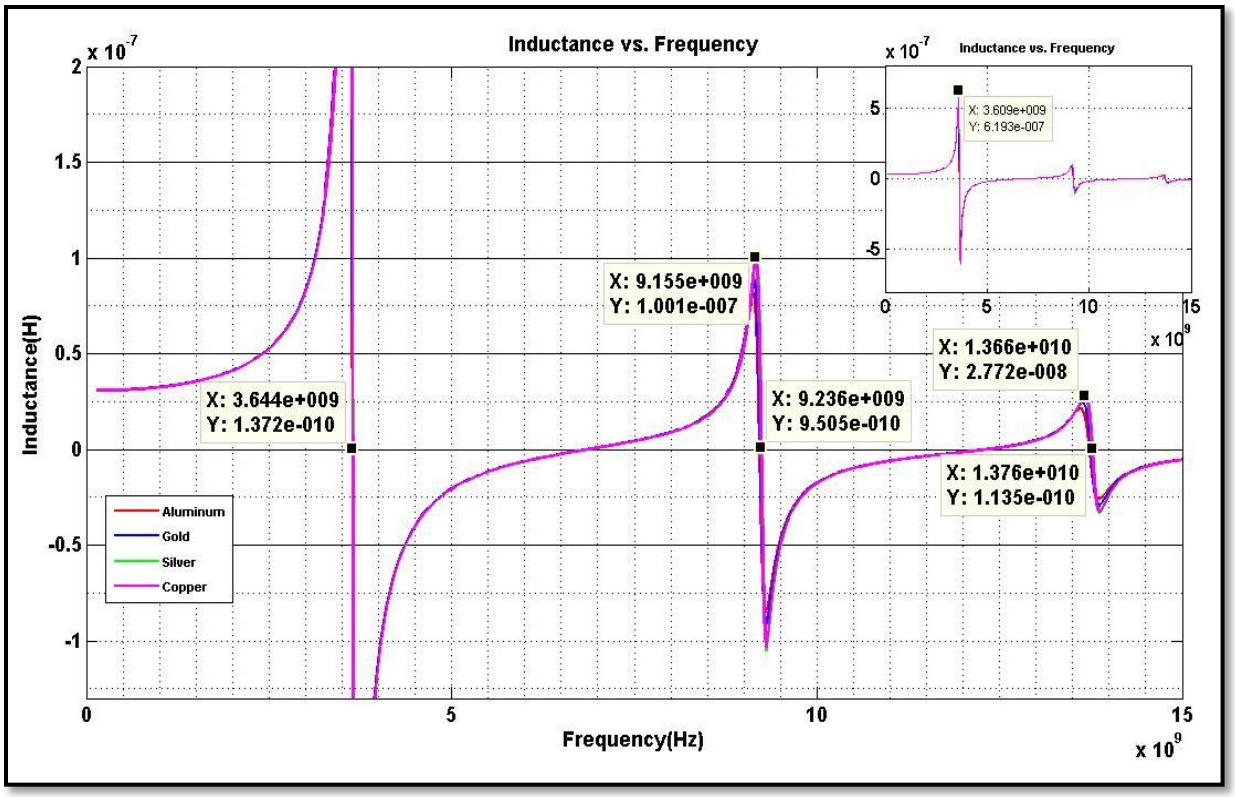
Inductance vs. Frequency
x 10^-7
Inductance(H)
Frequency(Hz)
x 10^9
Aluminum
Gold
Silver
Copper
X: 3.644e+009
Y: 1.372e-010
X: 9.155e+009
Y: 1.001e-007
X: 9.236e+009
Y: 9.505e-010
X: 1.366e+010
Y: 2.772e-008
X: 1.376e+010
Y: 1.135e-010
Inductance vs. Frequency
X: 3.609e+009
Y: 6.193e-007

(c)

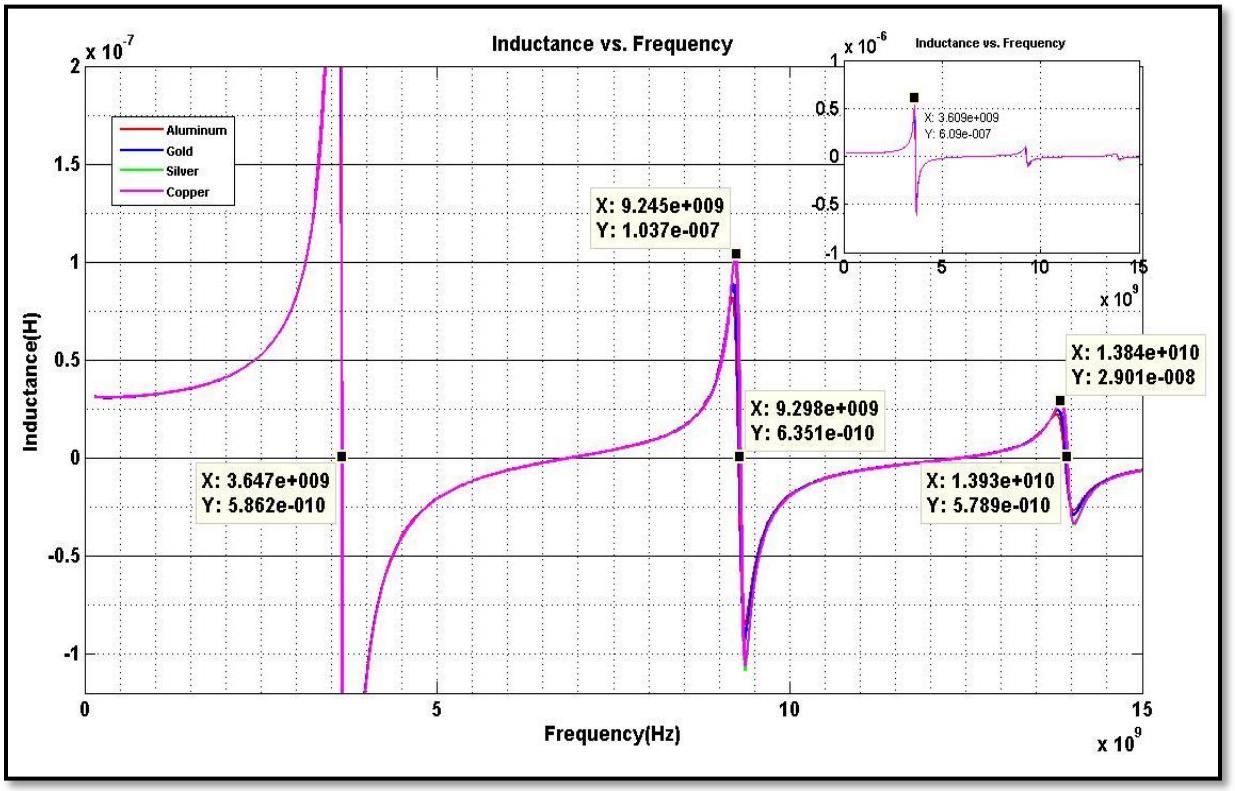
Inductance vs. Frequency
x 10^-7
Inductance(H)
Frequency(Hz)
x 10^9
Aluminum
Gold
Silver
Copper
X: 3.647e+009
Y: 5.862e-010
X: 9.245e+009
Y: 1.037e-007
X: 9.298e+009
Y: 6.351e-010
X: 1.384e+010
Y: 2.901e-008
X: 1.393e+010
Y: 5.789e-010
Inductance vs. Frequency
x 10^-6
X: 3.609e+009
Y: 6.09e-007

(d)

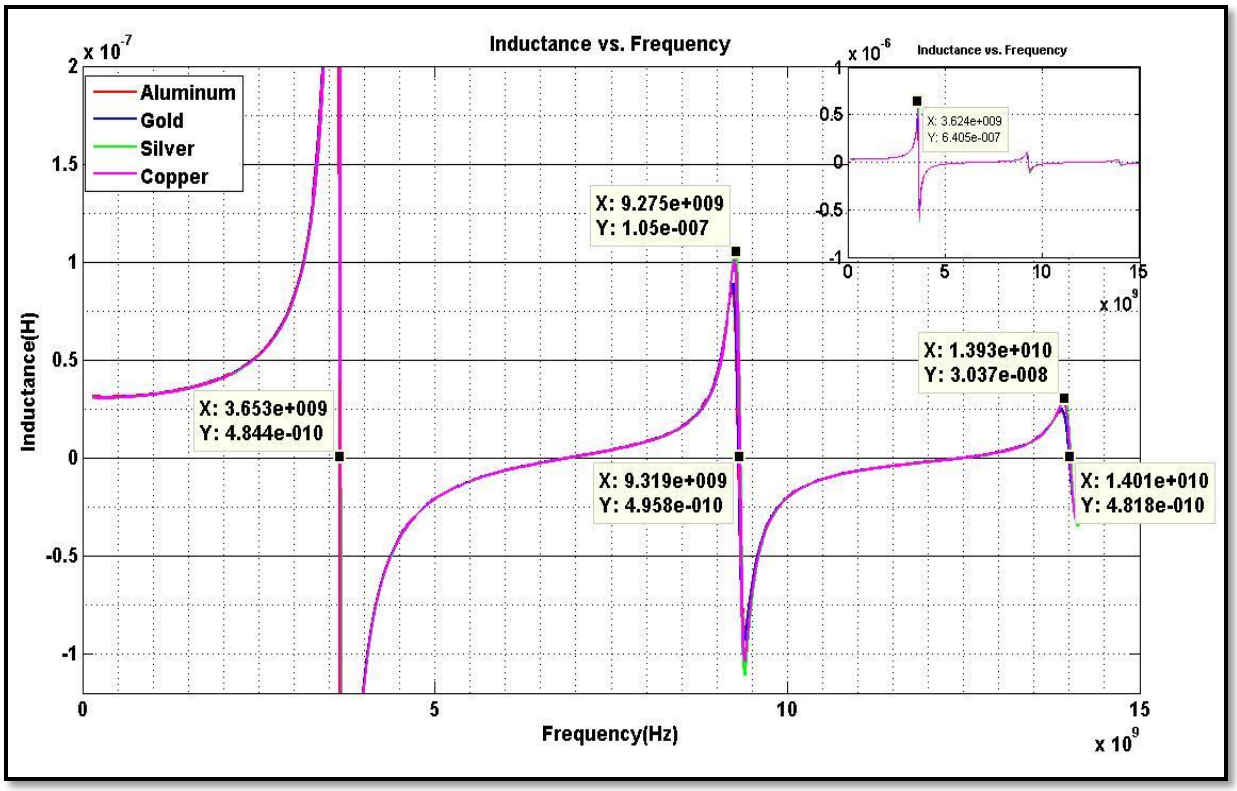

(e)

Figure 4.5-1: The inductance for a core thickness of (a) 5 μm, (b) 20 μm, (c) 40 μm, (d) 60 μm, and (e) 80 μm

4.5.2 Resistance

Figure 4.5-2 shows the resistance for varying core thickness. The resistance graphs display similar characteristics as observed in Section 3.4.2. As the resistance values observed is extremely high, a logarithmic plot of the resistance versus frequency is provided as an inset. All the four metals display common curve characteristics with unique peaks. The plot for aluminum in Figure 4.5-2 (b) is hidden under the copper curve. The resistance has its peak at the resonant frequencies. Silver shows the least resistance over the entire range of frequency with increasing core thickness. The peak resistance is seen to be increasing with increasing core. The increase in resistance can be due to the fact that the core material itself contributes to the series resistance.

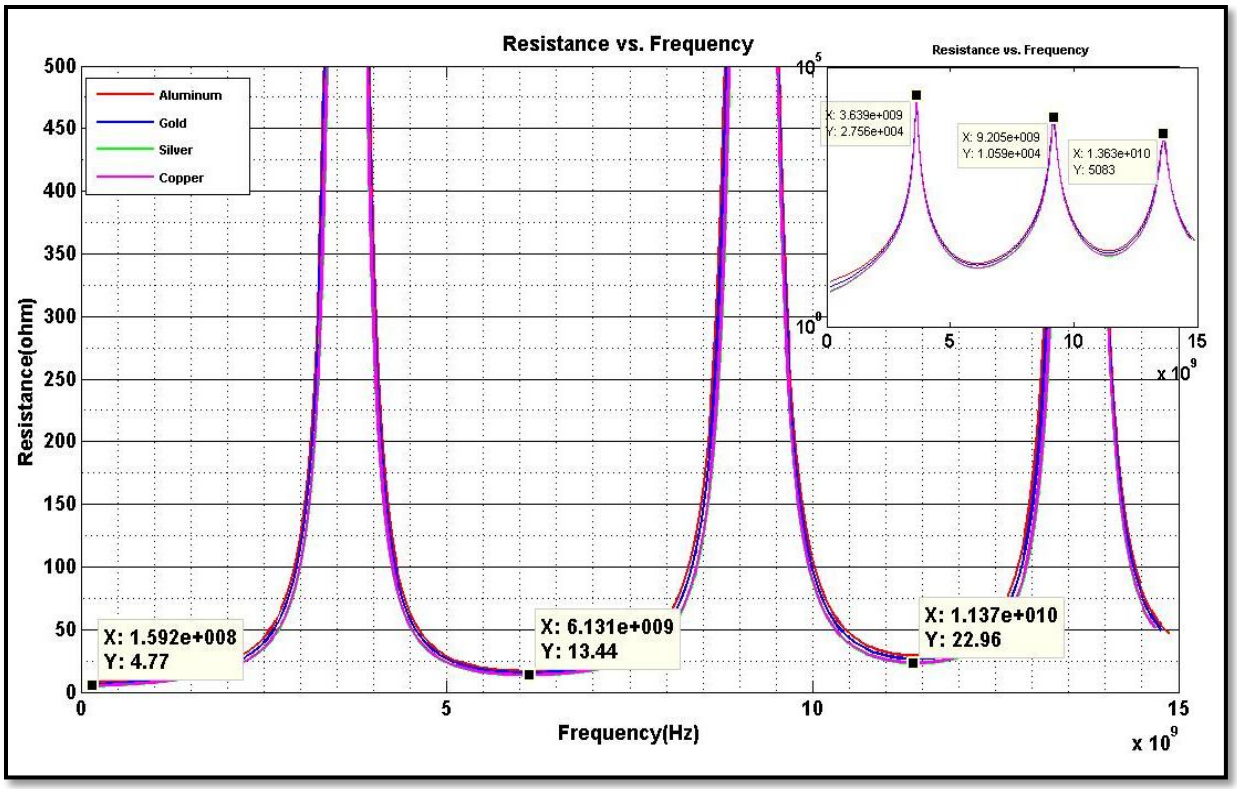
Resistance vs. Frequency
Aluminum
Gold
Silver
Copper
Resistance(ohm)
Frequency(Hz)
X: 1.592e+008
Y: 4.77
X: 6.131e+009
Y: 13.44
X: 1.137e+010
Y: 22.96
x 10^9
Resistance vs. Frequency
X: 3.639e+009
Y: 2.756e+004
X: 9.205e+009
Y: 1.059e+004
X: 1.363e+010
Y: 5083

(a)

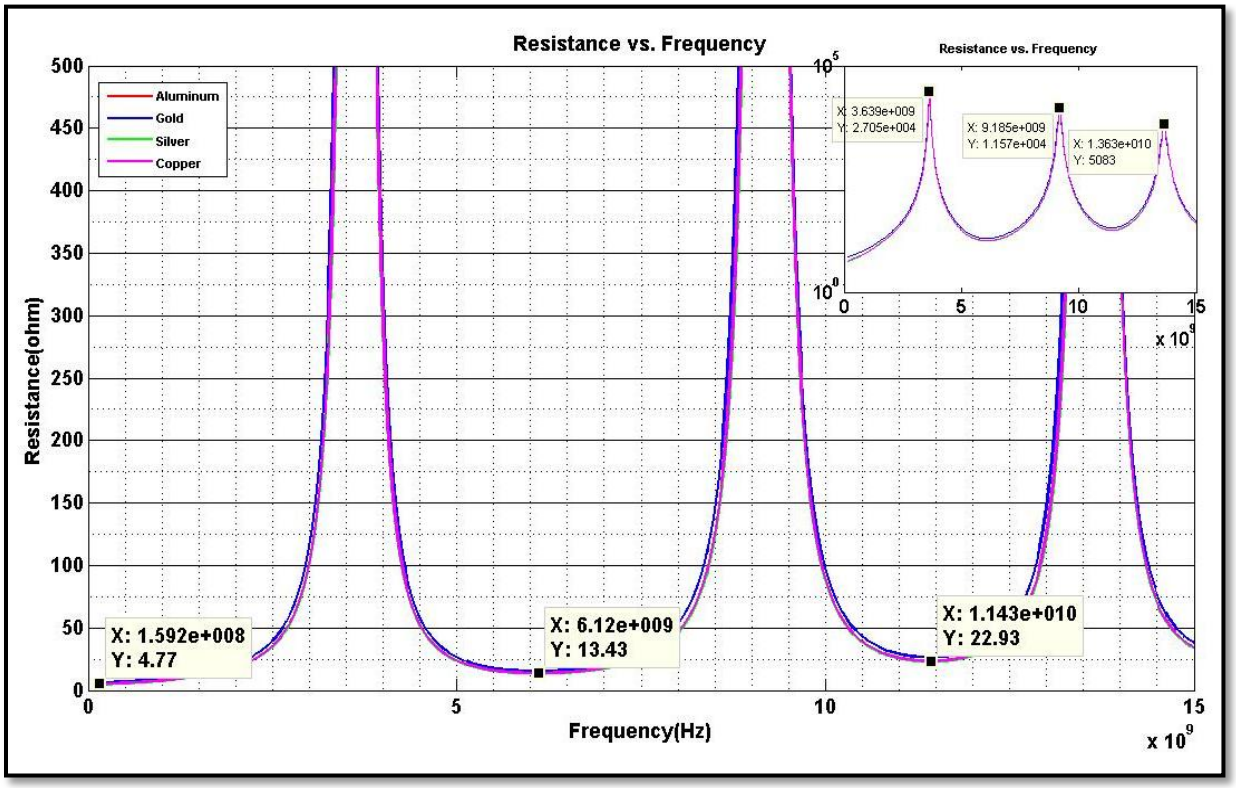
Resistance vs. Frequency
Aluminum
Gold
Silver
Copper
Resistance(ohm)
Frequency(Hz)
X: 1.592e+008
Y: 4.77
X: 6.12e+009
Y: 13.43
X: 1.143e+010
Y: 22.93
x 10^9
Resistance vs. Frequency
X: 3.639e+009
Y: 2.705e+004
X: 9.185e+009
Y: 1.157e+004
X: 1.363e+010
Y: 5083

(b)

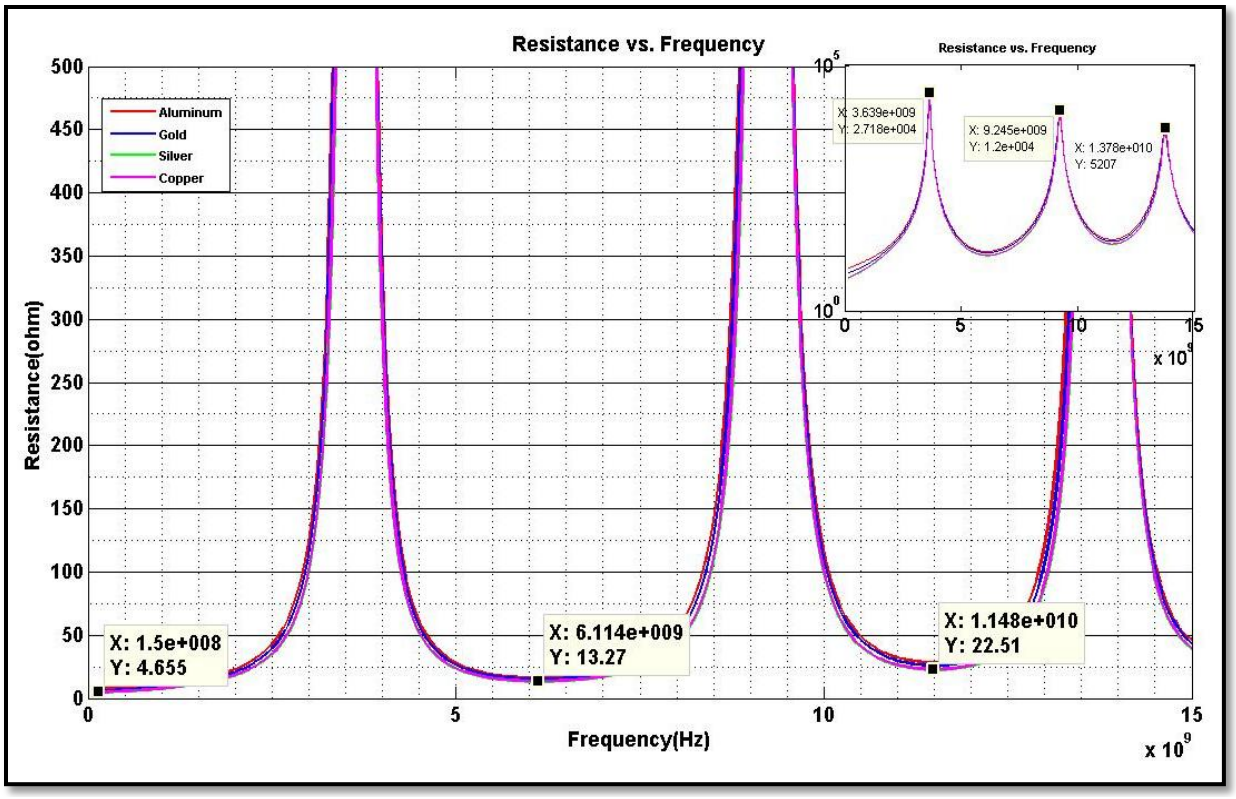
Resistance vs. Frequency
Aluminum
Gold
Silver
Copper
Resistance(ohm)
Frequency(Hz)
x 10^9
X: 1.5e+008
Y: 4.655
X: 6.114e+009
Y: 13.27
X: 1.148e+010
Y: 22.51
Resistance vs. Frequency
X: 3.639e+009
Y: 2.718e+004
X: 9.245e+009
Y: 1.2e+004
X: 1.378e+010
Y: 5207

(c)

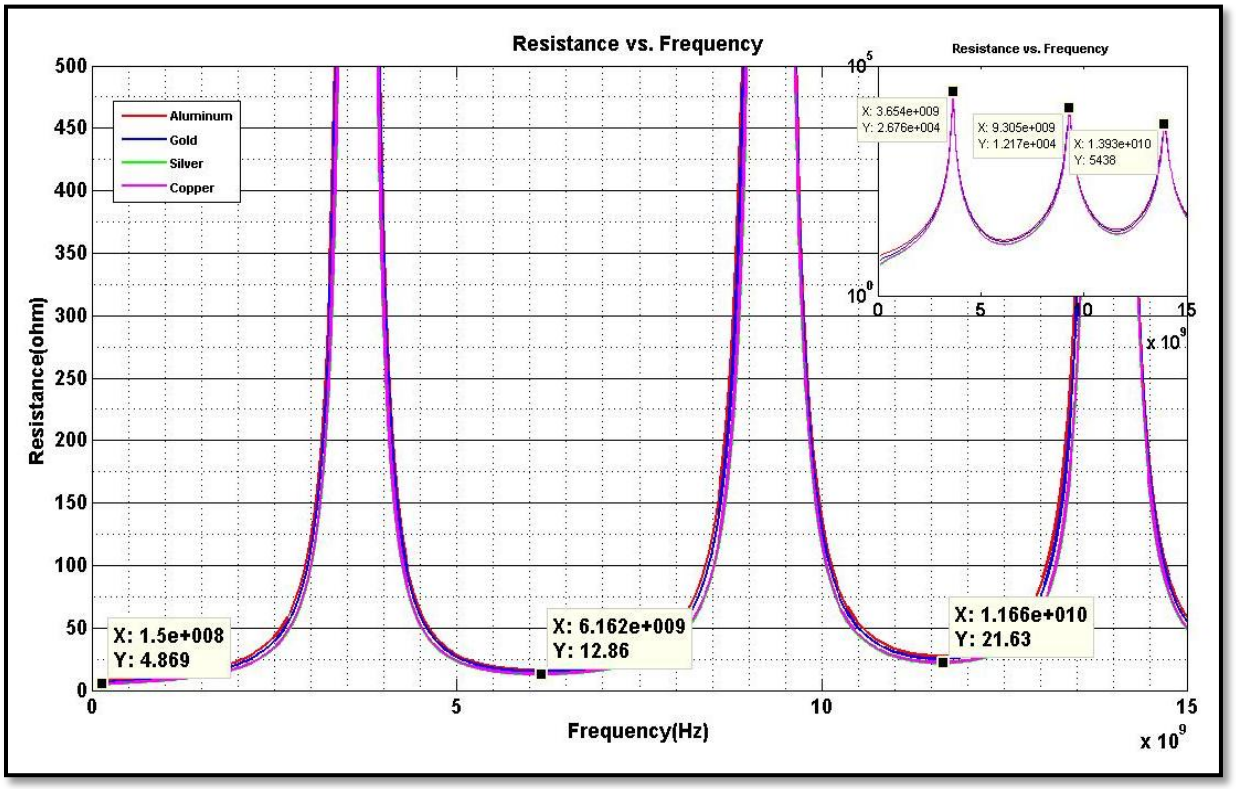
Resistance vs. Frequency
Aluminum
Gold
Silver
Copper
Resistance(ohm)
Frequency(Hz)
x 10^9
X: 1.5e+008
Y: 4.869
X: 6.162e+009
Y: 12.86
X: 1.166e+010
Y: 21.63
Resistance vs. Frequency
X: 3.654e+009
Y: 2.676e+004
X: 9.305e+009
Y: 1.217e+004
X: 1.393e+010
Y: 5438

(d)

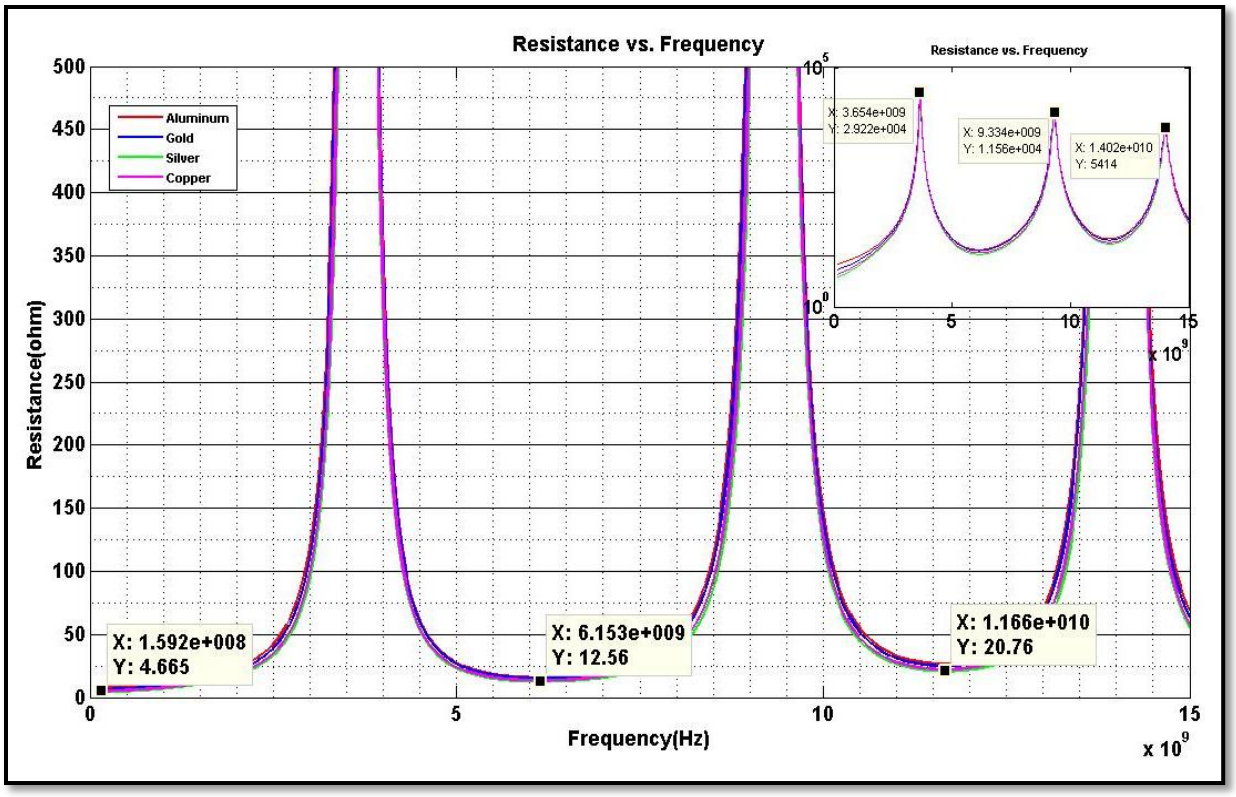

(e)

Figure 4.5-2: The resistance for a core thickness of (a) 5 μm, (b) 20 μm, (c) 40 μm, (d) 60 μm, and (e) 80 μm

4.5.3 Quality Factor

Figure 4.5-3 shows the quality factor of the inductor structure for increasing core thickness. It is similar to the graphs obtained in Section 3.4.3. All the four metals display similar curve characteristics but have unique peaks at lower frequencies. With the increase in frequency, the peaks have almost the same values. Silver shows the best quality factor for all core thicknesses. The curve for aluminum in Figure 4.5-3 (b) is under the curve for copper and is not visible. The quality factor curve for aluminum rises sharply in Figure 4.5-3 (b) compared to Figure 4.5-3 (a) but reduces again to its initial value for all further increase in core thickness. It is observed that the first peak of the quality factor in general has improved by a very small amount (0.2 – 0.5) with the increase in core thickness for all the metals. It appears that the quality factor is almost independent of the core thickness. One would expect a deterioration of the quality factor at higher frequencies due to core losses coming into play for greater core thickness but the effect of the losses do not seem to be too pronounced to affect the quality factor.

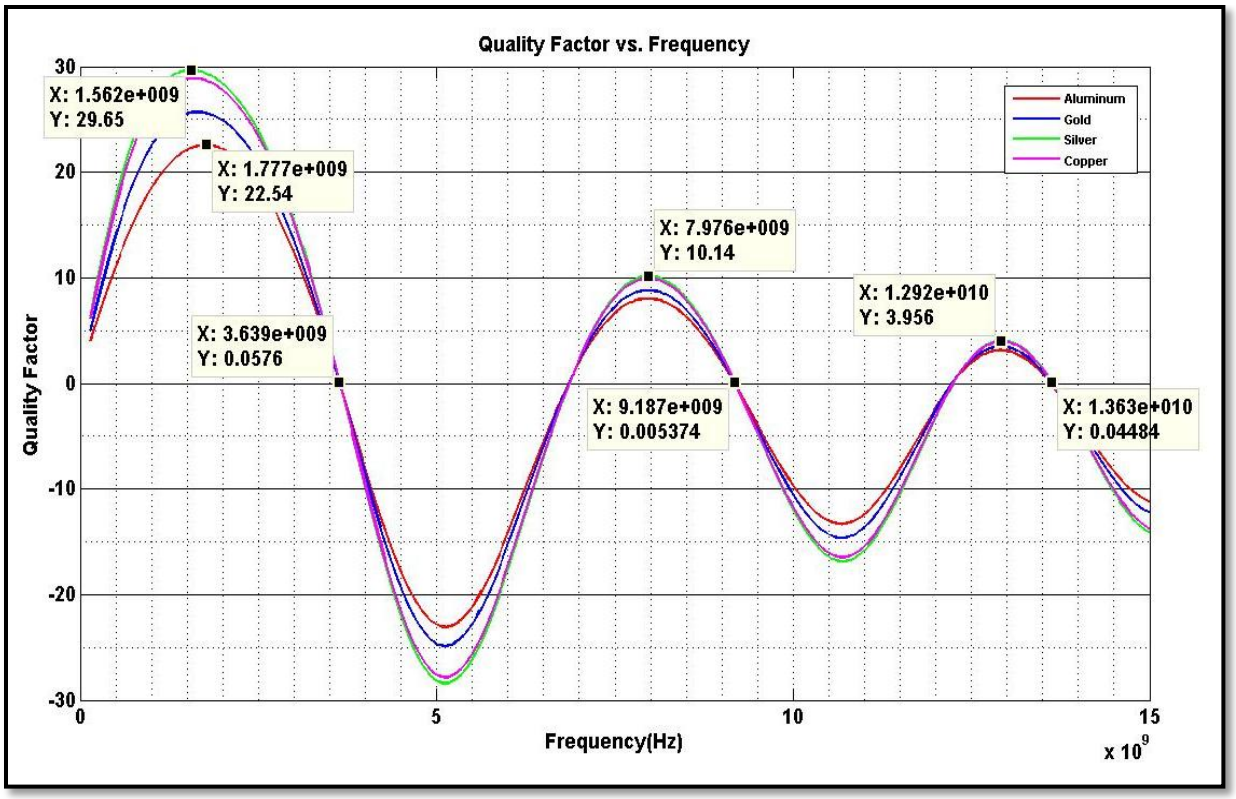
Quality Factor vs. Frequency
X: 1.562e+009
Y: 29.65
X: 1.777e+009
Y: 22.54
X: 7.976e+009
Y: 10.14
X: 1.292e+010
Y: 3.956
X: 3.639e+009
Y: 0.0576
X: 9.187e+009
Y: 0.005374
X: 1.363e+010
Y: 0.04484
Aluminum
Gold
Silver
Copper
Quality Factor
Frequency(Hz)
x 10^9

(a)

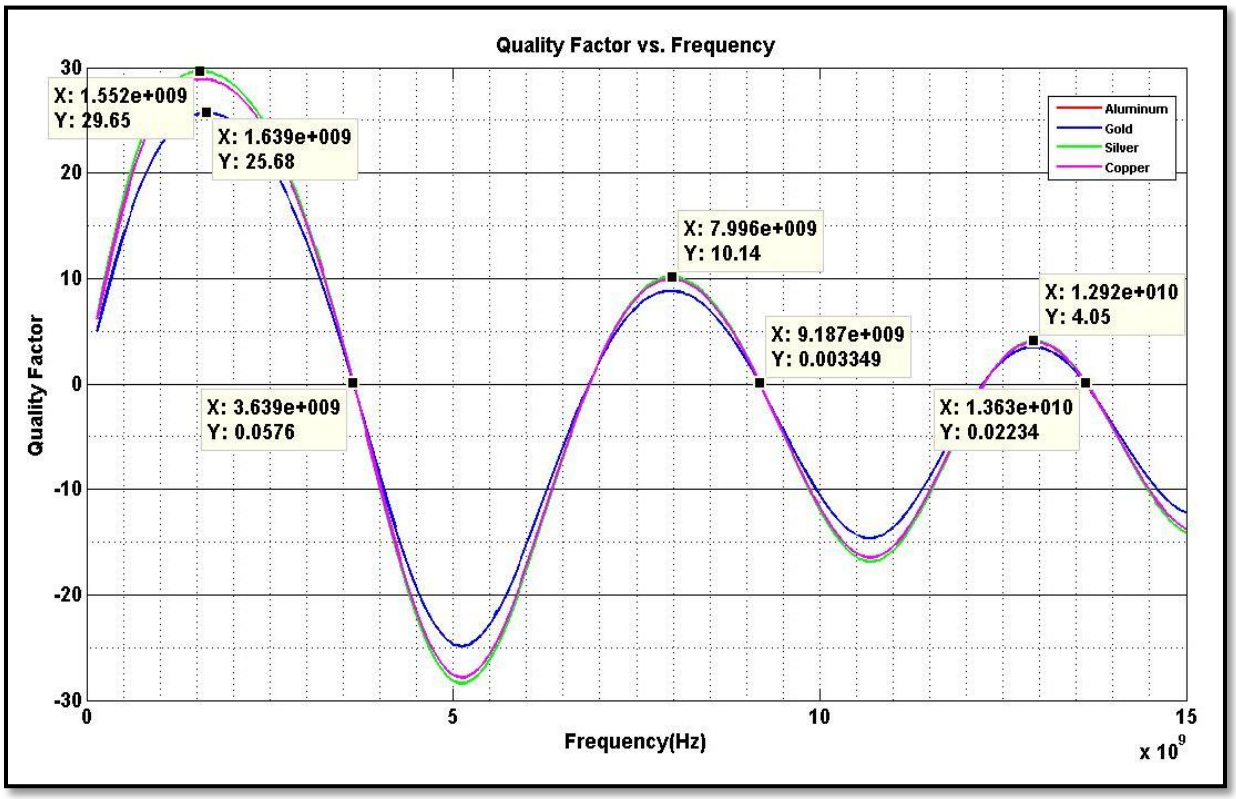
Quality Factor vs. Frequency
X: 1.552e+009
Y: 29.65
X: 1.639e+009
Y: 25.68
X: 7.996e+009
Y: 10.14
X: 1.292e+010
Y: 4.05
X: 9.187e+009
Y: 0.003349
X: 3.639e+009
Y: 0.0576
X: 1.363e+010
Y: 0.02234
Aluminum
Gold
Silver
Copper
Quality Factor
Frequency(Hz)
x 10^9

(b)

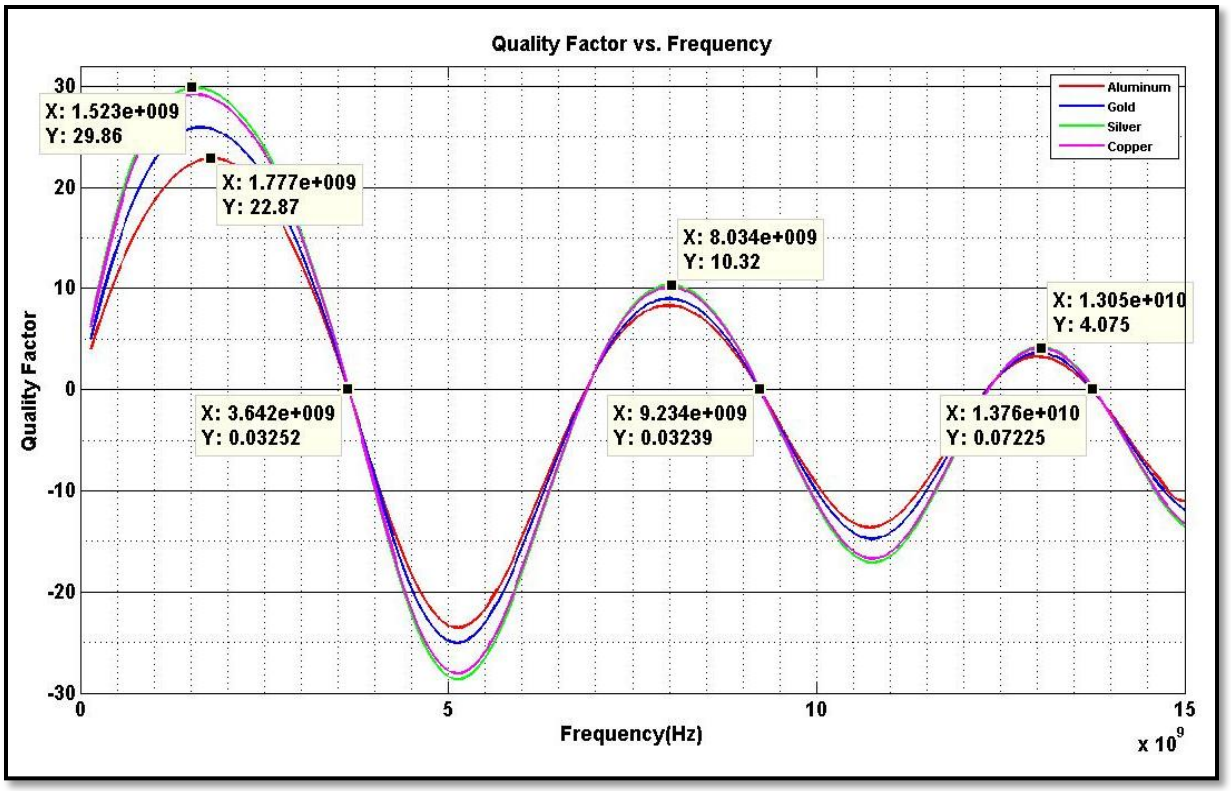
Quality Factor vs. Frequency
Aluminum
Gold
Silver
Copper
X: 1.523e+009
Y: 29.86
X: 1.777e+009
Y: 22.87
X: 8.034e+009
Y: 10.32
X: 1.305e+010
Y: 4.075
X: 3.642e+009
Y: 0.03252
X: 9.234e+009
Y: 0.03239
X: 1.376e+010
Y: 0.07225
Quality Factor
Frequency(Hz)
x 10^9

(c)

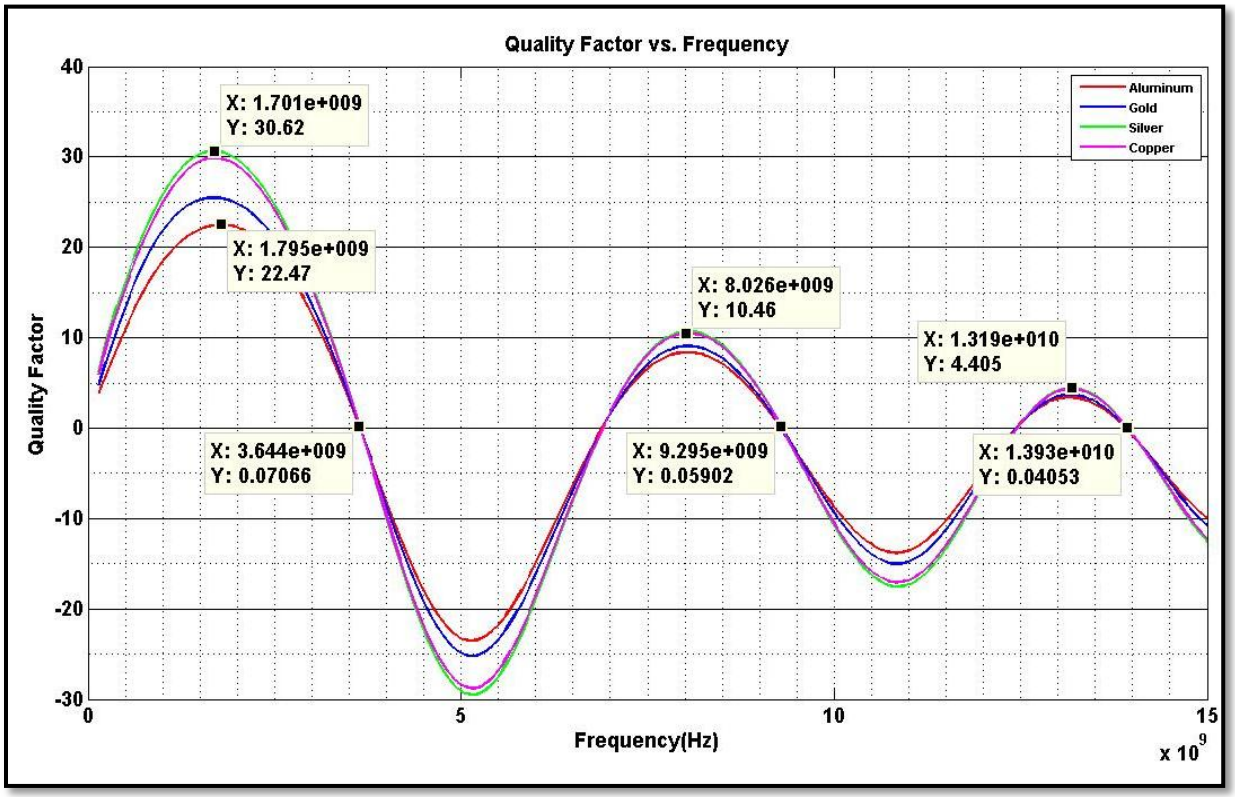
Quality Factor vs. Frequency
Aluminum
Gold
Silver
Copper
X: 1.701e+009
Y: 30.62
X: 1.795e+009
Y: 22.47
X: 8.026e+009
Y: 10.46
X: 1.319e+010
Y: 4.405
X: 3.644e+009
Y: 0.07066
X: 9.295e+009
Y: 0.05902
X: 1.393e+010
Y: 0.04053
Quality Factor
Frequency(Hz)
x 10^9

(d)

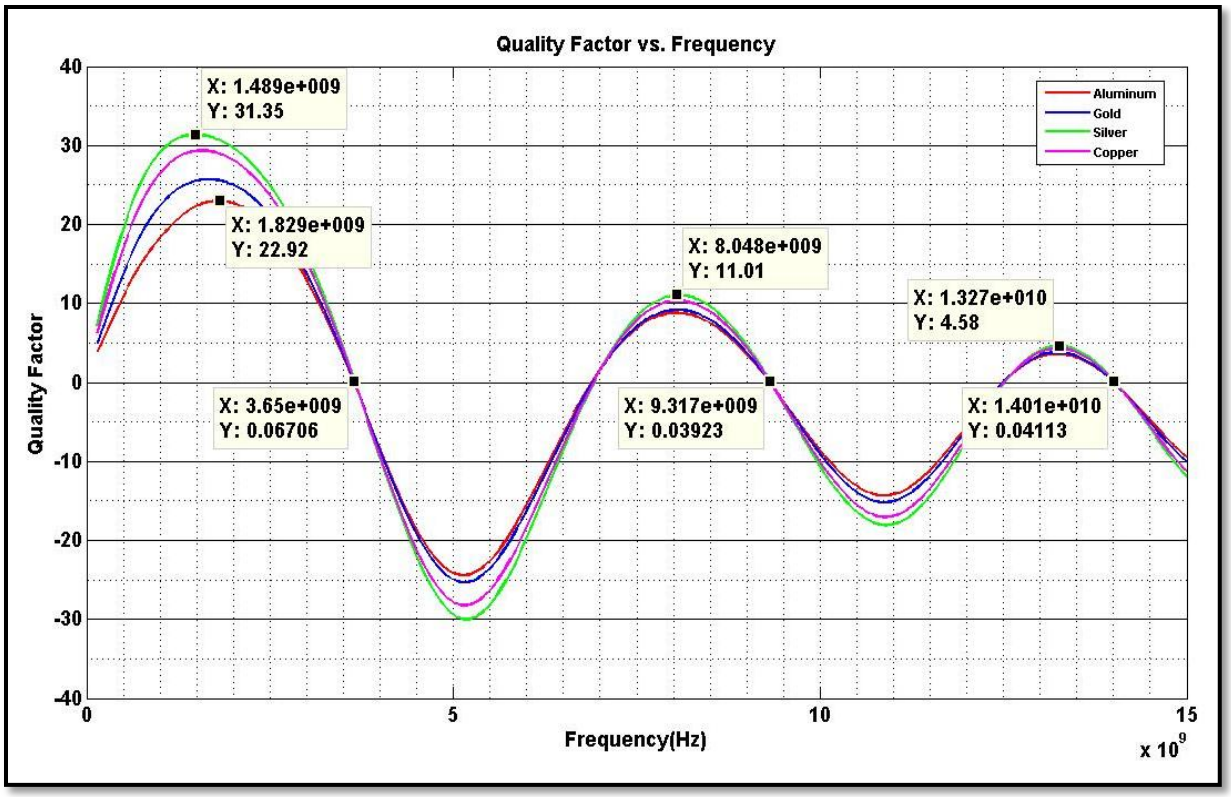

(e)

Figure 4.5-3: The quality factor for a core thickness of (a) 5 μm, (b) 20 μm, (c) 40 μm, (d) 60 μm, and (e) 80 μm

4.6 Effect of variable thickness of the core for 10 μm thick metal

Increasing the thickness of the metallic winding increases the magnetic coupling area and hence an increase in inductance can be expected. But this also means the turn to turn capacitances have a larger value, which could affect the quality factor of the circuit. To observe the effect of varying core thickness for a thicker metal winding we simulate an inductor with 29 turns, each turn being 10 μm thick and 20 μm in width separated by 40 μm spacing while maintaining other parameters constant. The magnetic core material used is constant and has a relative permeability of 120. Below are the results.

4.6.1 Inductance

Figure 4.6-1 shows the inductance of the structure for increasing core thickness. All the metals exhibit similar behavior and peaks in Figure 4.6-1 (a). Although the peak

inductance for copper occurs at a higher frequency, the value of the peak is the same as that of silver. The inductance as seen from previous results in Section 4.5.1 does not increase much with increase in core thickness. The resonant frequency is seen to be increasing with core thickness. The inductance values of the lower peaks increase by a small amount (2-3 nH).

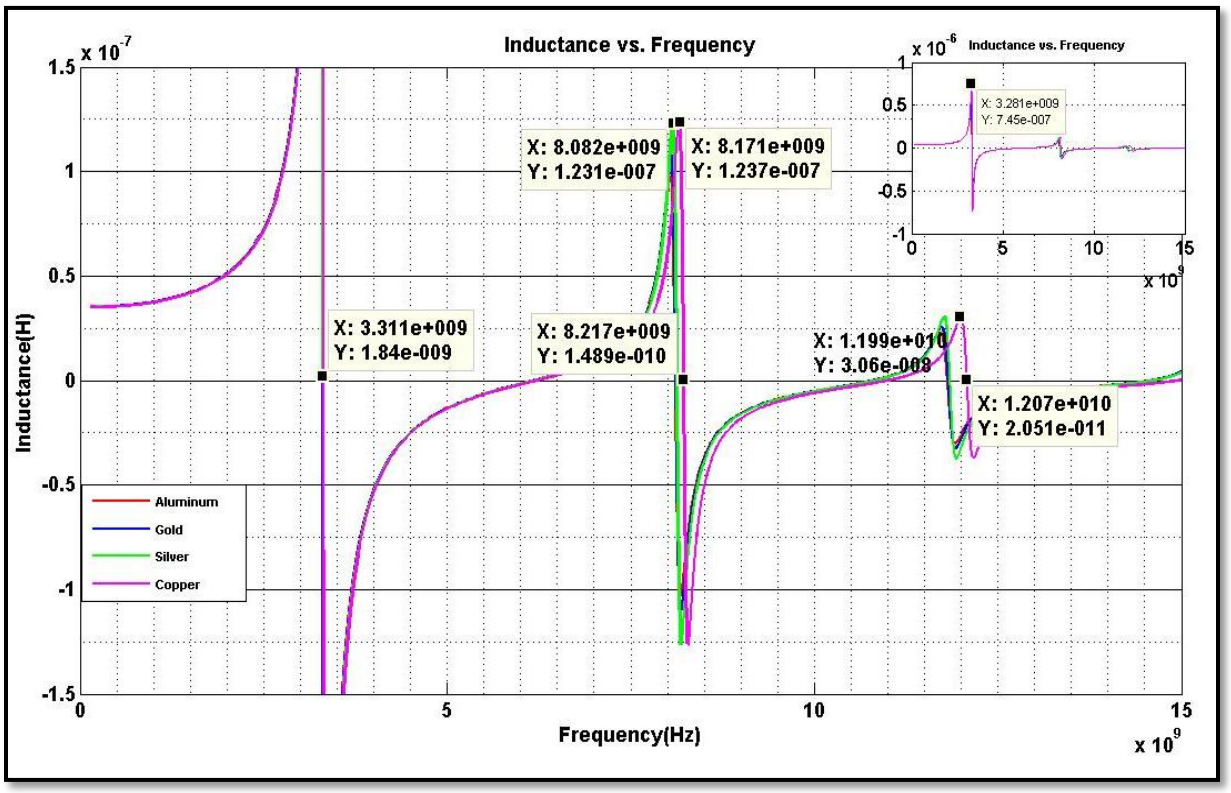

(a)

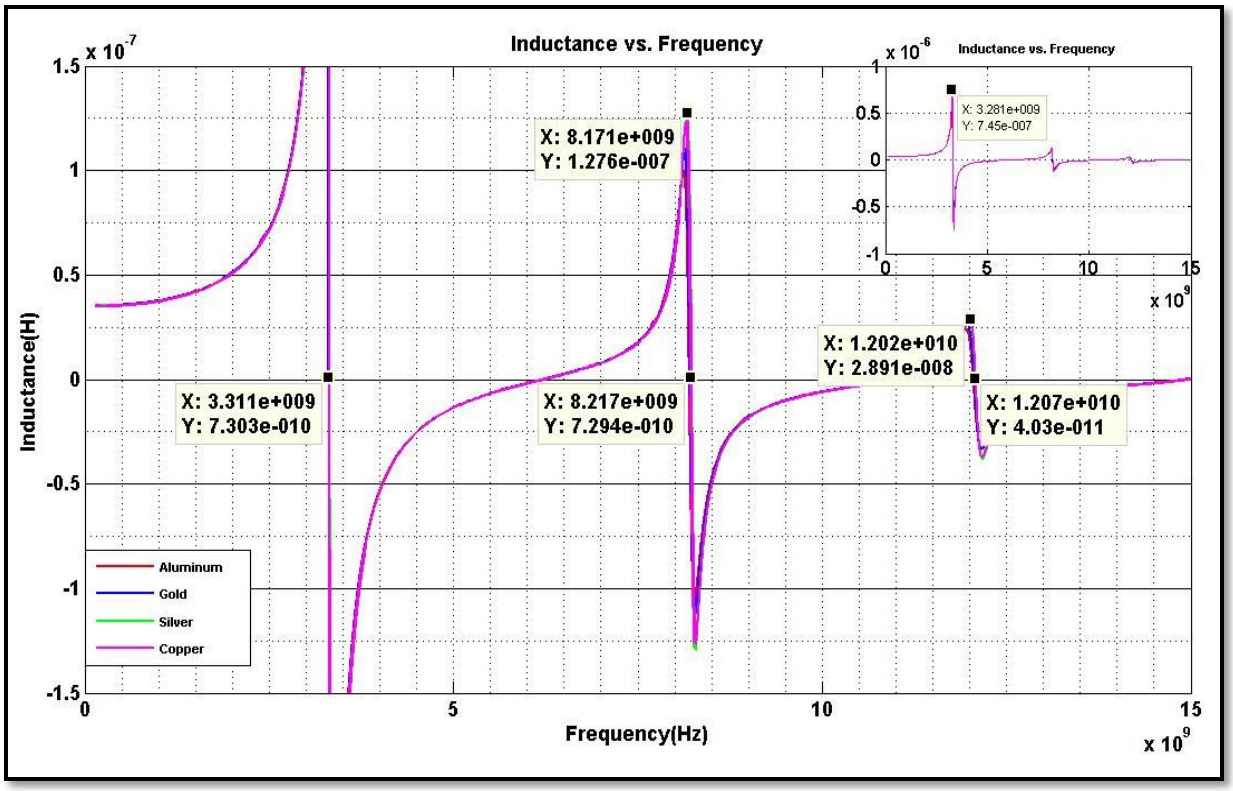
Inductance vs. Frequency
x 10^-7
Inductance(H)
Frequency(Hz)
x 10^9
X: 8.171e+009
Y: 1.276e-007
X: 3.311e+009
Y: 7.303e-010
X: 8.217e+009
Y: 7.294e-010
X: 1.202e+010
Y: 2.891e-008
X: 1.207e+010
Y: 4.03e-011
Aluminum
Gold
Silver
Copper
x 10^-6
Inductance vs. Frequency
X: 3.281e+009
Y: 7.45e-007

(b)

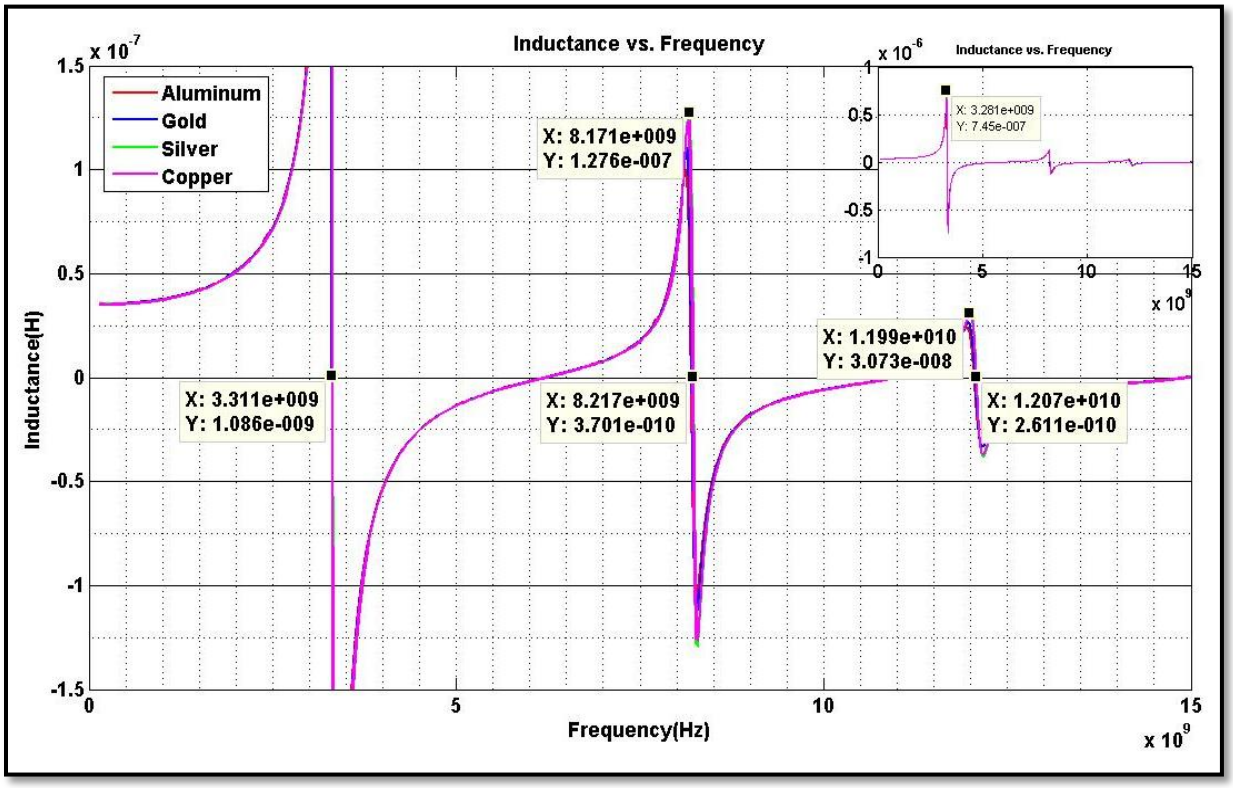
Inductance vs. Frequency
x 10^-7
Inductance(H)
Frequency(Hz)
x 10^9
Aluminum
Gold
Silver
Copper
X: 8.171e+009
Y: 1.276e-007
X: 3.311e+009
Y: 1.086e-009
X: 8.217e+009
Y: 3.701e-010
X: 1.199e+010
Y: 3.073e-008
X: 1.207e+010
Y: 2.611e-010
x 10^-6
Inductance vs. Frequency
X: 3.281e+009
Y: 7.45e-007

(c)

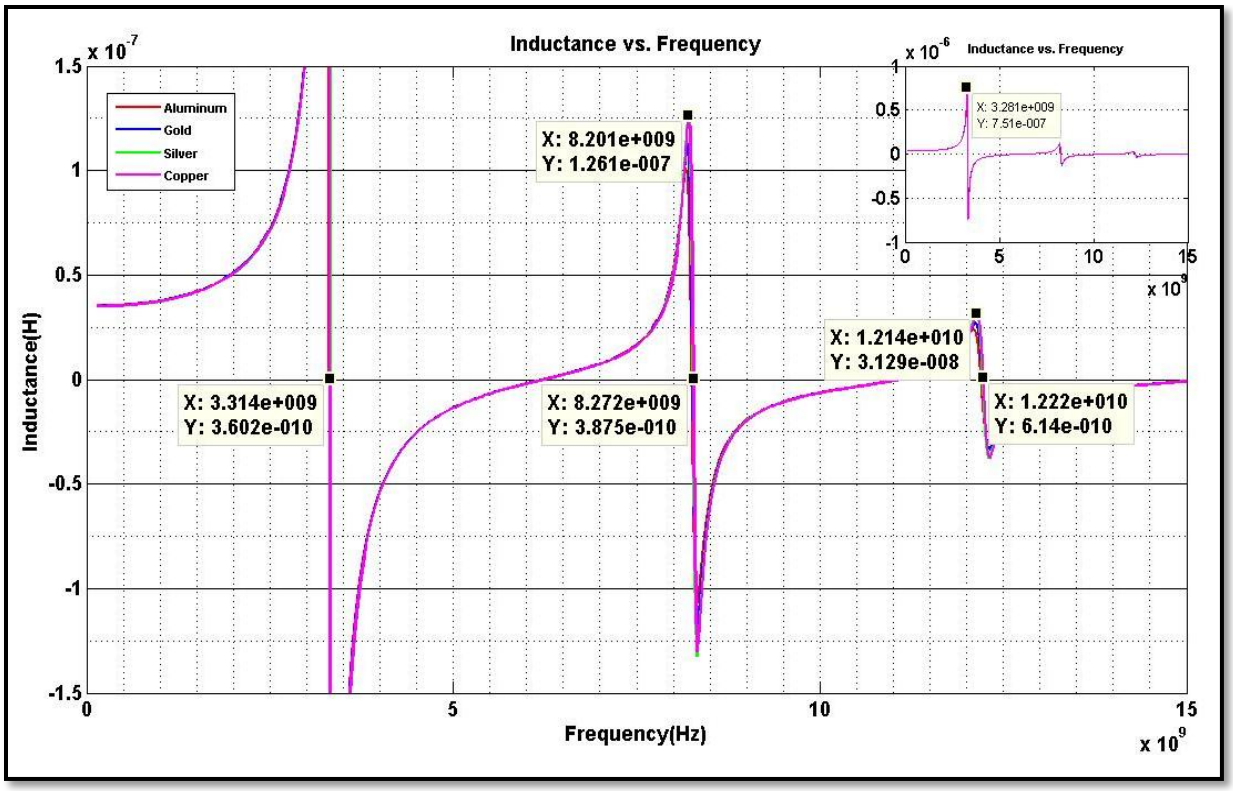

(d)

Figure 4.6-1: The inductance for a core thickness of (a) 10 μm, (b) 30 μm, (c) 50 μm, and (d) 70 μm

4.6.2 Resistance

Figure 4.6-2 shows the resistance of the structure. The resistance has a similar pattern as observed in the previous results of 5 μm thick metal. An inset containing a logarithmic plot of resistance versus frequency is provided as the resistance values are very high. It is observed that copper stands out separately from the other metals in Figure 4.6-2 (a) as seen earlier in the inductance graph. At lower frequencies, the metals have the same peaks. With the increase in core thickness, the resistance peaks increase by a very small amount. For a core thickness of 70 μm, the maximum resistance increase is about 300- 500 Ω and can be deduced as a contribution by the core material.

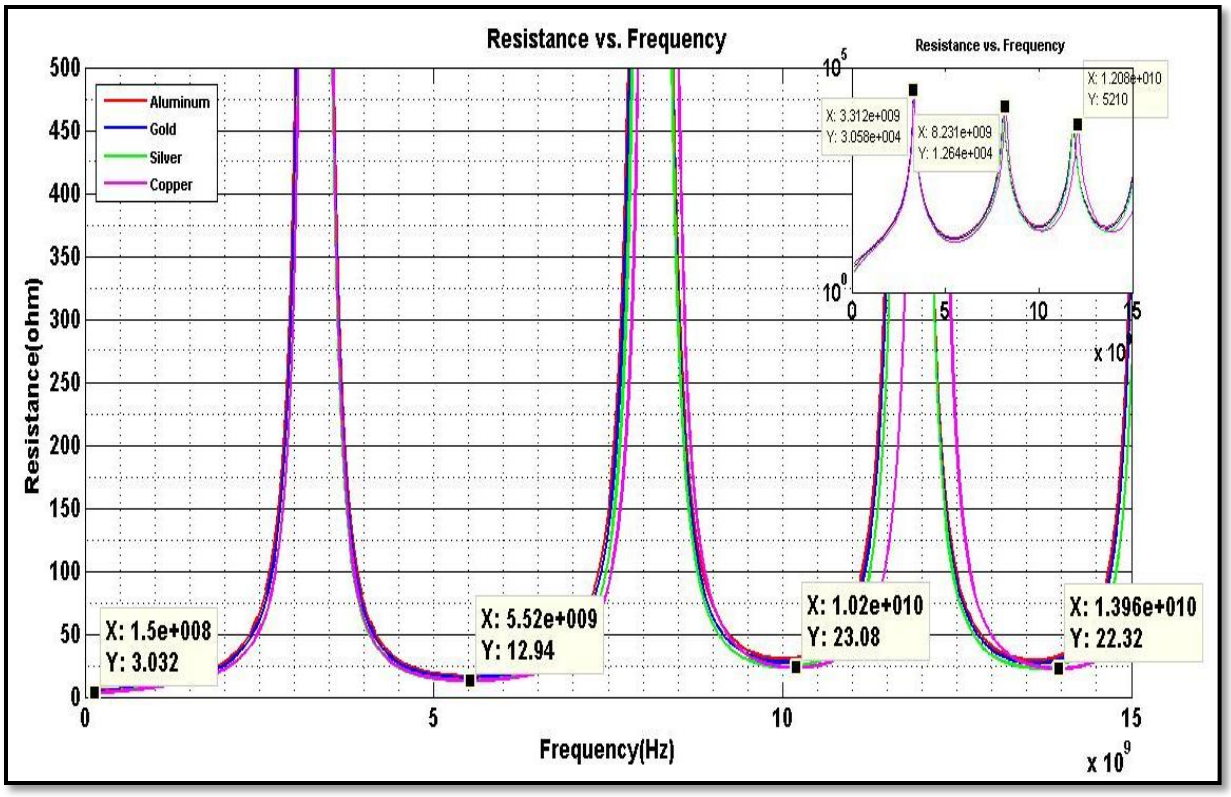
Resistance vs. Frequency
Aluminum
Gold
Silver
Copper
Resistance(ohm)
Frequency(Hz)
x 10^9
X: 1.5e+008
Y: 3.032
X: 5.52e+009
Y: 12.94
X: 1.02e+010
Y: 23.08
X: 1.396e+010
Y: 22.32
Resistance vs. Frequency
X: 3.312e+009
Y: 3.058e+004
X: 8.231e+009
Y: 1.264e+004
X: 1.208e+010
Y: 5210
x 10^9

(a)

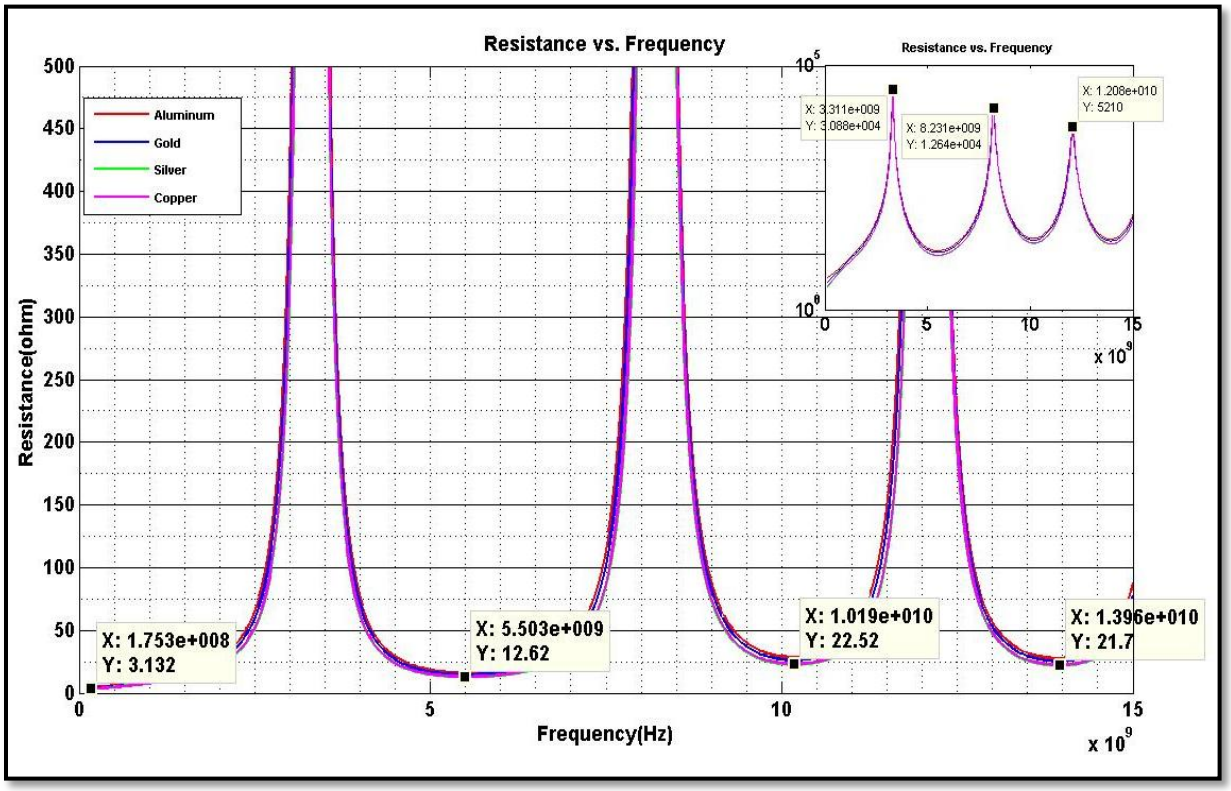
Resistance vs. Frequency
Aluminum
Gold
Silver
Copper
Resistance(ohm)
Frequency(Hz)
x 10^9
X: 1.753e+008
Y: 3.132
X: 5.503e+009
Y: 12.62
X: 1.019e+010
Y: 22.52
X: 1.396e+010
Y: 21.7
Resistance vs. Frequency
X: 3.311e+009
Y: 3.088e+004
X: 8.231e+009
Y: 1.264e+004
X: 1.208e+010
Y: 5210
x 10^9

(b)

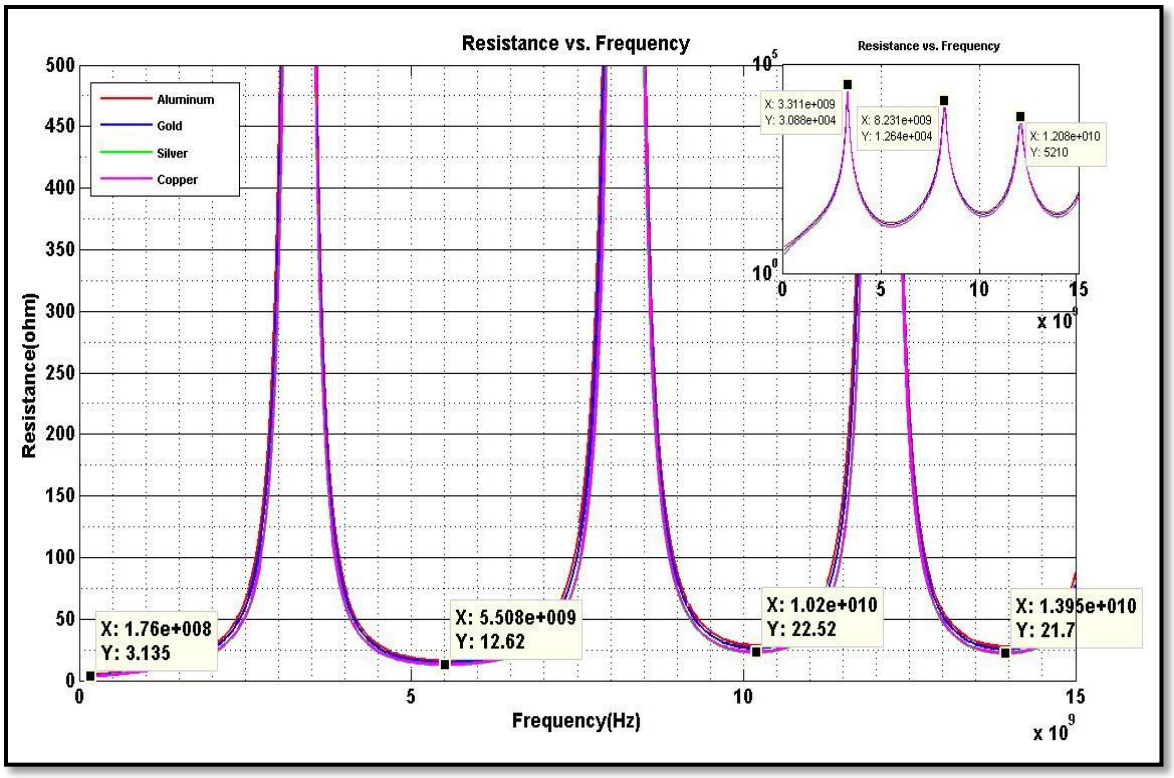

(c)

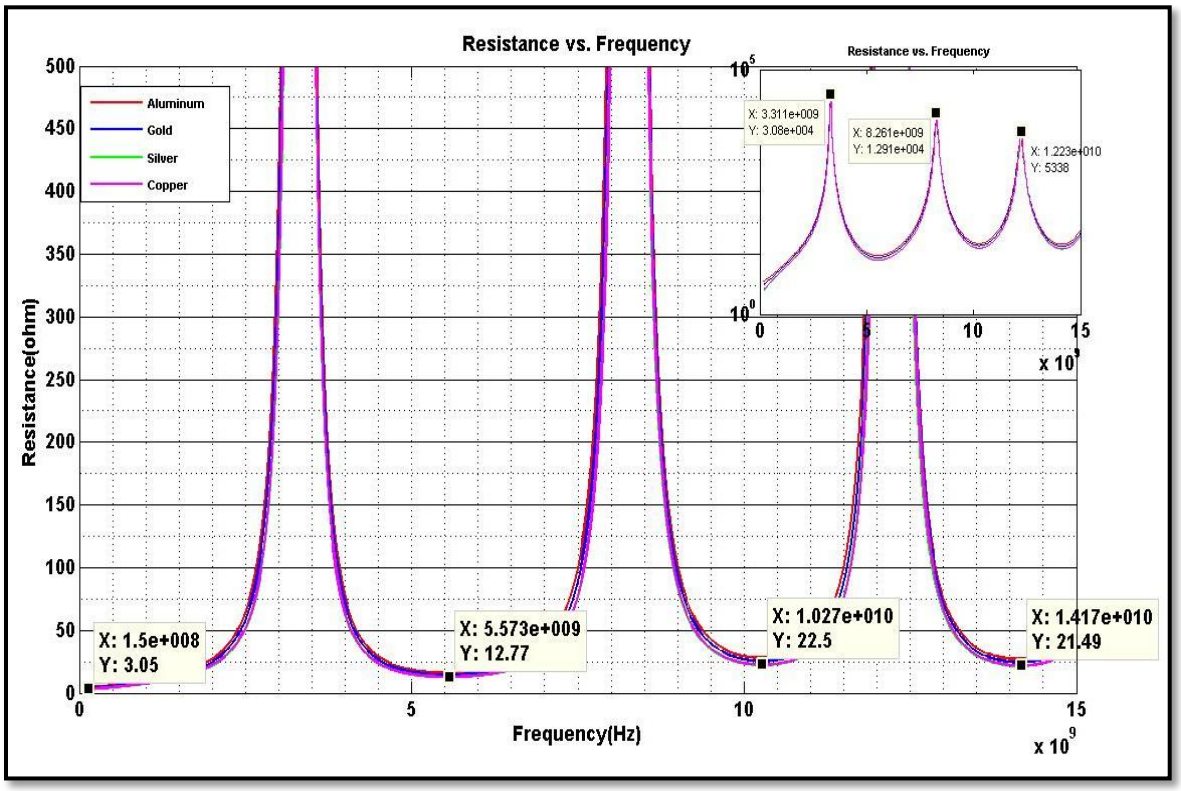

(d)

Figure 4.6-2: The resistance for a core thickness of (a) 10 μm, (b) 30 μm, (c) 50 μm, and (d) 70 μm

4.6.3 Quality Factor

Figure 4.6-3 shows the quality factor for the structure. All four metals display similar curves and are clearly visible at the least core size. With the increase in the core size, the curves for various metals begin to overlap each other and show a damping sinusoid of the almost the same frequency. The peaks are clearly distinguishable at lower frequencies but overlap at higher frequencies. There is only a slight improvement in quality factor with increase in thickness for the given structure indicating that the quality factor is least affected by core size.

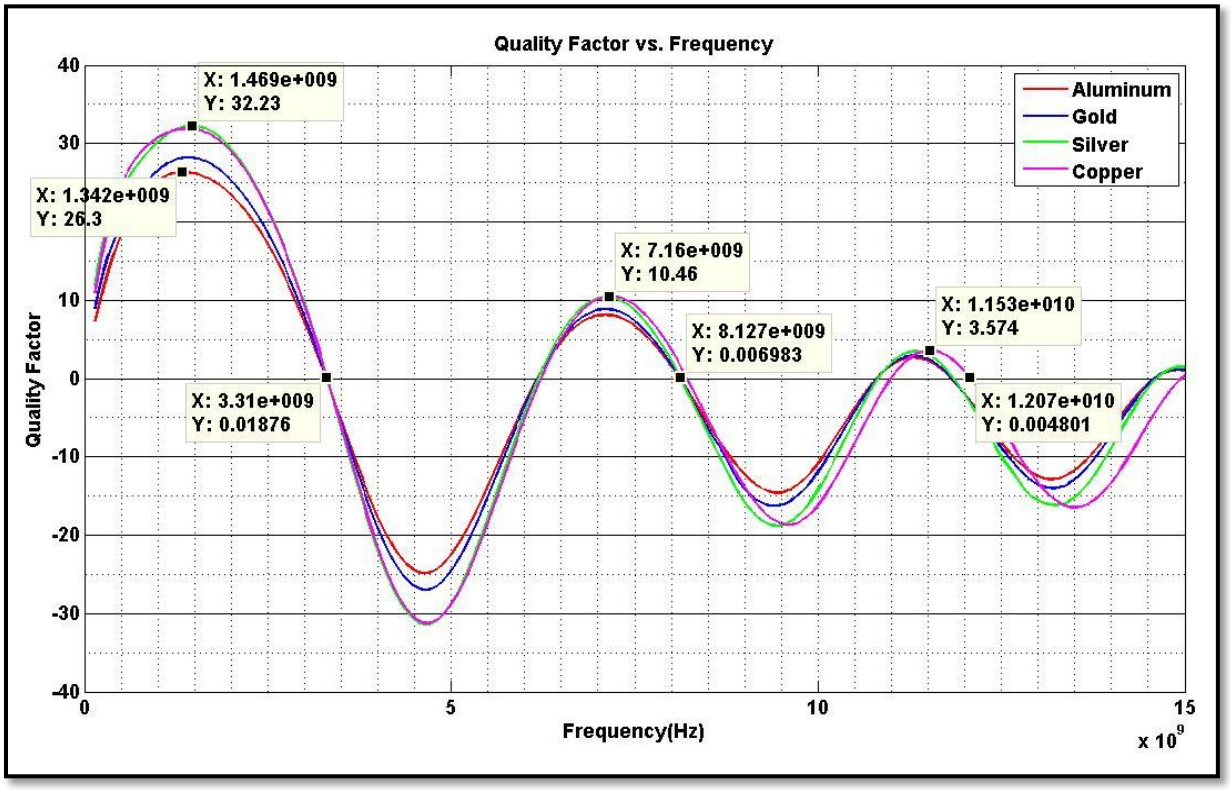

(a)

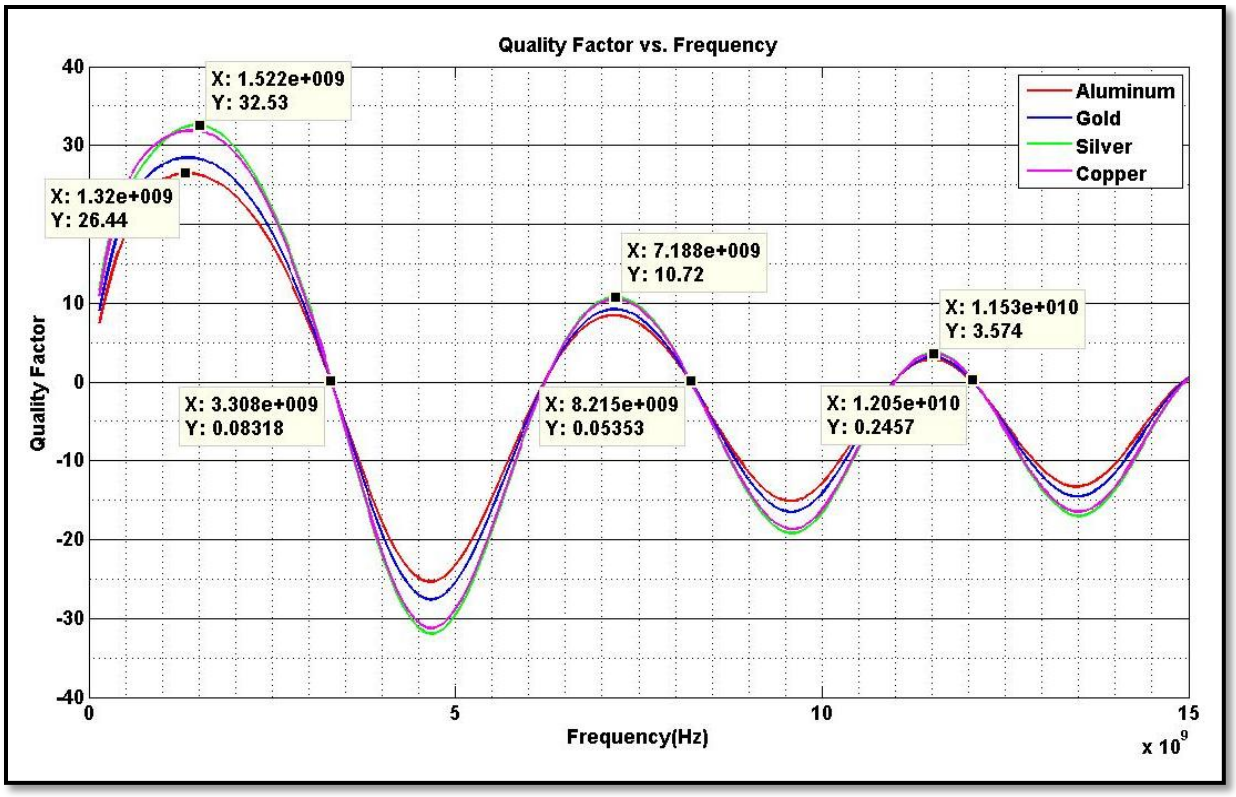
Quality Factor vs. Frequency
X: 1.522e+009
Y: 32.53
X: 1.32e+009
Y: 26.44
X: 7.188e+009
Y: 10.72
X: 1.153e+010
Y: 3.574
X: 3.308e+009
Y: 0.08318
X: 8.215e+009
Y: 0.05353
X: 1.205e+010
Y: 0.2457
Aluminum
Gold
Silver
Copper
Quality Factor
Frequency(Hz)
x 10^9

(b)

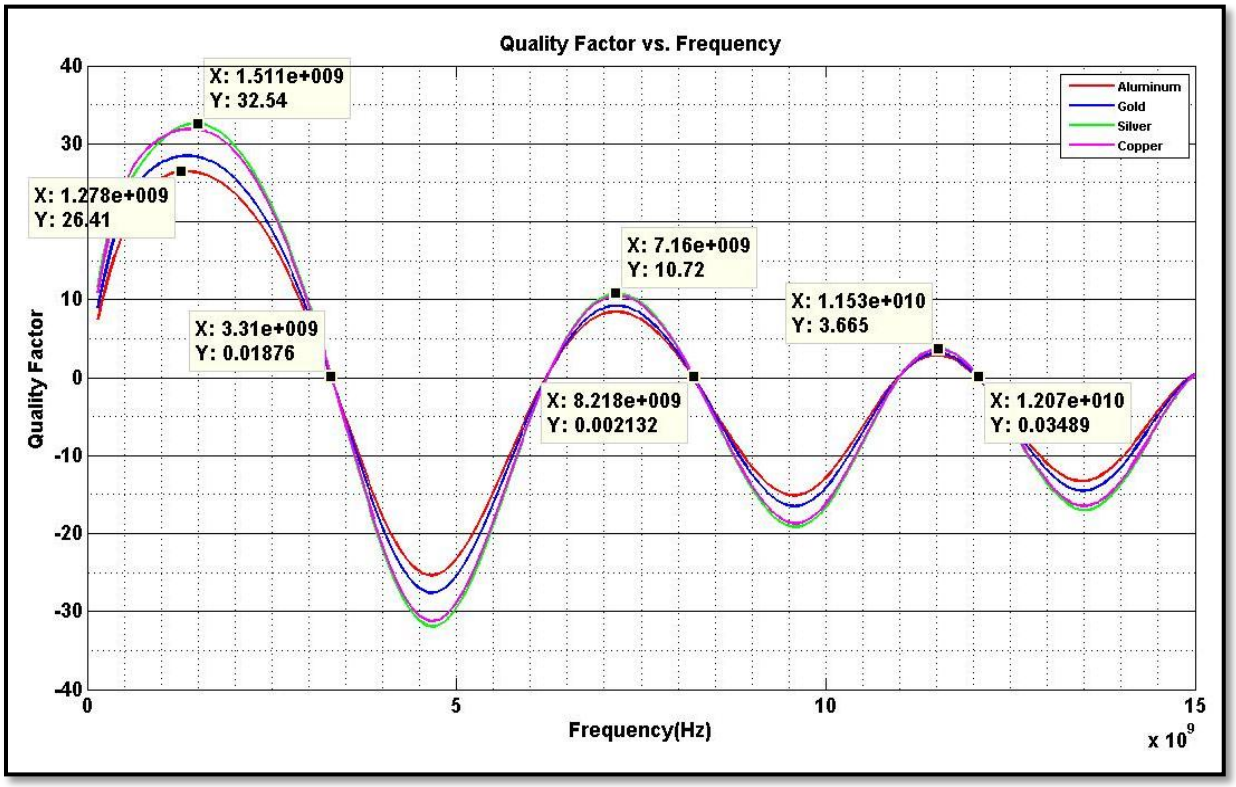
Quality Factor vs. Frequency
X: 1.511e+009
Y: 32.54
X: 1.278e+009
Y: 26.41
X: 7.16e+009
Y: 10.72
X: 1.153e+010
Y: 3.665
X: 3.31e+009
Y: 0.01876
X: 8.218e+009
Y: 0.002132
X: 1.207e+010
Y: 0.03489
Aluminum
Gold
Silver
Copper
Quality Factor
Frequency(Hz)
x 10^9

(c)

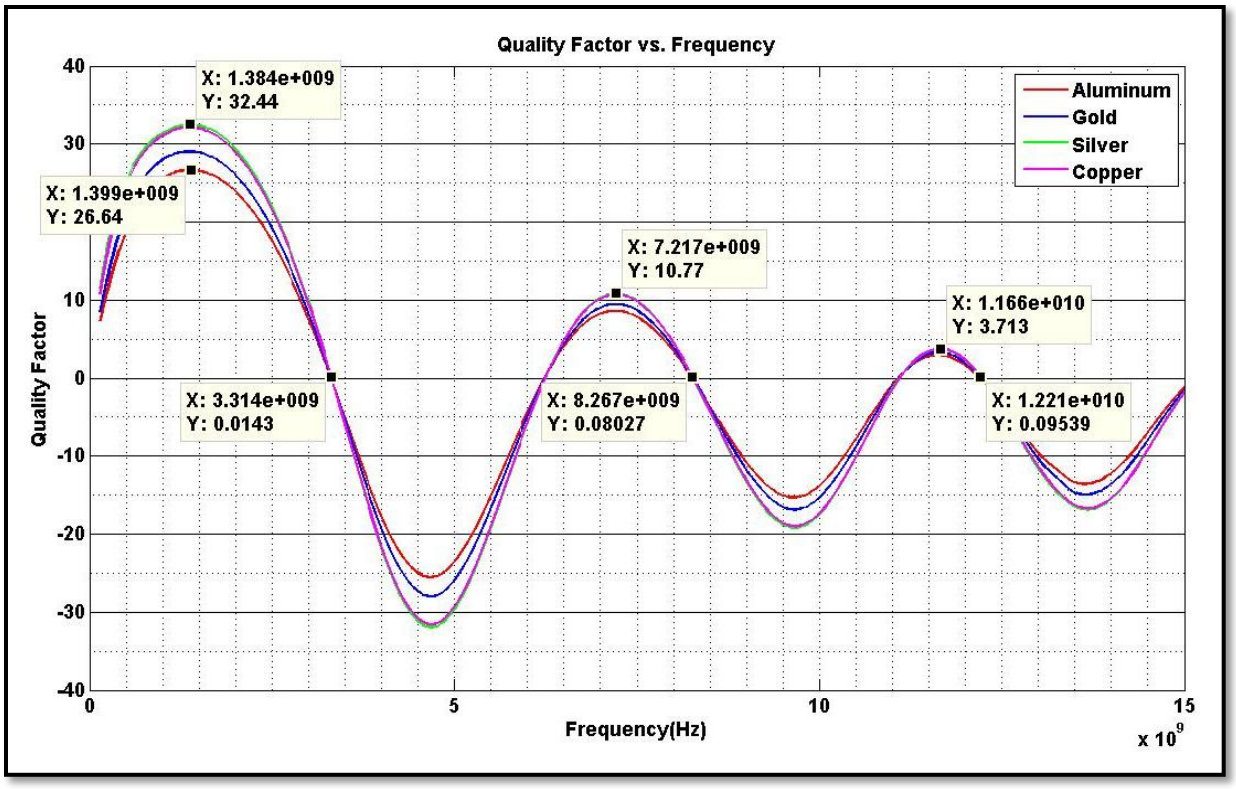

(d)

Figure 4.6-3: The quality factor for a core thickness of (a) 10 μm, (b) 30 μm, (c) 50 μm, and (d) 70 μm

4.7 Tabular comparison of data for varying metal thickness

Sections 4.5 and 4.6 show the graphical results for 5 μm and 10 μm thick metallic windings. It would prove to be useful to see a tabular comparison of the effect of increasing the thickness of the winding on the inductance, resistance, quality factor and resonant frequency. As the simulations were not carried out for the same core thickness, the table may not give an accurate comparison but it still gives a reasonable comparison. The larger core thickness for the metal (silver) of 5 μm has been compared with a smaller core thickness for the thicker metal (silver) of 10 μm.

4.7.1 Tabular comparison of cores with thickness 20 µm versus 10 µm

The inductance for the thicker coil is 158 nH larger than that of the thinner coil. The thicker coil shows better results compared to the thinner coil at the given core thickness when comparing quality factors. It is worth noticing that the resistances observed for the thicker coil are higher than the thinner coil.

5 µm thick winding core=20 µm		**10 µm thick winding core=10 µm**	
Inductance (silver)			
Frequency	**Peak Value**	**Frequency**	**Peak Value**
3.609 GHz	**587.4 nH**	**3.281 GHz**	**745 nH**
9.12 GHz	**101 nH**	**8.02 GHz**	**123.1 nH**
13.54 GHz	**27.44 nH**	**11.7 GHz**	**30.6 nH**
Resistance (silver)			
Frequency	**Peak Value**	**Frequency**	**Peak Value**
3.63 GHz	**27.05 kΩ**	**3.31 GHz**	**30.58 kΩ**
9.18 GHz	**11.57 kΩ**	**8.231 GHz**	**12.64 kΩ**
13.63 GHz	**5.083 kΩ**	**12.08 GHz**	**5.210 kΩ**
Quality Factor (silver)			
Frequency	**Peak Value**	**Frequency**	**Peak Value**
1.522 GHz	**29.65**	**1.469 GHz**	**32.23**
7.996 GHz	**10.14**	**7.16 GHz**	**10.46**
12.92 GHz	**4.05**	**11.53 GHz**	**3.57**

Table 4.7-1: Comparing cores of thickness 20 µm vs. 10 µm

4.7.2 Tabular comparison of cores with thickness 40 µm versus 30 µm

With the increase in core thickness, the inductance of the thinner coil improves by 32 nH, but the inductance and quality factor for the thicker coil are still better than the thinner coil at the given core thickness.

5 µm thick winding core=40 µm		**10 µm thick winding core=30 µm**	
Inductance (silver)			
Frequency	**Peak Value**	**Frequency**	**Peak Value**
3.6 GHz	**619 nH**	**3.281 GHz**	**745 nH**
9.155 GHz	**100 nH**	**8.17 GHz**	**127.6 nH**
13.66 GHz	**27 nH**	**12.02 GHz**	**28.91 nH**
Resistance (silver)			
Frequency	**Peak Value**	**Frequency**	**Peak Value**
3.63 GHz	**27.18 kΩ**	**3.31 GHz**	**30.8 kΩ**
9.245 GHz	**12 kΩ**	**8.231 GHz**	**12.64 kΩ**
13.78 GHz	**5.207 kΩ**	**12.08 GHz**	**5.210 kΩ**
Quality Factor (silver)			
Frequency	**Peak Value**	**Frequency**	**Peak Value**
1.522 GHz	**29.86**	**1.522 GHz**	**32.53**
8.03 GHz	**10.32**	**7.188 GHz**	**10.72**
13.05 GHz	**4.075**	**11.53 GHz**	**3.57**

Table 4.7-2: Comparing cores of thickness 40 µm vs. 30 µm

4.7.3 Tabular comparison of cores with thickness 60 µm versus 50 µm

The inductance and quality factor still show better results compared to the thinner coil. The resistance of the thicker coil has now reduced and is almost comparable to that of the thinner coil.

5 µm thick winding core=60 µm		**10 µm thick winding core=50 µm**	
Inductance (silver)			
Frequency	**Peak Value**	**Frequency**	**Peak Value**
3.6 GHz	**609 nH**	**3.281 GHz**	**745 nH**
9.24 GHz	**103 nH**	**8.17 GHz**	**127.6 nH**
13.84 GHz	**29.01 nH**	**11.99 GHz**	**30.73 nH**
Resistance (silver)			
Frequency	**Peak Value**	**Frequency**	**Peak Value**
3.65 GHz	**26.76 kΩ**	**3.31 GHz**	**30.8 kΩ**
9.3 GHz	**12.17 kΩ**	**8.231 GHz**	**12.64 kΩ**
13.93 GHz	**5.438 kΩ**	**12.08 GHz**	**5.210 kΩ**
Quality Factor (silver)			
Frequency	**Peak Value**	**Frequency**	**Peak Value**
1.701 GHz	**30.62**	**1.511 GHz**	**32.54**
8.026 GHz	**10.46**	**7.16 GHz**	**10.72**
13.19 GHz	**4.405**	**11.53 GHz**	**3.66**

Table 4.7-3: Comparing cores of thickness 60 µm vs. 50 µm

4.7.4 Tabular comparison of cores with thickness 80 µm versus 70 µm

The inductance of the thicker coil has improved by 6 nH and the resistance has reduced further and differs only by a few ohms from that of the thinner coil. Again the results of the thicker coil are better than the thinner coil.

5 µm thick winding core=80 µm		10 µm thick winding core=70 µm	
Inductance (silver)			
Frequency	**Peak Value**	**Frequency**	**Peak Value**
3.65 GHz	**640.5 nH**	**3.281 GHz**	**751 nH**
9.33 GHz	**105 nH**	**8.21 GHz**	**126.1 nH**
14.02 GHz	**30.3 nH**	**12.14 GHz**	**31.29 nH**
Resistance (silver)			
Frequency	**Peak Value**	**Frequency**	**Peak Value**
3.65 GHz	**29. 22 kΩ**	**3.31 GHz**	**30.8 kΩ**
9.33 GHz	**11.56 kΩ**	**8.261 GHz**	**12.91 kΩ**
14.02 GHz	**5.414 kΩ**	**12.23 GHz**	**5.339 kΩ**
Quality Factor (silver)			
Frequency	**Peak Value**	**Frequency**	**Peak Value**
1.489 GHz	**31.35**	**1.384 GHz**	**32.44**
8.048 GHz	**11.01**	**7.217 GHz**	**10.77**
13.27 GHz	**4.58**	**11.66 GHz**	**3.713**

Table 4.7-4 : Comparing cores of thickness 80 µm vs. 70 µm

Thus we can conclude that a thicker coil and smaller core thickness can achieve a desirable result.

4.8 Gallium Arsenide as a substrate

Gallium Arsenide (GaAs) is a compound consisting of gallium and arsenic. As a result its electrical and chemical properties are quite different from silicon [27]. Its electrical properties include higher electron mobility and saturated velocity that enable it to function at frequencies beyond 200 GHz. It has a higher bandgap, which makes it insensitive to variations in temperature. The high bandgap provides a high resistance and, thus, makes GaAs a more ideal substrate than Si. The high resistance of this substrate acts

as a natural insulator for the metal windings, reducing the substrate losses [28]. Organic materials such as polyimide have a number of positive features, such as a low dielectric constant, low internal stress, and are easier to process in thick film formation, so they are very suitable as insulator films for three-dimensional interconnects [29]. The permittivity of GaAs used is 13.1 with a conductivity of $5x10^{-8}$ S/m. The polyimide insulator used has a permittivity of 3.5. We show the simulation results of an inductor using silver for the metallic windings having GaAs as the substrate and polyimide as the insulator and compare it with a silicon substrate.

4.8.1 Coil structure with 10 µm thick magnetic core

A coil structure consisting of 35 turns where each is 10 µm thick by 30 µm wide and separated by a spacing 20 µm was simulated for gallium arsenide and silicon substrates respectively. The thickness of the magnetic core used is 10 µm with a permeability of 120. Both simulations have been performed for silver. Figure 4.8-1 shows the results of the simulation.

Figure 4.8-1 (a) shows that the inductance of the structure with a gallium arsenide substrate has a higher inductance peak and smaller resonant frequency compared to the silicon substrate. Only the first peak shows an inductance improvement of 20 nH where as the rest of the peaks are almost the same. Figure 4.8-1 (b) shows that the resistance of the gallium arsenide structure has a higher resistance compared to silicon, which is as expected. Figure 4.8-1 (c) shows the quality factor of GaAs being only a fraction larger than that of the silicon substrate.

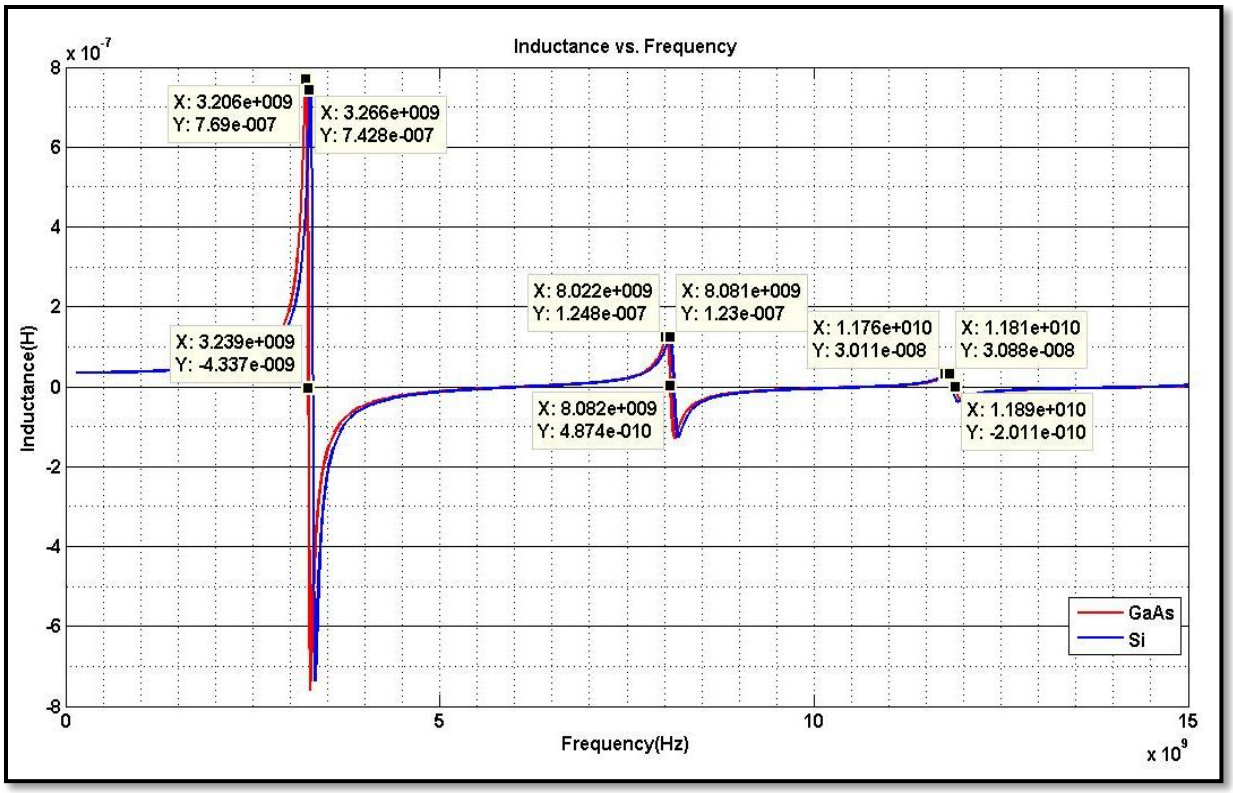
Inductance vs. Frequency
x 10^-7
Inductance(H)
Frequency(Hz)
x 10^9
X: 3.206e+009
Y: 7.69e-007
X: 3.266e+009
Y: 7.428e-007
X: 3.239e+009
Y: -4.337e-009
X: 8.022e+009
Y: 1.248e-007
X: 8.081e+009
Y: 1.23e-007
X: 8.082e+009
Y: 4.874e-010
X: 1.176e+010
Y: 3.011e-008
X: 1.181e+010
Y: 3.088e-008
X: 1.189e+010
Y: -2.011e-010
GaAs
Si

(a)

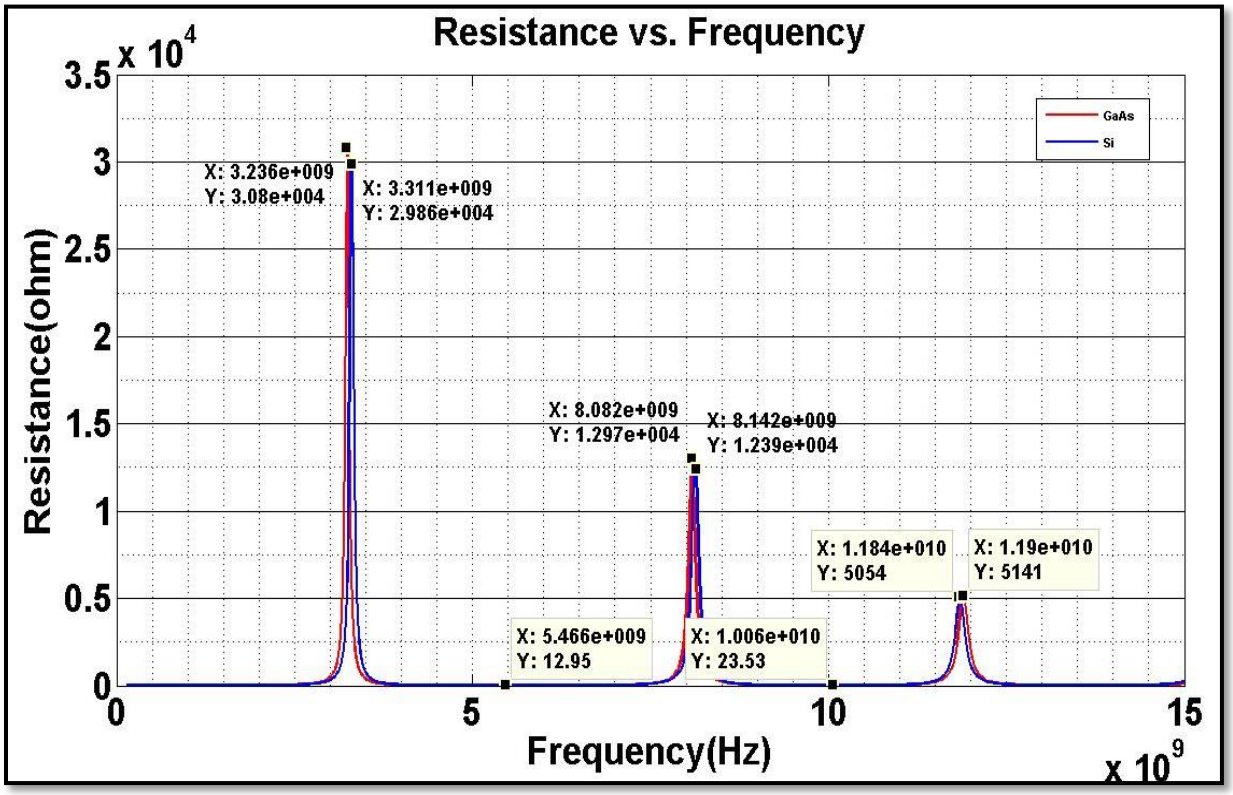
Resistance vs. Frequency
x 10^4
Resistance(ohm)
Frequency(Hz)
x 10^9
GaAs
Si
X: 3.236e+009
Y: 3.08e+004
X: 3.311e+009
Y: 2.986e+004
X: 8.082e+009
Y: 1.297e+004
X: 8.142e+009
Y: 1.239e+004
X: 1.184e+010
Y: 5054
X: 1.19e+010
Y: 5141
X: 5.466e+009
Y: 12.95
X: 1.006e+010
Y: 23.53

(b)

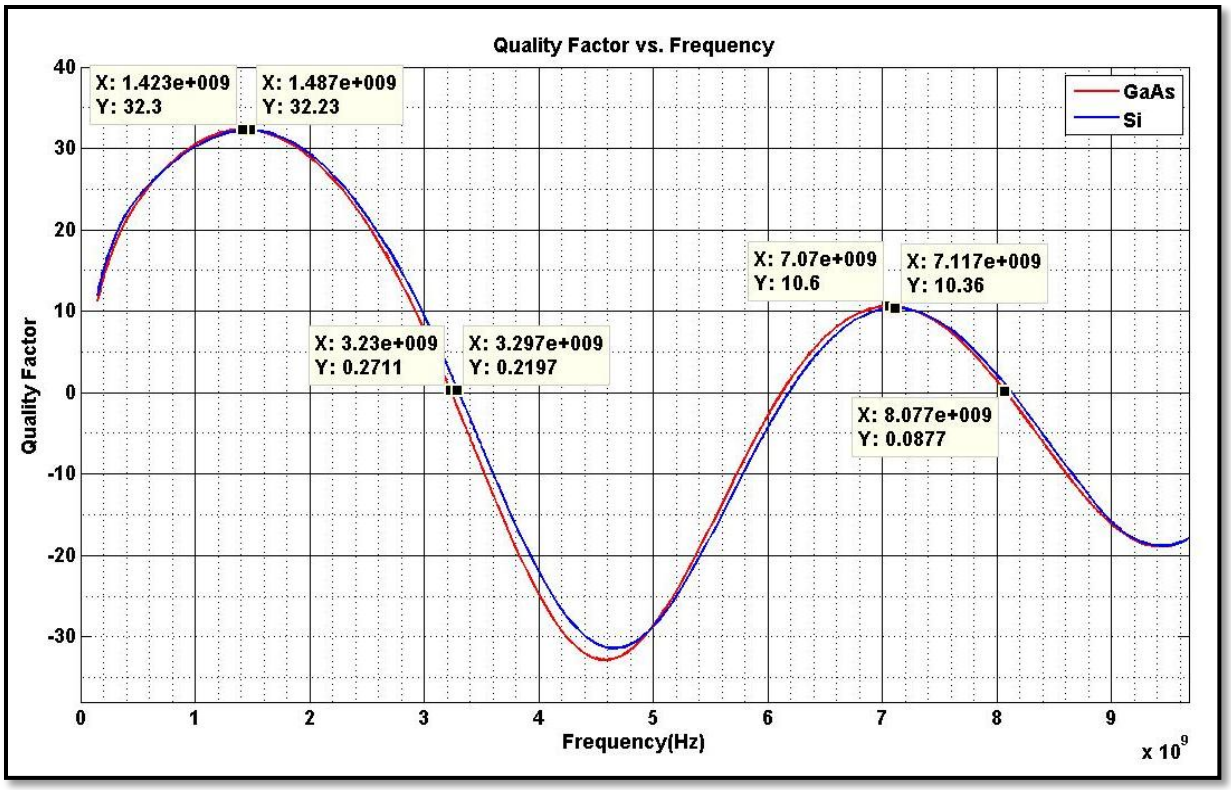

(c)

Figure 4.8-1: Effect of GaAs and Si substrate on (a) inductance (b) resistance, and (c) quality factor of an inductor consisting of 35 turns where each are 10 µm thick, 30 µm wide and separated by a spacing 20 µm and a 10 µm-thick magnetic core with a permeability of 120.

4.8.2 Coil structure with 70 µm thick magnetic core

A coil structure consisting of 35 turns, where each turn is 10 µm thick by 30 µm wide and separated by a spacing 20 µm was simulated for gallium arsenide and silicon substrates respectively. The thickness of the magnetic core used is 70 µm with a permeability of 120. Both simulations have been performed for silver. Figure 4.8-2 shows the results of the simulation.

Figure 4.8-2 (a) show the inductance of the structure. As observed previously, the inductance for gallium arsenide substrate has a higher peak compared to the silicon substrate at lower frequencies. The GaAs peaks are almost 6 nH more than their silicon counterparts. At higher frequency, the peaks share the same value. Figure 4.8-2 (b) shows that the resistance of the gallium arsenide structure has a resistance higher by 100 Ω compared to silicon. Figure 4.8-2 (c) shows the quality factor of GaAs being only a fraction larger than that of the silicon substrate. The inductance increase with GaAs is almost 14 nH more and proves to be a better alternative to silicon.

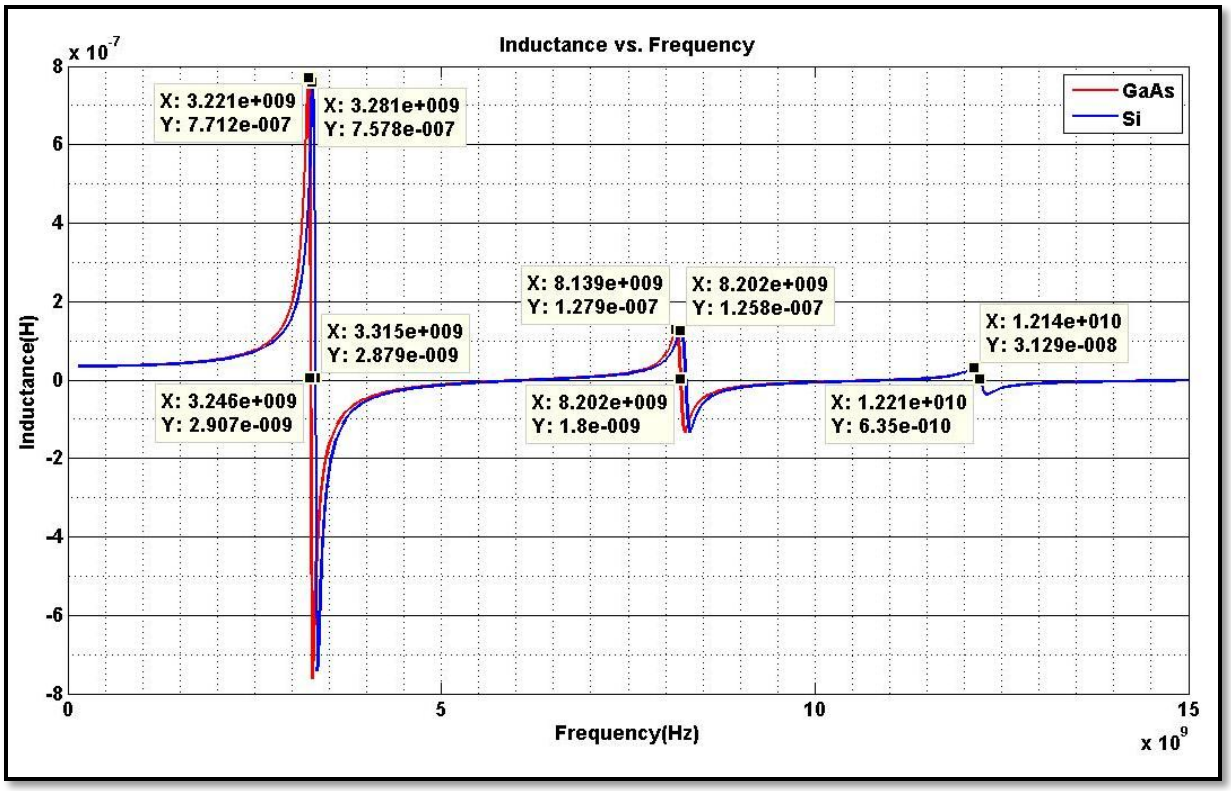
Inductance vs. Frequency
x 10^-7
Inductance(H)
Frequency(Hz)
x 10^9
GaAs
Si
X: 3.221e+009
Y: 7.712e-007
X: 3.281e+009
Y: 7.578e-007
X: 3.315e+009
Y: 2.879e-009
X: 3.246e+009
Y: 2.907e-009
X: 8.139e+009
Y: 1.279e-007
X: 8.202e+009
Y: 1.258e-007
X: 8.202e+009
Y: 1.8e-009
X: 1.214e+010
Y: 3.129e-008
X: 1.221e+010
Y: 6.35e-010

(a)

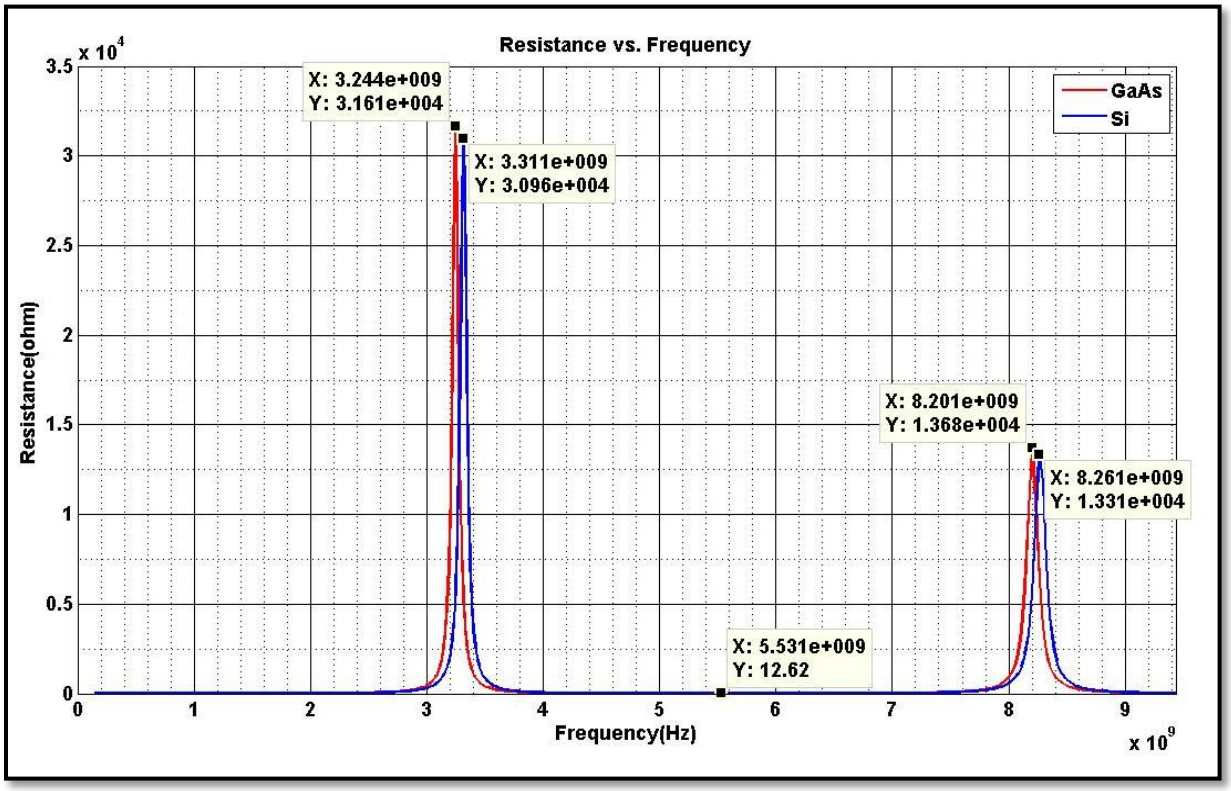
Resistance vs. Frequency
x 10^4
Resistance(ohm)
Frequency(Hz)
x 10^9
GaAs
Si
X: 3.244e+009
Y: 3.161e+004
X: 3.311e+009
Y: 3.096e+004
X: 8.201e+009
Y: 1.368e+004
X: 8.261e+009
Y: 1.331e+004
X: 5.531e+009
Y: 12.62

(b)

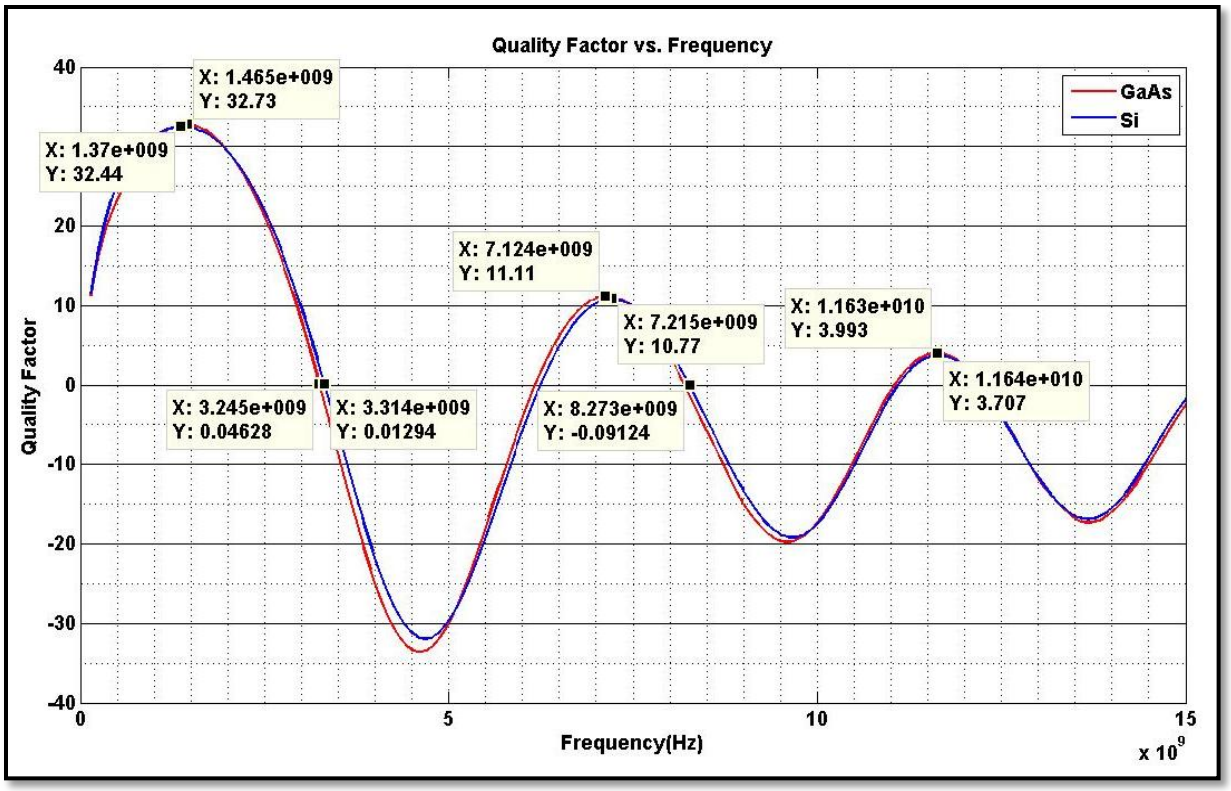

(c)

Figure 4.8-2: Effect of GaAs and Si substrate on (a) inductance, (b) resistance, and (c) quality factor of an inductor consisting of 35 turns where each is 10 µm thick, 30 µm wide and separated by a spacing 20 µm and a 70 µm-thick magnetic core with a permeability of 120

Chapter 5: Conclusions and Future Work

In this thesis we have described the modeling and design of a three-dimensional inductor. The inductor was designed in Momentum, ADS and further exported to Electromagnetic Professional to simulate the structure and obtain the s-parameters from which the values for series inductance, resistance and quality factor were derived. The structure was designed keeping in mind the process rules followed at VT MT SPL.

The three-dimensional inductor with a magnetic core was simulated for four types of metals – aluminum, gold, copper, and silver while varying various parameters such as the thickness of the coil, thickness of the core, spacing between turns, number of turns, type of substrate and magnetic core permeability. The results of these simulations help us narrow a choice for the optimum inductor structure.

It is observed from these simulations that the most feasible metals that can be used as windings in order of preference are silver, copper and aluminum. Gold is a very expensive metal and is rarely used in fabrication of coils. Silver displays the best results and then copper because of their higher conductivity.

The first set of simulations run for air core vs. magnetic core show a range of random unintelligible data being displayed between the frequency ranges of 150 MHz - 5 GHz, which is difficult to account for. The introduction of the core with μ_r=120 and μ_r=1500 show an increase in inductance as expected from the equations. As the Co-Fe nanoparticles have a μ_r=120 and we intend to fabricate the inductor with this magnetic core, all further simulations were carried on with respect to μ_r=120.

The losses in the substrate and the low quality factor were improved by nearly three points by increasing the silicon dioxide insulating layer between the substrate and the coil to 5 µm.

Increasing the spacing between turns helped increase the quality factor but reduced the inductance upon very large spacing. A spacing of 40 µm showed the highest Q for the given structure. Large spacing implies lower number of turns for a given area meaning lower inductance. Hence, there is a tradeoff between number of turns and spacing. The parasitic capacitances form a parallel resonant circuit with the inductor and cause resonance in the circuit, creating damped oscillations. These oscillations disappear with the increase in spacing between turns.

Increasing the thickness of the core to a large value improves the inductance value and quality factor. Better results are found for a smaller thickness of the core but with thicker coil windings.

Lastly to combat the substrate losses, gallium arsenide was used as the substrate and the results were compared with silicon. The quality factor for GaAs was the same as that of Si for lower frequencies but at higher frequencies, GaAs showed better results for lower core thickness. At higher core thickness, GaAs behaved very similarly compared to silicon. The effect of using GaAs as a substrate may show enhanced improvements once the inductor is fabricated.

In all, an optimum inductor can be designed considering the tradeoffs from the above results. Although a peak value of 751 nH on Si substrate and 771 nH on GaAs substrate was achieved, we observe that this value does not stay constant for a range of frequencies and the results can be improved with a better understanding of how to combat parasitics.

5.1 Future Work

As discussed above, the existing inductor structure can be improved to provide better and stable results over a larger frequency range. An in-depth understanding of the factors that cause the deviations in simulated versus expected results is essential in designing a more robust inductor. The random variations at lower frequencies and, the small increase in inductance for high permeability, which parasitic combinations cause the peaks in inductance and resistance, are but two of the questions that need to be clearly answered in order to understand the complex relationship between the structure of the inductor and its inductances as a function of frequency.

Different coil structures/geometries and materials can be simulated and compared for performance and improvements. Including the effects of neighboring coils/devices on the inductor will provide a real world scenario with new challenges and concerns. Finally, the inductor needs to be fabricated on an integrated circuit employing the necessary process steps at VT MT SPL and verified for functionality and performance in the RF range.

Bibliography

[1] T. Lee, "The Design of CMOS Radio-Frequency Integrated Circuits," 2nd edition Cambridge University Press, 2004.

[2] J. Wight, *et al.*, "On-Die Synthesized Inductors: Boon or Bane?," *Microwave Magazine, IEEE,* vol. 11, pp. 95-104, 2010.

[3] H. Ronkainen, *et al.*, "IC compatible planar inductors on silicon," *Circuits, Devices and Systems, IEEE Proceedings -,* vol. 144, pp. 29-35, 1997.

[4] H. J. De Los Santos, "On the ultimate limits of IC inductors-an RF MEMS perspective," in *Electronic Components and Technology Conference, 2002. Proceedings. 52nd*, 2002, pp. 1027-1031.

[5] J. R. Long and M. A. Copeland, "The modeling, characterization, and design of monolithic inductors for silicon RF IC's," *Solid-State Circuits, IEEE Journal of,* vol. 32, pp. 357-369, 1997.

[6] S. Musunuri and P. L. Chapman, "Fabrication and characterization of PDMA inductors," in *Power Electronics Specialists Conference, 2004. PESC 04. 2004 IEEE 35th Annual*, 2004, pp. 4460-4466 Vol.6.

[7] Z. Jun, *et al.*, "Development of three-dimensional inductors using plastic deformation magnetic assembly (PDMA)," *Microwave Theory and Techniques, IEEE Transactions on,* vol. 51, pp. 1067-1075, 2003.

[8] S. R. Kythakyapuzha, "Modeling of Spiral Inductors and Transformers", M.S. thesis, Kansas State University, Manhattan, Kansas, 2001.

[9] D. W. Lee, *et al.*, "Design and fabrication of integrated solenoid inductors with magnetic cores," in *Electronic Components and Technology Conference, 2008. ECTC 2008. 58th*, 2008, pp. 701-705.

[10] K. Shirakawa, *et al.*, "Thin Film Inductor with Multilayer Magnetic Core," *Magnetics in Japan, IEEE Translation Journal on,* vol. 8, pp. 169-176, 1993.

[11] M. Frommberger, *et al.*, "Integration of crossed anisotropy magnetic core into toroidal thin-film inductors," *Microwave Theory and Techniques, IEEE Transactions on,* vol. 53, pp. 2096-2100, 2005.

[12] F. Hettstedt, *et al.*, "Toroid microinductors with magnetic nanocomposite cores," in *Microwave Conference, 2007. European*, 2007, pp. 270-273.

[13] Y. Chen, *et al.*, "Ferrite-Partially-Filled on-Chip RF Inductor Fabricated Using Low-Temperature Nano-Powder-Mixed-Photoresist Filling Technique for Standard CMOS," in *Electron Devices Meeting, 2007. IEDM 2007. IEEE International*, 2007, pp. 1038-1040.

[14] M. Danesh and J. R. Long, "Differentially driven symmetric microstrip inductors," *Microwave Theory and Techniques, IEEE Transactions on*, vol. 50, pp. 332-341, 2002.

[15] M. Froramberger, *et al.*, "A new approach to RF thin film microinductors," in *Microwave Conference, 2004. 34th European*, 2004, pp. 1361-1364.

[16] Polar Instruments, "An Introduction to S-parameters," www.polarinstruments.com/support/cits/s_parameters.ppt

[17] Anon., "S Parameter Design," *Agilent Technologies application note, AN 154,* 2006.

[18] Anderson, R. W., "S-parameter techniques for faster, more accurate network design," *Hewlett-Packard Application Note 95-1*, 5952-1130, 1997.

[19] D. M. Pozar, "Microwave Engineering," Reading, MA: Addison-Wesley, 1990.

[20] Agilent Technologies, http://www.home.agilent.com/agilent/product.jspx?cc=US&lc=eng&ckey=1297143

[21] ANSYS, http://www.ansoft.com/products/hf/hfss/

[22] Mentor Graphics, http://www.mentor.com/electromagnetic-simulation/products/ie3d-ssd

[23] Agilent Technologies, http://www.home.agilent.com/agilent/product.jspx?cc=US&lc=eng&ckey=1887116&nid=-33748.0.00&id=1887116&cmpid=zzfindeesof-momentum

[24] Sonnet, http://www.sonnetsoftware.com/products/cst/

[25] Kevni Büyüktas, Klaus Koller, Karl-Heinz Müller, and Angelika Geiselbrechtinger, “A New Process for On-Chip Inductors with High *Q*-Factor Performance,” *International Journal of Microwave Science and Technology*, vol. 2010, Article ID 517187, 9 pages, 2010.

[26] R. Soohoo, "Magnetic thin film inductors for integrated circuit applications," *Magnetics, IEEE Transactions on,* vol. 15, pp. 1803-1805, 1979.

[27] S. M. Sze, "Semiconductor Devices Physics and Technology," J. Wiley, New York, 1985.

[28] I. Bahl, "Lumped Elements for RF and Microwave Circuits," Norwood, MA: Artech House, 2003.

[29] S. Sugitani, *et al.*, "Three-dimensional interconnect with excellent moisture resistance for low-cost MMICs," *Advanced Packaging, IEEE Transactions on,* vol. 26, pp. 133-140, 2003.